The black hole information paradox for small Schwarzschild de Sitter black holes; and no-boundary extremal surfaces in slow roll inflation and other cosmologies

by

Kaberi Goswami

A thesis submitted in partial fulfillment of the requirements for the degree of Doctor of Philosophy

to

Chennai Mathematical Institute

April 2025

Chennai Mathematical Institute,
Plot H1, SIPCOT IT Park, Siruseri, Kelambakkam,
Chennai, Tamil Nadu, India 603103

Advisor:

Dr. K. Narayan, *Chennai Mathematical Institute (CMI).*

Doctoral Committee Members:

1. Dr. K G Arun, *Chennai Mathematical Institute (CMI).*
2. Dr. Suresh Govindarajan, *Indian Institute of Technology Madras (IITM).*

Declaration

This thesis titled *Study of black hole information paradox for a small Schwarzschild de Sitter black hole and no-boundary extremal surfaces in the slow roll inflation and other cosmologies* is a presentation of my original research work, carried out with my collaborators and under the guidance of Dr. K. Narayan at Chennai Mathematical Institute. This work has not formed the basis for the award of any degree, diploma, associateship, fellowship or other titles in Chennai Mathematical Institute or any other university or institution of higher education.

Kaberi Goswami
April 2025

In my capacity as the supervisor of the candidate's thesis, I certify that the above statements are true to the best of my knowledge.

Dr. K. Narayan
August 2020

Thesis Outline

This thesis is based on the publications [1],[2],[3],[4]. This work was performed in collaboration with the co-authors of this article. This thesis is divided into two parts. The first five chapters of the thesis are included in part one, titled "The black hole information paradox for small Schwarzschild de Sitter black holes". Chapters 6 and 7 are included in part two, titled "No-boundary extremal surfaces in slow roll inflation and other cosmologies". The various Chapters of this thesis are organized as follows: Chapter 1 provides a brief introduction and motivation for the study of the black hole information paradox and its possible resolution. Then in Chapter 2, we study Timelike quantum extremal surfaces in some of the cosmological backgrounds, in particular, de Sitter space in the Poincaré slicing and FRW universes under certain conditions. In Chapter 3, we study the information paradox for a small Schwarzschild black hole in a frozen de Sitter background, while considering the observer in the static diamond of the background geometry, in a generic 2-dimensional dilaton gravity theory. We have shown that including a self-consistent island at late times of the black hole evaporation process leads to the falling page curve and resolves the paradox. In Chapter 3, we further study the information paradox for the same small Schwarzschild de Sitter black hole while considering the radiation collected by some meta observer close to the future boundary. Here we have also shown that islands arising from both sides black hole horizon resolve the information paradox. Chapter 5 discusses the overall conclusion and possible future directions for the study of the black hole information paradox. Next, in Chapter 6, we review previously studied de Sitter extremal surfaces from various places. Finally, in Chapter 7, we study no-boundary extremal surfaces in slow-roll inflation, with perturbations to no-boundary global dS preserving the spatial isometry. It turns out that the area of the no-boundary extremal surface has both the real and imaginary finite corrections at leading order in the slow-roll parameter that match those in the semiclassical expansion of the Wavefunction (or action), and corroborate the cosmic brane interpretation discussed previously.

Appendices A, B, and C show all the mathematical computations and technical details of Chapters 3, 4 and 7, respectively.

Acknowledgments

I owe the completion of this work to the incredible individuals I have met throughout my life and my time at CMI. In retrospect, returning to academia after two years of completing my master's was the best decision of my life. During the six years of my PhD, I learnt a lot about Physics, life, sociopolitical issues, especially the lives of people around us, those who serve us every day beyond a normal human's capacity.

First and foremost, I am extremely grateful to have Narayan as my advisor. I thank him for his exceptional guidance and support throughout my PhD days. His curiosity and excitement about research ideas during discussions encouraged me to keep going. I would like to thank him for being amazingly supportive in the final year of my PhD.

I would like to thank K. G Arun at CMI and Suresh Govindarajan at IITM, Chennai, for being my doctoral committee members.

I thank Amitabh Virmani at CMI, Chennai, for helpful discussions during our collaboration on one of the projects.

I thank my amazing friends and collaborators, Gopal Yadav, Soumya Adhikari, and Pavan Dharanipragada, for many enjoyable physics discussions and chats on different topics.

I thank my amazing friends Alok Laddha and Ronak Soni for many helpful discussions on Physics and other topics, and for being an incredible support during the hard times of my PhD. My time in CMI was absolutely enjoyable because of these guys. Especially, I would like to thank Alok for being an exceptionally amazing human being and supportive friend in every aspect of our friendship.

I thank all my friends at CMI and IMSc for being with me during the Ph.D. days. Their love and support kept me going during my Ph.D. I thank my batchmates Ankit, Parthapratim and Pankaj for making my stay enjoyable. I thank all my juniors Aleek, Harsh, Pitish, Hitesh, Anirban, Aditya, Siva Shankar, Khusboo, Sayantan, and my seniors, Sayantani, Shanmugapriya, Athira, Manu, Aneesh and Debangshu, for many beautiful memories during this journey. My heartfelt thanks to my non-academic friends Panda, Ajit bhaiya, Mala akka, Barun da, Soutam da, for working endlessly to make our lives comfortable.

I also thank my friends at other institutions for chatting and discussing during our meetings at various schools, workshops, and conferences.

I thank Jan de Boer at the University of Amsterdam and Daniel Grumiller at TU Wien for hosting me for an academic visit during the summer, 2024.

I thank Preeti for being my best friend and sharing our friendship for over ten years now. She has been very emotionally supportive throughout these years.

One of the main reasons for being extremely grateful to be in CMI is that I met my Puguu here. I thank him for being there for me through all the ups and downs over these years, helping me understand socio-political issues, showing unconditional love, support, kindness, social intelligence, and a strong personality, which was precious throughout this journey. I want to thank him for being my backbone in every aspect of my life.

I thank my Ma, Baba, and Krishna for their unconditional love and care. I am grateful for the freedom and support they provided, which shaped me into who I am today.

Kaberi Goswami
April 2025

Dedicated to ma, baba, Krishna, puguu and meowws

List of publications

This thesis is based on the following publications.

1. Kaberi Goswami, K. Narayan and Hitesh K. Saini, *Cosmologies, singularities and quantum extremal surfaces*, JHEP 03 (2022) 201; [arXiv:2111.14906 [hep-th]].

2. Kaberi Goswami and K. Narayan, *Small Schwarzschild de Sitter black holes, quantum extremal surfaces and islands*, JHEP 10 (2022) 031; [arXiv:2207.10724 [hep-th]].

3. Kaberi Goswami and K. Narayan, *Small Schwarzschild de Sitter black holes, the future boundary and islands*, JHEP 05 (2024) 016; [arXiv:2312.05904 [hep-th]].

4. Kaberi Goswami, K. Narayan and Gopal Yadav, *No-boundary extremal surfaces in slow-roll inflation and other cosmologies*, JHEP 03 (2025) 193; [arXiv:2409.14208 [hep-th]].

Other publication not included in this thesis :

5. Soumya Adhikari, Pavan Dharanipragada, Kaberi Goswami and Amitabh Virmani, *Attractor saddle for 5D black hole index*, JHEP 03 (2025) 180; [arXiv:2411.12413 [hep-th]].

Contents

Part I

The black hole information paradox for small Schwarzschild de Sitter black holes

Chapter 1

Black hole information paradox: Introduction

The black hole information paradox [1] has seen fascinating progress over the last few years: In this context, it is perhaps best to regard this, not as a detailed understanding of black hole microstates, but as the tension between the apparent unbounded growth of the entanglement entropy of Hawking radiation [2] outside the black hole and the quantum mechanics expectation that entanglement entropy must become small at late times to recover the purity of the original matter state (see *e.g.* [3], [4], which review various aspects of the information paradox). This falling Page curve [5], [6], reflecting the original purity can be recovered when nontrivial, spatially disconnected, island saddles for quantum extremal surfaces are included [7], [8], [9], [10], [11].

Quantum extremal surfaces are extrema of the generalized gravitational entropy [12, 13] obtained from the classical area of the entangling RT/HRT surface [14]-[17] after incorporating the bulk entanglement entropy of matter. Effective 2-dimensional models allow explicit calculation, where 2-dim CFT techniques enable detailed analysis of the bulk entanglement entropy. The island, arising as a nontrivial solution to extremization (near the black hole horizon, and only at late times), reflects new replica wormhole saddles [10, 11] and serves to purify the early Hawking radiation thereby lowering the entanglement entropy. There is a large body of literature on various aspects of these issues, reviewed in *e.g.* [18, 20, 21]: see *e.g.* [22]-[179] for a partial list of investigations on black holes in various theories, and also cosmological contexts. It is important to note that several of these investigations are simply applications of the island proposal, which appears to be self-consistent, even if it cannot be rigorously derived in those contexts (see *e.g.* [20] for an overall critical perspective, as well as [94], [95], and [96]).

The above lightning introduction briefly states the problem of the black hole information paradox and its possible resolution via the study of the island formula, and we give a detailed discussion about the basics of the various aspects of this study in the following sections. In sec. 1.1, we begin with the basic definition and properties of the entanglement entropy of the discrete system and the continuum QFT. Then we briefly discuss the entanglement entropy in CFT_2 for both single and multiple intervals in sec. 1.2. For the review on the basics of entanglement entropy, we have been following [17]. In sec. 1.3, we introduce holography starting with the basics of AdS geometry, conformal field theory, and followed by the statement of AdS/CFT correspondence and its dictionary. Followed by this sec. 1.4 discusses briefly the idea of holographic entanglement entropy via the RT formulation. Next in sec. 1.5, we give preliminaries about the thermal aspects of a black hole, which include black hole thermodynamics, Euclidean black hole, and different stages of the black hole evaporation process. In sec. 1.6, we state the idea of considering a black hole as a quantum mechanical system according to the Central Dogma. In sec. 1.7 we briefly mention two different notions of entropy. In sec. 1.8, we review Hawking's original paradox [1] by following [18], [19], and sec. 1.9 discusses the resolution of the black hole information paradox for a 2-dimensional black hole coupled to a heat bath in a generic 2-dimensional dilaton gravity theory via the island formulation. This formulation is giving us the true Gravitational fine-grained entropy of the Hawking radiation, which follows the Page curve like evolution, and for this we have followed the review on black hole information paradox [9], [18] by Almheiri et. al. In the final sec. 1.10, we give a simple example of the black hole information paradox and its resolution for a 2-sided eternal black hole coupled to a heat bath in JT gravity, followed by a recent lecture [19] by Mahajan.

1.1 Introduction to Entanglement entropy

Entanglement entropy is a measure of how quantum information is stored in a quantum state. It can be defined in quantum mechanics, quantum field theory, and also in quantum gravity. In holographic systems, entanglement entropy is encoded in geometric features of the bulk geometry.

1.1.1 Definition and basics

A bipartite system is a system with Hilbert space equal to the direct product of two factors,

$$\mathcal{H}_{AB} = \mathcal{H}_A \otimes \mathcal{H}_B \tag{1.1}$$

Considering the general state of the full system ρ, we can construct an operator that acts on one of the factors, say $\mathcal{H}_A$, by tracing out the other (in this case $\mathcal{H}_B$). This operator is the *reduced density matrix* ρ_A and our definition can be formalized as

$$\rho_A = \mathrm{Tr}_B\, \rho \tag{1.2}$$

The definition here is capturing the state of the degrees of freedom in A, assuming complete ignorance of what happens in B. The von Neumann entropy of the reduced density matrix, which is often referred to as the *entanglement entropy*, is given by

$$S_A = -\,\mathrm{Tr}_A\,(\rho_A \log \rho_A) \tag{1.3}$$

It is also convenient to define another set of 'entropies' called the Rényi entropies, which are simply defined in terms of the moments of the reduced density matrix:

$$S_A^{(q)} = \frac{1}{1-q}\,\log \mathrm{Tr}_A(\rho_A{}^q) \tag{1.4}$$

The canonical definition here requires that $q \in \mathbb{Z}_+$, but it is effective to analytically continue the definition to $q \in \mathbb{R}_+$. Now, if we consider $q \to 1$, then the Rényi entropies converge to S_A, i.e.,

$$S_A = \lim_{q\to 1} S_A^{(q)}. \tag{1.5}$$

1.1.2 Entanglement entropy in quantum field theory

Now, we have a d-dimensional relativistic QFT on some Lorentzian spacetime B, which we take to be globally hyperbolic. Since B_d is globally hyperbolic, we pick a Cauchy slice Σ_{d-1} which is an (achronal) spacelike slice, defined in the QFT, at a particular time. On Σ_{d-1}, we then have a state of the system. This could be a pure state given by a wavefunctional $\Psi[\Phi(x)]$, or more generally a density matrix ρ_Σ (x now defines a coordinate chart on Σ_{d-1}). We choose some spacetime codimension-1 region A on the Cauchy slice, which allows for a spatial bipartitioning of the form $A \cup A_c = \Sigma_{d-1}$. The boundary of the region is the entangling surface ∂A, which we note is a codimension-2 hypersurface in B. Here, some UV divergence arises from the short distance entanglement between the degrees of freedom inside and outside the entangling surface. These can be regulated by introducing an explicit UV regulator ϵ.

The reduced density matrix $\rho_A = \mathrm{Tr}_{\mathcal{H}_{A_c}}(\rho_\Sigma)$ captures the entanglement between A and A_c. Tracing over the complementary region A_c amounts to integrating over all field configurations

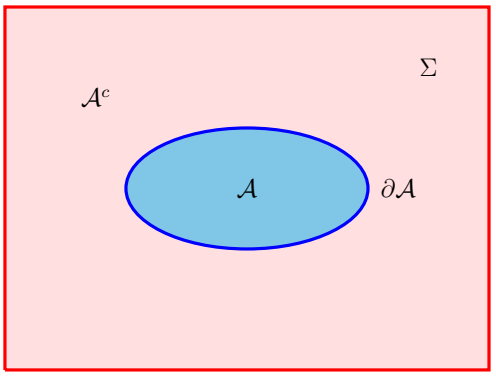

Figure 1.1: A continuum QFT which has been spatially bipartitioned into two components on a Cauchy slice Σ.

in that domain, i.e., for $x \in A_c$ to obtain ρ_A. The explicit path integral construction that computes the matrix elements of ρ_A is given in many places [23, 24, 25, 26, 17]. The Euclidean framework is most appropriate when we consider static states for which time evolution is trivial. Then the Rényi entropies can be computed by considering a functional integral on a "branched cover" geometry, known as the replica construction, and therefrom pass to the entanglement entropy itself by invoking an analytic continuation.

1.1.3 General properties of Entanglement entropy

1.1.3.1 Area law

As we have seen before, entanglement entropy is a UV divergent quantity due to the entanglement between the modes right across the entangling surface. The reason is that any state in local QFT has a short-range correlation in ultra-violet. We anticipate that the number of EPR pairings across the entangling surface will directly correlate with the divergence. Given that the leading contribution in entanglement entropy would be proportional to the area of the entangling surface, this would anticipate a sub-extensive behaviour of entanglement. This notion was a major factor in the original emphasis on this quantity [27] to compare its behaviour to that of the Bekenstein-Hawking entropy for black holes.

We can demonstrate that the leading divergent terms in the UV limit $\epsilon \to 0$ in d-dimensional free field theories do follow the area law [28]:

$$S_A = \gamma \, \frac{\text{Area}(\partial A)}{\epsilon^{d-2}} + \cdots \tag{1.6}$$

Where we have ignored the less divergent terms. This leading diverging term is proportional to the area of the region A's boundary and does not depend on the size of A, as would be expected based on physical considerations.
There is a thorough derivation of the area law for gapped interacting systems for d = 2 [29], even if explicit calculations of the entanglement entropy of interacting field theories (apart from holographic theories) are relatively intractable. However, two-dimensional conformal theories (d = 2) are an exception, as they show a logarithmic divergence and do not adhere to an area law.

1.1.3.2 Entropy inequalities

- Subadditivity: For a bipartite system $\mathcal{H}_{A_1} \otimes \mathcal{H}_{A_2}$ we have

$$S_{A_1} + S_{A_2} \geq S_{A_1 A_2} \,. \tag{1.7}$$

  This is frequently trivially satisfied in QFTs for overlapping regions, i.e., $A_1 \cap A_2 \neq 0$.

- Mutual information: For such a bipartite system, define the mutual information as

$$I(A_1 : A_2) = S_{A_1} + S_{A_2} - S_{A_1 A_2} \geq 0 \,. \tag{1.8}$$

  This is non-negative, and it follows from the inequality subadditivity. Roughly, $I(A_1 : A_2)$ measures the amount of information that A_1 has about A_2 (or vice-versa).

- Relative entropy: Given, two density matrices ρ and σ, define the relative entropy $S(\rho||\sigma)$. It provides a measure of distinguishability between the two states.

$$S(\rho||\sigma) = \mathrm{Tr}\, \rho \log \rho - \mathrm{Tr}\, \rho \log \sigma \,. \tag{1.9}$$

  Relative entropy has two important properties: positivity and monotonicity. Positivity implies that the relative entropy is non-negative for any two density matrices and vanishes only when the two are equal, i.e.,

$$S(\rho||\sigma) \geq 0 \,, \qquad S(\rho||\sigma) = 0 \implies \rho = \sigma \,. \tag{1.10}$$

- Triangle inequality: Relative entropy implies the triangle inequality

$$| S_{A_1} - S_{A_2} | \leq S_{A_1 A_2} \,. \tag{1.11}$$

- Strong subadditivity: This inequality applies to a tripartite system $\mathcal{H} = \mathcal{H}_{A_1} \otimes \mathcal{H}_{A_2} \otimes \mathcal{H}_{A_3}$

$$S_{A_1A_2} + S_{A_2A_3} \geq S_{A_1A_2A_3} + S_{A_2}, \tag{1.12}$$

$$S_{A_1A_2} + S_{A_2A_3} \geq S_{A_1} + S_{A_3}\,. \tag{1.13}$$

1.2 Entanglement entropy in CFT_2

Consider a two-dimensional theory with conformal invariance, i.e. a CFT_2 and these theories can be described by giving

- The central charge c,
- A set of the quasi-primary operators $\mathcal{O}_{h,\bar{h}}$ which have definite scaling dimensions $\{h, \bar{h}\}$ under local Weyl rescaling, and
- The OPE coefficients C_{ij}^k which appear in the OPE: $\mathcal{O}_i\mathcal{O}_j \sim C_{ij}^k\,\mathcal{O}_k$.

These two-dimensional CFTs also possess an infinite-dimensional global symmetry algebra, called the Virasoro algebra.

1.2.1 Entanglement entropy for a single interval in CFT_2

Consider a vacuum state of the CFT_2 on $\mathbb{C}$ at an instant of time $t = 0$, and define A to be a single interval $-a < x < a$. As we have mentioned before for computing the entanglement entropy in QFT, the replica construction here has also been done by taking the q copies of original complex plane with slits cut out along A and to glue them cyclically to construct the manifold B_q. This constructs a q-sheeted surface with a prescribed branching at $\{x = \pm a, t = 0\}$. Now we want to compute the partition function $Z[B_q]$ and to do that we have to upgrade the field $\phi(x,t)$, which lives on a single complex plane, to a set of fields $\phi_k(x,t)$ with $k = 1, 2, \cdots, q$ that live on the q-copies. In order to glue all the q copies, we need to impose boundary conditions on the fields

$$\phi_k(x, 0^+) = \phi_{k+1}(x, 0^-)\,, \qquad x \in A = \{x | x \in (-a, a)\} \tag{1.14}$$

These boundary conditions can be thought of by passing from the basis of q-independent fields to a composite field $\varphi(x,t)$ living on B, obeying twisted boundary conditions. The scaling

dimension of the twist operator is [30]

$$h_q = \bar{h}_q = \frac{c}{24}\left(q - \frac{1}{q}\right). \tag{1.15}$$

The partition function of the theory on B_q can be written down in terms of correlation functions of the twist fields:

$$\mathcal{Z}[B_q] = \prod_{k=0}^{q-1} < \mathcal{T}_q(-a,0)\,\mathcal{T}_q(a,0) >_B \tag{1.16}$$

Considering the twist fields as conformal primaries with scaling dimension given by (1.15), the partition function turns out to be

$$\mathcal{Z}[B_q] = \left(\frac{2a}{\epsilon}\right)^{-\frac{c}{6}\left(q-\frac{1}{q}\right)} \tag{1.17}$$

Here ϵ is the UV regulator. Then we find that the entropy becomes

$$S_A^{(q)} = \frac{c}{6}\left(1 + \frac{1}{q}\right)\log\frac{2a}{\epsilon}. \tag{1.18}$$

It is now trivial to analytically continue from $q \in \mathbb{Z}_+$ to $q \sim 1$ and the entanglement entropy for region A becomes

$$S_A = \frac{c}{3}\log\frac{2a}{\epsilon}. \tag{1.19}$$

This formula 1.19 is for computing entanglement entropy for a subregion A in a flat Minkowski background. We will now write down the formula for computing the single-interval entanglement entropy in a general curved background. The metric in the curved background is related to the flat metric by a Weyl factor:

$$ds^2 = \frac{1}{\Omega(t,x)^2}\left(-dt^2 + dx^2\right). \tag{1.20}$$

The entanglement entropy becomes

$$S(2a) = \frac{c}{6}\log(-(x^+(a) - x^+(-a))(x^-(a) - x^-(-a))) - \frac{c}{6}\log\Omega(a) - \frac{c}{6}\log\Omega(-a). \tag{1.21}$$

The final two terms are extra contributions from the Weyl factor in the metric. So the entropy has two extra pieces in the case of curved background.

1.2.2 Entanglement entropy for disconnected multiple interval in $\mathbf{CFT}_2$

The computation of entanglement entropy for multiple intervals is rather complicated even in 2-dimensional CFT's. Take a disjoint union of m spatial intervals $A = \cup_{i=1}^{m} A_i$. Now, according to the replica method, we need to construct the q-fold $\mathbb{Z}_q$ symmetric branched cover spacetime of the original geometry with $2m$ branching points. For every two copies of the replicated geometry, each pair of regions will now conspire to create a single handle. This suggests that the branched cover spacetime is a higher genus Riemann surface. Therefore, calculating the R´enyi entropy involves computing the CFT's partition function on this Riemann surface (or, alternatively, a suitable correlator of 2mq twist operators).

1.3 Introduction to Holography

The AdS/CFT correspondence is an exact mapping between any theory of quantum gravity in an asymptotically AdS_{d+1} spacetime and an ordinary CFT_d, without gravity. This mapping is called the duality and it is conjectured by Maldacena in 1997 [31]. Since the gravitational theory exists in one more dimension in the bulk as compared to the boundary, it is holographic. Any physical (gauge-invariant) quantity that can be calculated in one theory may also be computed in the dual theory, according to the principle of duality. The field theory can be in any of the states in the Hilbert space, and the AdS/CFT correspondence at a general level asserts that each such state maps to an analogous state in the closed string Hilbert space. The isomorphism between Hilbert spaces is the central feature of the correspondence. However, the mapping between the two theories is highly nontrivial. For instance, simple computations on one side frequently correspond to incalculable, strongly coupled quantities on the other side. Some reviews discussing the correspondence and its evidence are [34, 35, 36, 37, 38, 39].

1.3.1 AdS geometry

The maximum symmetric solution of Einstein's equations with a negative cosmological constant is known as anti-de Sitter space. The AdS_{d+1} spacetime can be defined as a hyperboloid in $\mathbb{R}^{d,2}$, i.e., the hypersurface, with a metric:

$$-X_{-1}^2 - X_0^2 + \sum_{i=1}^{d} X_i^2 = -l_{AdS}^2\,, \qquad ds^2_{\mathbb{R}^{d,2}} = -dX_{-1}^2 - dX_0^2 + \sum_{i=1}^{d} dX_i^2\,. \tag{1.22}$$

For general dimension AdS_{d+1} , the metric in global coordinates is

$$dS^2 = l^2(-\cosh^2\rho dt^2 + d\rho^2 + \sinh^2\rho d\sigma_{d-1}^2) \tag{1.23}$$

To understand the global structure of this spacetime, it is convenient to change the radial coordinate via $\tanh\rho = \sin r$ so that $r \in [0, \frac{\pi}{2})$. Then, the metric becomes

$$dS^2 = \frac{l^2}{\cos^2 r}(-\ dt^2 + dr^2 + \sinh^2 r d\sigma_{d-1}^2) \tag{1.24}$$

which is conformal to a solid cylinder whose boundary at $r = \frac{\pi}{2}$ is $\mathbb{R} \times S^{d-1}$. The conformal boundary of AdS is timelike in contrast to flat space. The metric for the Poincaré patch of AdS_{d+1}, which can be coordinatized as (nb: $\mathbf{x}_{d-1} = \{x_1, x_2, \cdots, x_{d-1}\} \in \mathbb{R}^{d-1}$)

$$ds^2 = \frac{l^2}{z^2}\left(-dt^2 + d\mathbf{x}_{d-1}^2 + dz^2\right). \tag{1.25}$$

In these coordinates, the boundary is at z = 0. These coordinates cover a wedge of the global cylinder.

1.3.2 Conformal Field Theory

A QFT with a certain spacetime symmetry, known as conformal invariance, is called a conformal field theory (CFT). Conformal invariance is a symmetry under local scale transformations. The correlation function of operators in the theory remains well-behaved under coordinate rescalings $x \to \lambda x$ due to conformal symmetry. Correlation functions of quasi-primary operators in CFT obey

$$\langle O_1(x_1)O_2(x_2)\cdots O_n(x_n)\rangle = \lambda^{\Delta_1+\Delta_2+\cdots+\Delta_n}\langle O_1(x_1)\cdots O_n(x_n)\rangle \tag{1.26}$$

where Δ_i is called the scaling dimension of the operator O_i. This scale invariance, along with the rotation and translation invarianc,e implies for 2pt functions

$$\langle O(x)O(y)\rangle \propto \frac{1}{|x-y|^{2\Delta}} \tag{1.27}$$

In a simple example of CFT, the 2pt function of a free massless scalar field in 4d is $(\langle\phi(x)\phi(y)\rangle) \propto \frac{1}{(x-y)^2}$.

1.3.3 AdS/CFT correspondence

Supersymmetric gauge theories, which are realized in the low energy limit of open string theories living on D-brane world volumes in string theory, are the prototypical examples of holographic field theories. One of the examples is the $\mathcal{N} = 4_{4d}$ $SU(N)$ Super Yang-Mills, which is the maximally supersymmetric four-dimensional QFT comprising of $SU(N)$ gauge fields, six adjoint scalars, and adjoint Weyl fermions. This theory is a supersymmetric extension of pure Yang-Mills theory and has an exact conformal invariance for any value of the coupling g_{YM}. There are no dimensionful parameters in the theory (all fields are massless) and the family of such theories can be characterized by two parameters: $\lambda = g_{YM}^2 N$, which is the dimensionless 't Hooft coupling, and a measure of the effective number of degrees of freedom $c_{eff} \propto N^2 - 1$. In the large N limit, which does correspond to the planar gauge theory limit, we obtain the classical master field of this theory in terms of string theory on $AdS_5 \times \mathbf{S}^5$. The strong coupling limit $\lambda \to \infty$ further truncates the dynamics to the two derivative Type IIB supergravity theory on the same background.

We assume that we have a CFT_d which satisfies the criterion for the existence of a holographic map $\lambda, c_{eff} \gg 1$, and consider the class of these which may be studied using classical gravitational dynamics in an asymptotically AdS_{d+1} spacetime, which we therefore call M_{d+1}. Now, in order to continue, a dictionary connecting field theory with gravitational observations is required.

1.3.4 AdS/CFT Dictionary

The duality between a string theory on the AdS bulk and a boundary CFT means that there is a one-to-one correspondence between fields in the bulk and operators in the boundary CFT. The dictionary between these bulk fields and boundary operators was first formulated by Gubser, Klebanov, Polyakov [32] and Witten [33], which states that

$$Z_{CFT}[h_0(x)] = Z_{String}[h(x, r \to 0) = h_0(x)] \ , \tag{1.28}$$

where $x = (t, \vec{x})$ are coordinates in the boundary, r is the bulk radial coordinate, and we choose coordinates such that $r \to 0$ is the boundary of AdS. $h(x, r)$ denotes a generic bulk field *e.g.* scalar field, vector field or bulk metric and $h_0(x)$ is the boundary value of the bulk field $h(x, r)$, which acts as the source for the dual operator in boundary CFT. $Z_{CFT}[h_0(x)]$ is the generating functional for correlation functions of operators $\mathcal{O}(x)$ in the boundary CFT given by

$$Z_{CFT}[h_0(x)] = \left\langle e^{i \int d^d x \, h_0(x) \, \mathcal{O}(x)} \right\rangle \ . \tag{1.29}$$

$Z_{String}[h(x, r \to 0) = h_0(x)]$ is the string partition function evaluated at the boundary of the AdS bulk. In the large N, large λ limit, where the classical supergravity description is valid, the string partition function is dominated by the classical supergravity action,

$$Z_{String}[h(x, r \to 0)] \approx e^{-S_{cl}[h(x,r\to 0)=h_0(x)]} \ . \tag{1.30}$$

Then, using the relation (1.28), we can compute the correlation functions of boundary operators from the bulk partition function as

$$\langle \mathcal{O}(x_1) \cdots \mathcal{O}(x_n) \rangle = \frac{\delta^n}{\delta h_0(x_1) \cdots \delta h_0(x_n)} e^{-S_{cl}[h(x,r\to 0)=h_0(x)]}\Big|_{h_0=0} \ . \tag{1.31}$$

1.4 Holographic entanglement entropy

In the previous section, we discussed a dictionary between the field theory states and asymptotically AdS geometries. Here, we want to compute the entanglement entropy in d-dimensional CFT via AdS/CFT correspondence. This can be computed as a geometric quantity in AdS, just like the thermal entropy in CFT, which is found from the area formula of AdS black hole entropy. In [14, 15], Ryu and Takayanagi (RT) first addressed this issue and provided a prescription for static time-independent scenarios. Hubeny, Rangamani, and Takayanagi (HRT) further expanded this prescription to include arbitrary time dependence and other general states in [16].

Motivation: We wish to determine the entanglement entropy of a certain spatial region A in a holographic CFT_d on a boundary geometry B_d. To compute entanglement entropy S_A for A, we need to smear out the rest of the region A_c. In the smearing-out process, the loss of information is measured by the quantity S_A. In the higher dimensional AdS spaces, this loss of information happens by hiding a part of bulk space inside a minimal surface γ_A. This surface covers the smeared region A_c from inside the bulk AdS space. The boundary of γ_A i.e. ∂A is the holographic screen for the hidden part in the bulk. A minimal surface implies the maximum amount of loss of information, which gives the entropy bound. These considerations lead to area law to compute the entanglement entropy.

General proposal: To calculate the entanglement entropy at some particular instant of time, we will assume that this area lies on some Cauchy slice $\Sigma \subset B_d$. Keep in mind that the entangling surface is ∂A and $\Sigma = A \cup A_c$ as usual.

Firstly, one needs to find a surface γ_A which is a codimension-2 *extremal* surface in the bulk spacetime M_{d+1} anchored on ∂A. The extremal surface γ_A is a local extremum of the area functional and is subject to the boundary conditions that $\gamma_A\big|_B = \partial A$. Since there may be more than one such surface, we must only take into account those that meet a homology constraint. This constraint demands that there should exist a spacelike, bulk codimension 1, smooth interpolating surface $R_A \subset M_{d+1}$ which is bounded by the extremal surface γ_A and the region A on the boundary. Finally, we should choose the extremal surface with the lowest area out of the entire family of extremal surfaces that satisfy the homology requirement. The holographic entanglement entropy is then given by the area of this surface in Planck units in an analogy with the black hole entropy formula of Bekenstein and Hawking.

$$S_A = \min_X \frac{\text{Area}(\gamma_A)}{4\,{G_N}^{d+1}} \tag{1.32}$$

This is famously known as the Ryu-Takayanagi (RT) proposal to compute the holographic entanglement entropy. The Hubeny-Rangamani-Takayanagi (HRT) prescription is a further generalization of the RT proposal in a time-dependent background. While the RT proposal was suitably covariantized by the HRT prescription of upgrading minimal surfaces to extremal surfaces.

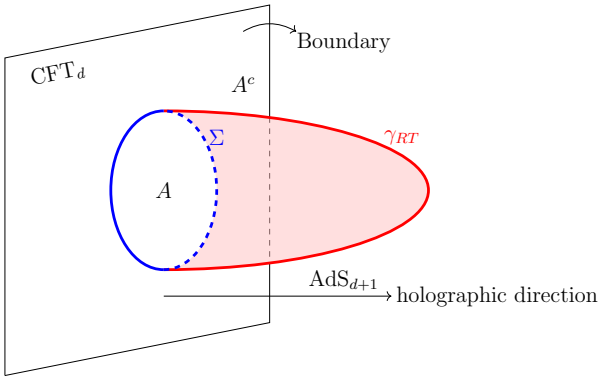

Figure 1.2: Pictorial representation of an RT surface in AdS_{d+1} for a subregion A of boundary CFT_d.

Aron Wall [40] came up with a reformulation of the HRT proposal in terms of a maximin construction, which provides a nice complementary perspective. Given a boundary region A, we pick a bulk Cauchy slice Σ_t such that $\partial\Sigma_t = A \cup A^c = \Sigma$. On this slice, we find a minimal surface γ. One then varies the choice of the bulk Cauchy slice, finding minimal surfaces on the entire family. We can imagine this construction by filling out the FRW wedge (a region in the bulk spacetime and each point on it remains spacelike separated from Σ) of Σ with Cauchy slices containing (spacetime codimension-2) minimal surfaces drawn on them. One is instructed to compute the area of the minimal surface on each slice and take the one from

this (infinite) family with the maximum area. This is the *maximin surface*.

$$\gamma^{A}_{\text{maximin}} = \gamma_* \in \{\gamma \subset \Sigma_t \text{ is minimal}\} \;\; \& \;\; \text{Area}\, \gamma \;\; \text{is maximal} \tag{1.33}$$

1.5 Thermal aspects of black hole

1.5.1 Black hole Thermodynamics

In classical general relativity, black holes have neither a temperature nor significant entropy. Bekenstein first introduced the concept of black hole entropy as a measure of the information about the black hole interior to an outside observer [41]. This paper sets the basis of the thermodynamic approach to black hole physics. In 1970s [42], [2] Hawking showed that when the classical gravitational field of a black hole is coupled with quantum fields like photons, a black hole can be considered as a thermodynamic object. Hawking also showed that the spectrum of particles that a black hole produces can be considered as black body radiation at a certain temperature, called the Hawking temperature, which is related to the Schwarzschild radius of the black hole via,

$$K_B T_H = \hbar \frac{c}{r_S} \frac{1}{4\pi} \; . \tag{1.34}$$

This gives evidence that a black hole can be viewed as an ordinary hot object from the outside. Further, it has been shown [43] that the black hole obeys versions of the laws of Thermodynamics.

A black hole responds dynamically when an object is dropped into it. After a brief ripple, the event horizon swiftly settles to a new equilibrium at a larger radius. In the 1970s it was noticed for the first time that the resulting small changes in the black hole geometry are constrained by equations similar to the laws of thermodynamics. For a rotating black hole, the equation is [43]

$$\frac{\kappa}{8\pi G_N} d\,(\text{Area}) = dM - \Omega dJ \; , \tag{1.35}$$

where κ is its surface gravity, M is its mass, J is its angular momentum, and Ω is the rotational velocity of the horizon. The above mentioned area refers to the area of the event horizon. If the black hole has temperature $T \propto \kappa$, and entropy $S_{\text{BH}} \propto \text{Area}$, then this looks exactly like the first law of thermodynamics in the form

$$T dS_{\text{BH}} = dM - \Omega dJ \; . \tag{1.36}$$

In addition, the area of the horizon always increases in the classical theory, suggesting a connection to the second law of thermodynamics. This suggests that the total entropy of a black hole has a contribution from the area of its event horizon and a contribution from the quantum fields outside the horizon. Thus, the total or 'generalized' entropy of a black hole is [41]

$$S_{\text{gen}} = \frac{\text{Area of horizon}}{4\hbar G_N} + S_{\text{outside}} \ , \tag{1.37}$$

where S_{outside} denotes the entropy of matter as well as gravitons outside the black hole, as it appears in the semiclassical description. The generalized entropy, including the contribution from the quantum fields, is also found to obey the second law of thermodynamics [44],

$$\Delta S_{\text{gen}} \geq 0 \ , \tag{1.38}$$

giving further evidence of being really an entropy. This result is stronger than the classical area theorem because it also covers phenomena like Hawking radiation. During black hole evaporation, when the Hawking radiation comes out, the area of the event horizon decreases, but the generalized entropy increases due to the entropy of Hawking radiation.

1.5.2 Euclidean black hole

In order to get another perspective on thermal aspects of black holes, we will now explore a bit more on the connection between Euclidean time and thermodynamics.
The metric of a Schwarzschild black hole is

$$ds^2 = -\left(1 - \frac{r_s}{r}\right) dt^2 + \frac{dr^2}{1 - \frac{r_s}{r}} + r^2 d\Omega_2^2 \ . \tag{1.39}$$

The Schwarzschild radius $r_s = 2G_N M$ sets the size of the black hole. In a black hole spacetime, the partition function at inverse temperature β is calculated by a Euclidean path integral in the geometry of a Euclidean black hole. This geometry can be achieved from the Schwarzschild metric 1.39 by doing an analytic continuation of the Lorentzian time t, which is a real time, to the Euclidean time t_E, which is imaginary i.e. by setting $t = it_E$,

$$ds_E^2 = \left(1 - \frac{r_s}{r}\right) dt_E^2 + \frac{dr^2}{1 - \frac{r_s}{r}} + r^2 d\Omega_2^2 \ , \qquad t_E = t_E + \beta \ . \tag{1.40}$$

In this geometry, the radial coordinate is restricted to $r > r_s$ and $r = r_s$ (the horizon) is the origin, which implies that Euclidean black holes do not have an interior. Here is a conical

singularity aries at $r = r_s$ and in order to remove the singularity we need to fix β to

$$\beta = 4\pi r_s \ . \tag{1.41}$$

This geometry is called as 'cigar' as depicted in the fig 1.3.

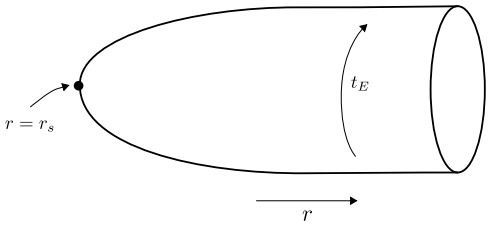

Figure 1.3: The Euclidean Schwarzschild black hole. The Euclidean time and radial directions have the geometry of a cigar, which is smooth at the tip, $r = r_s$. At each point we also have a sphere of radius r.

In this geometry for $r \gg r_s$, there is a Euclidean time circle of circumference β, which is the inverse temperature as seen by an observer far away. As we have mentioned previously, the Euclidean path integral on this geometry is interpreted as the partition function,

$$Z(\beta) = \text{Path integral on the Euclidean black hole} \sim e^{-I_{\text{classical}}} Z_{\text{quantum}} \ . \tag{1.42}$$

It has contributions from both gravity and quantum fields. In the semiclassical limit, the gravitational part comes from the classical saddle solution of the Einstein-Hilbert action and is found by evaluating the on-shell action on the geometry 1.40. The quantum part is obtained by computing the partition function of the quantum fields on this geometry 1.40.
Now if we apply the standard thermodynamic formula to this result,

$$S = (1 - \beta\partial_\beta) \log Z(\beta) \tag{1.43}$$

It will further give us the generalised entropy 1.37.

1.5.3 Evaporating black hole

The Hawking process can be interpreted as pair creation of entangled particles near the horizon, with one particle escaping to infinity and the other falling toward the singularity. Hawking radiation carries energy away to infinity and therefore reduces the mass of the black hole. Eventually, the black hole evaporates away completely. The different stages of the black hole evaporation is the following:

a) After stellar collapse, when the black hole just formed, outside of the black hole is nearly stationary.

b) The Hawking process creates an entangled pair of particles, one trapped behind the horizon and the other escaping to infinity gives rise to the Hawking radiation. The black hole starts to shrink as its mass is carried away by the radiation.

c) Eventually, the black hole interior, i.e. the angular direction, shrinks to size zero. This is singularity.

d) At the end, when the black hole completely evaporates away, there is a smooth spacetime containing only Hawking radiation but no black hole.

The pictorial representation of the different stages of the black hole formation and evaporation is shown in fig 1.4.

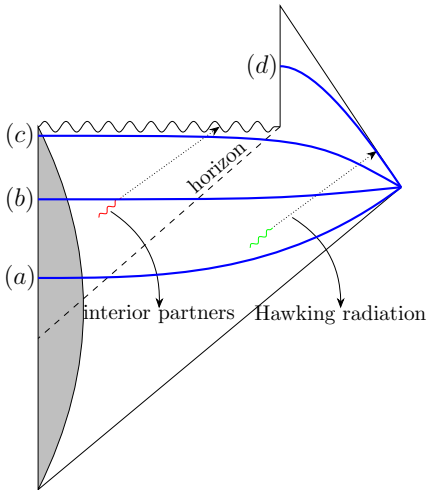

Figure 1.4: Penrose diagram for the formation and evaporation of a black hole. Spatial slices (a)-(d) correspond to the above mentioed different stages of black hole evaporation.

1.6 Black hole as an ordinary quantum system

An object described by a finite, but large, number of degrees of freedom that obey the ordinary laws of physics, which in turn imply the laws of thermodynamics. Thus, the above results we reviewed suggest that the black hole can be regarded as an ordinary system, obeying the laws of thermodynamics. Now, we are going to state an important idea called the 'Central dogma', which is crucial in development of this subject.

> **Central Dogma:** As seen from the outside, a black hole can be described in terms of a quantum system with Area/$4G_N$ degrees of freedom, which evolves unitarily under time evolution.

According this hypothesis, the black hole and the whole spacetime around it can be replaced by a quantum system. This quantum system interacts with the outside via a unitary Hamiltonian.

1.7 Fine-grained and coarse-grained entropy

We have two notions of entropy: a) Fine-grained or von Neumann entropy and b) Coarse-grained entropy. In this section, we will talk about the definitions and basic properties of these two entropies.

a) **Fine-grained entropy/von-Neuman entropy:** Given the density matrix, ρ, describing the quantum state of the system, the von-Neuman entropy of the quantum state is given by

$$S_{vN} = -Tr[\rho \log \rho] \tag{1.44}$$

It quantifies the precise information, which we do not know, about the quantum state. For the pure state, it vanishes, which indicates complete knowledge about the quantum state.
properties:

1. It remains invariant under unitary time evolution $\rho \to U\rho U^{-1}$.
2. Given a quantum system composed of two parts A and B, the full Hilbert space is $H = H_A \times H_B$ and. Then we can define the von Neumann entropy for the subsystem A by first forming a density matrix ρ_A obtained by taking a partial trace over the system B. The entropy of ρ_A can be non-zero, even if the full system is in a pure state. This happens when the original pure state contains some entanglement between the subsystems A and B. In this case $S(A) = S(B)$ and $S(A \cup B) = 0$.

b) **Coarse-grained entropy:** Given some density matrix ρ describing the system, for which we only measure a subset of simple, or coarse-grained observables A_i. Now, we pick all possible density matrices $\tilde{\rho}$ which give the same result as our system for the observables that we are considering, $Tr[\tilde{\rho}A_i] = Tr[\rho A_i]$. Then we compute the von Neumann entropy $S(\tilde{\rho})$. Finally, we maximize this over all possible choices of $\tilde{\rho}$. This will give us the coarse-grained entropy of the system.

Thermodynamic entropy is the simplest example of the coarse-grained entropy. In this case, the observables are often chosen to be the approximate energy and the volume. The thermodynamic entropy is obtained by maximizing the von Neumann entropy among all states with that approximate energy and volume.

1. Coarse-grained entropy increases under unitary time evolution and obeys the second law of thermodynamics.
2. The generalized entropy, defined in 1.37, is the coarse-grained entropy of the black hole.
3. The fine-grained entropy is always less than the coarse-grained entropy, $S_{vN} \leq S_{coarse}$. The reason is simply because S_{coarse} provides a measure of the total number of degrees of freedom available to the system, thus, it sets an upper bound on how much the system can be entangled with something else.

1.7.1 Semiclassical entropy

If we consider a gravity theory with the semiclassical approximation, then basically we have a classical geometry and quantum fields defined on that classical geometry. S_{semi} is the von-Neumann entropy of quantum fields, which appears in 1.37 (including gravitons), and is there on the semiclassical geometry. In other words, this is the fine-grained entropy of the density matrix calculated by the standard replica methods of quantum field theory in curved spacetime.

1.8 Hawking's original paradox

In this section, we will briefly discuss Hawking's Black hole information problem. In the 1970s [42], [2] Hawking showed that the quantum effects are not only crucial near the black hole singularity. The quantum effects near the black hole horizon also cause a decreasing horizon radius and eventually disappear. In the study of the evolution of the von Neumann entropy of black holes or Hawking radiation as a function of time, Hawking considered a semi-classical approximation of the gravity theory. In his analysis, the gravitational field of a black hole is treated classically, while the matter fields, like the photon and neutrino fields, are considered quantum mechanically. Before the black hole starts to evaporate, the matter fields in a quantum field theory remain in a vacuum state, which is also an entangled state. Once the black hole starts to evaporate, the vacuum state splits into two parts across the horizon, and one part ends up in the black hole interior, and the other part ends up in the exterior. This is how a black hole produces particles due to the quantum effects near the black hole horizon. The exterior part, which comes from the splitting of a vacuum state across the horizon, gives rise to the Hawking radiation.

Consider a black hole formed from the collapse of a matter, which was in a pure state. Once the black hole forms completely, it emits a thermal gas of particles due to the quantum effects discussed previously. Due to evaporation, the horizon radius gradually decreases, and the interior of the black hole eventually disappears. In the final stage of the evaporation, only the gas of particles remains at some finite temperature with a non-zero entropy. Now, initially we have considered that the matter, which forms the black hole, was in some pure state with zero entropy. However, a black hole's entire formation and evaporation process creates a final state with non-zero entropy. This entropy quantifies the amount of our ignorance about the precise state of a system. So the non-zero value of entropy at the final state of Hawking radiation implies the fact that during the black hole formation and evaporation process, the information about the black hole's initial state is getting lost. This is famously known as the black hole information loss problem.

The Page Curve

Consider a black hole that forms and starts to evaporate. The thermal aspects of Hawking radiation arise because the entangled pair of particles, which formed the vacuum state in the quantum field theory, are splitting into two parts across the horizon. Due to the presence of the horizon, one of the members of the pair can go to infinity, giving rise to the Hawking radiation, and the other member is trapped in the black hole interior. We will call them the "outgoing Hawking quantum" and the "interior Hawking quantum" respectively. These

two parts together form a pure state. However, if we consider only one member, say the outgoing Hawking quantum, we will find it in a mixed state, that is, a thermal state at the Hawking temperature. Now we will study the evolution of the entropy of Hawking radiation as a function of time and restate Hawking's paradox [1].

Hawking's calculation shows us that the entropy initially grows linearly with time up to a certain value of time, the so-called Page time. The linear growth is due to the entanglement between the Hawking radiation outside the black hole horizon and the black hole interior. During the same time, due to the black hole evaporation, the mass of the black hole evaporates away, and the area of the event horizon reduces, which causes a decrease in the thermodynamic entropy of the black hole. The above-mentioned Page time is the time when the initially growing von Neumann entropy of the Hawking radiation coincides with the decreasing thermodynamic entropy of the black hole. Page time has an important significance in the study of the evolution of the entropy of Hawking radiation, as we will see below.

After the Page time, when almost half of the black hole had evaporated, Hawking predicted that the entropy of Hawking radiation should keep on increasing until the black hole completely evaporated away, and the final state of the Hawking radiation will end up in a mixed state with non-zero entropy. However, according to the quantum unitarity principle, the time evolution of a quantum mechanical system is unitary. This implies the initial pure state of the system should remain pure under time evolution. But the entire process of black hole formation and evaporation seems to turn pure states into mixed states.

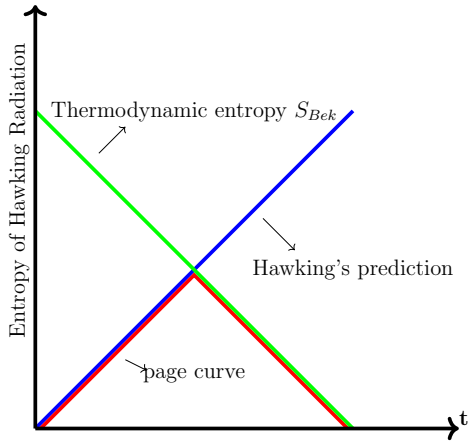

Figure 1.5: Pictorial representation of the evolution of entanglement entropy of Hawking radiation

From the idea of the Page curve-like evolution shown by Don Page in [5], it has been predicted that the entropy of Hawking radiation after Page time should start to decrease. Thus, the evolution of the entropy of Hawking radiation should follow the Page curve, and at the final

stage of the evaporation, the entropy should go to zero. This further implies the fact that the final state of the Hawking radiation will again be a pure state.

1.9 Resolution of black hole information paradox

1.9.1 Generic 2-dimensional dilaton gravity theory

The action for a generic 2d dilaton gravity theory is given by

$$I_{\text{grav}}[g_{ij}^{(2)}, \phi] = \int d^2y\sqrt{-g}\left(\frac{1}{16\pi G_N^{(2)}}\phi R^{(2)} + U(\phi)\right), \tag{1.45}$$

The Einstein-Hilbert term in action is purely topological, and extra dilaton ϕ gives non-trivial dynamics to the theory. $U(\phi)$ is called the dilaton potential, which becomes linearly dependent on ϕ in the case of JT gravity [45]-[51]. Now, if a matter CFT_2 consists of fields χ is added to the theory, the action becomes

$$I[g_{ij}^{(2)}, \phi, \chi] = I_{\text{grav}}[g_{ij}^{(2)}, \phi] + I_{\text{CFT}}[g_{ij}^{(2)}, \chi]\,. \tag{1.46}$$

To take the semi-classical limit in the 2d dilaton gravity theory, we need to consider the central charge of the matter CFT_2 to lie within $1 \ll c \ll \frac{\phi}{4G_N^{(2)}}$. This implies that the presence of the matter fields does not create any back reaction in the classical geometry, and the geometry thus does not change in the presence of any quantum fields.

1.9.2 Two-dimensional black hole coupled to heat bath

Now we consider an evaporating black hole in the two-dimensional gravity theory and couple it to a bath, where the Hawking radiation is being collected. As we mentioned previously, the gravity is coupled to a matter CFT_2, and the same CFT_2 is considered to be present in the bath. The bath is in a fixed non-gravitational spacetime. Here in our case, the 2d gravity theory has AdS_2 geometry, and the matter CFT_2 lives in it with a conformal boundary condition at the asymptotic AdS_2 boundary. This gravity theory coupled to matter CFT_2 and the CFT_2 living in the non-gravitational bath are joined along the boundary of both the spacetime, allowing them to freely exchange energy. The entire set-up has 2 different pictures:

- 2d Gravity: One side has 2d gravity coupled to a matter CFT_2 and the other side has the same CFT_2.

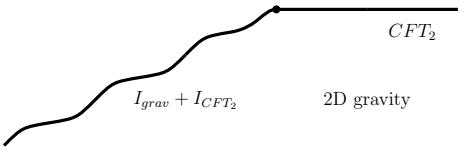

Figure 1.6: The 2d dilaton gravity theory plus matter CFT_2 on the left side, coupled with a bath containing the same matter CFT_2 on the right side.

- Quantum mechanical system: Nearly AdS_2 gravity with a black hole is replaced by a holographic one-dimensional non-gravitational quantum mechanical system on the boundary. It is coupled to the CFT_2 living in the non-gravitational bath.

Figure 1.7: The dual holographic quantum mechanical system is coupled with the bath CFT_2.

1.9.3 von Neumann entropy of the boundary QM system

Now, we will discuss the gravitational formula for the von Neumann or fine-grained entropy of a quantum mechanical theory, which is dual to 2d gravity theory. Considering the entire boundary quantum theory in a particular state, we want to compute the entropy of some boundary subregion A. We need to first consider a candidate co-dimension one region y, which is homologous to A, in the bulk geometry. The bulk geometry of this co-dimension one region is dual to the state of the boundary theory. Then, we define a Generalized entropy-like quantity

$$S_{\text{gen}}(y) = \frac{\phi(y)}{4G_N^{(2)}} + S_{\text{Bulk-}2d}[\mathcal{I}_y]\,. \tag{1.47}$$

Where $\mathcal{I}_y$ is the interval between y and the boundary. $S_{\text{Bulk-}2d}[\mathcal{I}_y]$ is the bulk von-Neumann entropy, which has contribution only from the bulk matter field χ present in the interval $\mathcal{I}_y$. This entropy has been computed ignoring the quantum fluctuation of ϕ, $g_{ij}^{(2)}$.

The entropy of region A will be the value of S_{gen} evaluated on the region y_* which minimizes the generalized entropy. So our goal is to look for an extremal surface by first extremizing $S_{\text{gen}}(y)$ with respect to y. Now, there could be more than one extremal surface, thus we need to find the global minimum of all extremum

$$S = \min_y \left\{ \text{ext}_y \left[\frac{\phi(y)}{4G_N^{(2)}} + S_{\text{Bulk-}2d}[\mathcal{I}_y] \right] \right\}\,, \tag{1.48}$$

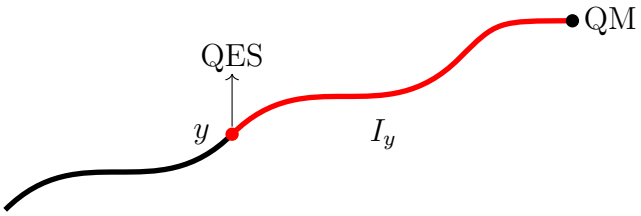

Figure 1.8: QES for the dual quantum mechanical system.

The surface that extremizes 1.48 is called the 'quantum extremal surface'. This will finally give us the true fine-grained entropy of the quantum mechanical system.

1.9.4 Entanglement entropy and entanglement wedge of an evaporating black hole and Hawking radiation

We consider a 2-dimensional gravity theory with a one-sided evaporating black hole in a nearly AdS_2 background, and it is attached to a non-gravitational bath, where the Hawking radiation is being collected.

To preserve global unitarity, the late-time Hawking radiation must be entangled with early Hawking radiation, and as we have seen previously, the black hole interior modes are also maximally entangled with the late Hawking radiation across a smooth horizon. However, this violates the principle of 'monogamy of entanglement', which states that a single quantum system cannot be entangled with two other systems at the same time. To resolve this paradox, this paper [4] suggests that at or before the page time, a "Firewall" or region of very high energy density should be created at the place of the smooth horizon due to the breaking of the entanglement between the interior mode and late-time Hawking radiation. It is known as the AMPS firewall paradox, and the same inconsistency has been pointed out earlier by Samir Mathur in the context of the fuzzball proposal [52].

In [53], it has been shown that the firewall paradox can be resolved by the "ER=EPR" proposal in the case of entangled black holes. The resolution is that the black hole interior mode is encoded in the early Hawking radiation. This implies that the late-time Hawking radiation is entangled with both the interior mode and the early Hawking radiation. In [54], Almheiri used the idea of entanglement wedge reconstruction to show how the ER=EPR proposal continues to resolve the firewall paradox for a two-sided black hole. In 2019 [7], Penington has shown that the firewall paradox for a one-sided evaporating black hole can be resolved in exactly the same way.

At the early stages of the black hole evaporation, just after the black hole forms and before the Hawking radiation starts to escape, there is no bath. Now, we want to compute the von Neumann entropy of a black hole. In this case, the extremal surface, called as vanishing extremal surface, turns out to cover the entire closed universe on the gravity side. Thus, in the generalized entropy 1.47, the area term becomes zero and only contribution comes from the bulk von-Neumann entropy $S_{\text{Bulk-}2d}[\mathcal{I}_y]$. Since the black hole forms from the collapse of the matter, which was in a pure state, the $S_{\text{Bulk-}2d}[\mathcal{I}_y]$ becomes zero. So overall, at the early stage, the fine-grained entropy of the black hole is zero.

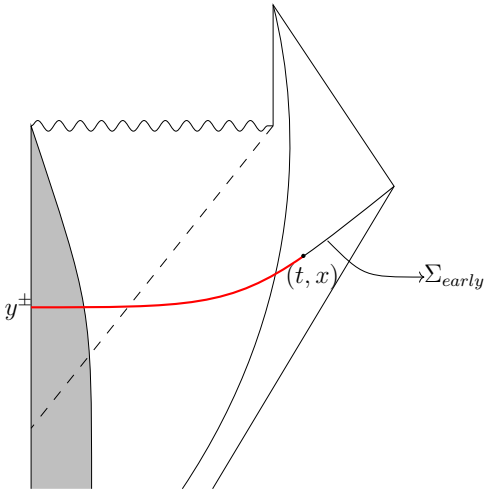

Figure 1.9: Penrose diagram for an evaporating black hole. At some early time slice (y^+, y^-) is the QES from the 2d point of view.

When the black hole starts to evaporate, then there is a bath. As black hole evaporation starts, the entangled pair of particles breaks across the horizon. The ingoing Hawking quanta go to the black hole interior, and the outgoing Hawking quanta give rise to the Hawking radiation. Thus initially, the von Neumann entropy of the black hole and the Hawking radiation start to grow monotonically.

1.9.5 Entanglement entropy of the black hole at late times

We replace the 2-dimensional gravity theory with the evaporating black hole by its dual quantum mechanical system at the boundary. This dual quantum mechanical system is now coupled with the non-gravitational CFT_2 on the bath side. Consider a late time slice Σ_{late} on the spacetime geometry of the evaporating black hole and take an interval $[0, x]$, which consists of the quantum mechanical degrees of freedom. We want to compute the von Neumann entropy of this interval, and it will give us the entropy of the black hole at late time t. At the later stage of the black hole evaporation, a non-vanishing extremal surface, which does not

cover the entire space beyond the black hole horizon, appears. S_{gen} for this surface has an area term as well as the bulk entropy term. In these papers [7], [8], it has been shown that after extremizing the generalized entropy 1.47, the quantum extremal surface (y^+, y^-) turns out to be just beyond the black hole horizon.

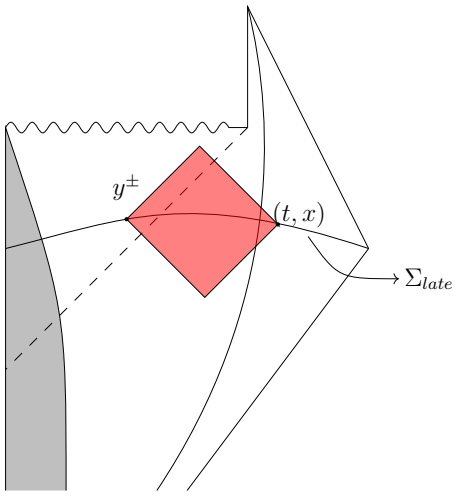

Figure 1.10: On a late time slice the extremal surface at (y^+, y^-) gives the entropy of the black hole and the red diamond is the entanglement wedge associated with that QES.

The entanglement wedge is the causal domain of the spacelike slice in between (t, x) and (y^+, y^-), as shown in Fig 1.10. The black hole entropy becomes

$$S_{BH}(t) = S_{Bek}(T(t)) + \cdots \tag{1.49}$$

Here T is the temperature of the black hole at time t. The leading contribution comes from the thermodynamic entropy of the black hole. As the black hole evaporates, the area of the horizon decreases, which leads to a decrease in thermodynamic entropy. Thus at late times, the black hole entropy decreases, and the evolution of von Neumann entropy of an evaporating black hole follows the Page curve, indicative of unitary black hole evaporation.

1.9.6 Entanglement entropy of Hawking radiation at late times

In our case, the Hawking radiation is being collected in the non-gravitational bath consisting of CFT_2. Now, we want to compute the von Neumann entropy of some state in the bath CFT_2. This will be the entropy of an interval in bath CFT_2 on the same late time slice Σ_{late} considered in the previous section. Now, we trace out the rest of the interval and compute the entropy in the usual way. It will reproduce Hawking's original answer, which says that the entropy of the Hawking radiation continues to grow after Page time. This is a violation of the principle of unitarity in black hole evaporation, and the information about the black

hole interior is getting lost during the evaporation. This is famously known as the black hole information problem, as we have discussed in the previous section. Recently, exciting works have been done in this line to show that this information problem is a paradox [7], [8]. In the next subsection, we discuss this in detail.

1.9.7 Gravitational von-Neumann entropy: Island formula

The state in bath CFT_2 is prepared by collecting Hawking radiation from an evaporating black hole using gravity theory. So basically, the state in the bath CFT_2 is entangled with some other system that lives in a gravitational theory. We need to define a new rule to compute entropy in effective theories involving gravity. The previous computation of the entropy of Hawking radiation [1] shows some wrong results, since it does not include the black hole interior region. Holographic computation suggests including the black hole interior region. Thus, the full system is now outgoing Hawking radiation plus the black hole interior.

To compute the entropy, we apply the RT/HRT prescription and include all possible **island** regions living in the interior of the black hole to extremize the entropy. Including an island causes an extra term, the island's boundary area in the entropy computation. In some cases, if the boundary quantum system is entangled with the fields living in the closed universe, for example, a completely evaporated black hole or before the Hawking radiation starts to come out, in that case, island regions cover the entire internal space. Then the area term in the generalized entropy becomes zero.

Now we will define the prescription to compute the entropy of a region A in the bath CFT_2 coupled to some system in gravity theory.

$$S(A) = \underset{Z}{\text{Min}}\, \underset{Z}{\text{Ext}} \left[\frac{S_{\text{eff}}(A \cup Z) + \text{Area}[\partial Z]}{4G_N} \right] \tag{1.50}$$

This new rule states that we need to extremize a generalized entropy-like functional over all possible islands Z, and this is done by minimizing over all possible extrema of the generalized entropy. S_{eff} is the entropy of a state in semi-classical gravity and the area term is the area of the island boundary. This new rule computes the gravitational fine-grained entropy of a semi-classical gravity state. This is the generalization of the previously defined prescription 1.48, which computes the fine-grained entropy of a quantum mechanical system without being entangled with some gravitational system. Here, Z is called the quantum extremal island. The fine-grained entropy of Hawking radiation computed using this new rule 1.50, called the **Island** formula, turns out to follow the Page curve, shown in red in Fig 1.12. This island contains the black hole interior modes, which are in the entanglement wedge of Hawking

radiation and are encoded in the Hawking radiation present in the reservoir. This is how the resolution of the firewall paradox can be achieved for a one-sided evaporating black hole.

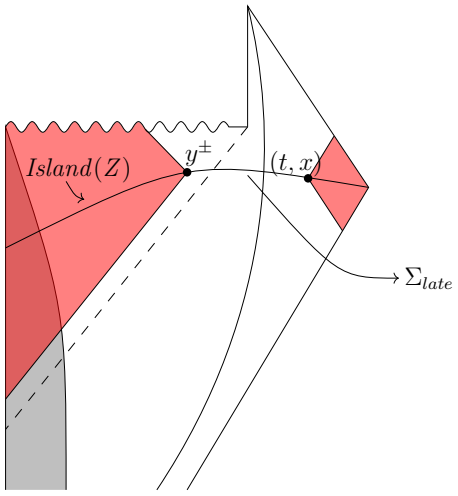

Figure 1.11: On the late time slice, the QES (y^+, y^-), which gives the entropy of Hawking radiation, remains the same as the black hole. The entanglement wedge for the Hawking radiation is the entire red diamond. One part of it is in the black hole interior, and the other part is in the bath.

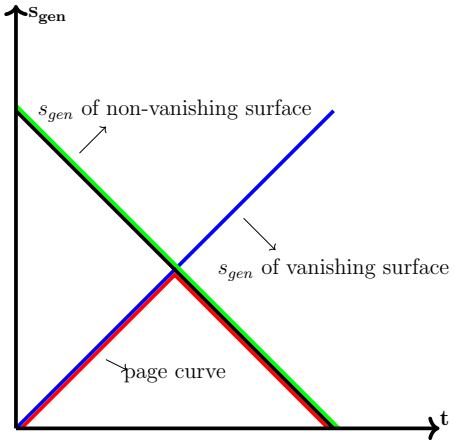

Figure 1.12: The Fig. shows a summary of the evolution of generalized entropy for different extremal surfaces.

For a complete and exact quantum state, we need to use $S(A) = -\mathrm{Tr}(\rho_A \log \rho_A)$ to compute the entropy of an exact state in a quantum field theory. If we prepare a state in quantum field theory using gravity theory, then we need to use this gravitational fine-grained entropy formula 1.50. One important point to keep in mind is that the gravity theory here is considered to be an effective field theory. RT/HRT prescription plays a special role here in the sense that, using this, we can compute the fine-grained entropy from the effective gravity theory. This entire prescription gives a hint towards the fact that there might be an exact description of gravity theory, where the entropy computation 1.50 is exact.

Although this entire prescription cannot tell us anything about the microstate of the system, i.e. the individual matrix element of the density matrix, which represents the state in the effective gravity theory. This description somehow knows the correct entropy of Hawking radiation. This is a surprising fact about the effective theory that, without knowing the microscopic details of the theory, one can compute the fine-grained entropy of its semiclassical gravity state.

In the case of holographic matter, the quantum extremal surface prescription reduces to this new rule. It also holds for matters containing general fields.

1.10 A simple example of the resolution of information paradox

In this section, we will discuss an example of the formulation of the information paradox and its resolution for a two-sided eternal black hole.

1.10.1 The setup

Let us consider a two-sided eternal black hole in AdS geometry. This geometry describes the thermofield double state of the boundary CFT at an inverse temperature β.

$$|\Psi_\beta^{\text{TFD}}\rangle = \frac{1}{\sqrt{Z(\beta)}} \sum_i e^{-\frac{\beta E_i}{2}} |E_i\rangle |E_i\rangle \,. \tag{1.51}$$

This black hole is stable and does not evaporate. But we can model the evaporation as follows:

The two-sided black hole can be replaced by a dual quantum mechanical system, as we have seen in the previous section. We coupled the left and right boundary quantum mechanical systems A_1 and A_2 with two heat baths B_1 and B_2, respectively. This entire combined system is defined by a left-right thermofield double state. Given the initial state and Hamiltonian, we evolve the combined system with time in the forward direction by the time evolution operator e^{-iHt}, where H is the total Hamiltonian of the combined system. Here we want to compute the time evolution of the entropy of $B_1 \cup B_2$, as a function of time.

The combined system $A_1B_1A_2B_2$ is in a pure state. So the entropy of $B_1 \cup B_2$ must be equal to $A_1 \cup A_2$ at any instant of time. In early times, the entropy of $B_1 \cup B_2$ increases linearly with time. But we will run into trouble if it increases indefinitely forever. The reason is the following:

The entropy of $A_1 \cup A_2$ has an upper bound $2S(\beta)$, where $S(\beta)$ = entropy of the thermal density matrix of one of the quantum systems A_1 or A_2. Thus, the entropy of $B_1 \cup B_2$ must have this upper bound, and it cannot increase linearly forever. When the entropy reaches its upper bound, at that time a phase transition happens, and the entropy curve becomes flat.

Gravity description of the above setup Gravitationally, $A_1 \cup A_2$ is the holographic dual to a two-sided eternal black hole in AdS geometry, and it is coupled to a flat space region with no gravity along the two AdS boundaries. Now, we evolve the combined system with time in the forward direction. During the evolution, we let the quantum fields from the black hole side leak into the flat space region without reflecting back in. This flat space region is considered as the heat bath in the setup, and the quantum fields, which leak into the bath, are considered to be the Hawking radiation. This leaking of quantum fields leads to the continuous loss of energy from the black hole, and it will start to shrink. The entropy of $B_1 \cup B_2$ is the entropy of Hawking radiation in our context.

The entropy of a two-sided eternal black hole has an upper bound $2S_{Bek}$, where S_{Bek} is the Bekenstein-Hawking entropy of the black hole. As we have seen, the entropy of the black hole and the Hawking radiation are equal at any instant in time. Thus, the entropy of Hawking radiation must also saturate at this upper bound. The Information paradox in the evolution of the entropy of Hawking radiation arises in our context since the semi-classical gravity predicts that the entropy of Hawking radiation increases linearly with time forever. In gravity, the Quantum extremal surface prescription with an allowed disconnected entanglement wedge reproduces the Page curve. These are also the replica wormhole solution of the Euclidean path integral computation of the entropy.

1.10.2 JT gravity

We will perform the computation of the entropy of Hawking radiation in JT gravity. This is a 2-dimensional dilaton gravity theory, and it is dual to a quantum mechanical system of Majorana fermions, known as the SYK model. In this subsection, we will discuss JT gravity briefly. The Euclidean action for the theory is given by

$$\begin{aligned} 16\pi G\, I_{\text{Euc}} = 16\pi G\,(I_0 + I_G) = &- \phi_0 \left(\int d^2x\, \sqrt{g}\, R + \int dx\, \sqrt{\gamma}\, 2K \right) \\ &- \left(\int d^2x\, \sqrt{g}\, \phi(R+2) + \int dx\, \sqrt{\gamma}\, 2\phi\,(K-1) \right). \end{aligned} \tag{1.52}$$

This gravitational action is dimensionally reduced from the higher-dimensional theory, and it describes the S-wave sector of the near-horizon limit of a near-extremal black hole. The action

I_0 is a purely topological term, and ϕ_0 gives the entropy of a black hole at zero temperature. The quantity $\phi_0 + \phi$ is the total dilaton, and it is also the transverse space area of a near extremal higher-dimensional black hole. Since ϕ is dynamical, the gravitational dynamics is governed by the action I_G. The theory has a specific set of boundary conditions for bulk fields. These are

$$g_{tt}\big|_{\text{bdry}} = \frac{1}{\epsilon^2}, \quad \phi\big|_{\text{bdry}} = \frac{\phi_{const}}{\epsilon}\,. \tag{1.53}$$

By varying the action 1.52 with respect to g_{ij} and ϕ, we obtain a set of equation of motion

$$R + 2 = 0\,, \tag{1.54}$$

$$\left(\nabla_k \nabla^k \phi\right)\, g_{ij} - \nabla_i \nabla_j \phi - \phi\, g_{ij} = 0\,. \tag{1.55}$$

and solving these equations of motion will finally give us the black hole solution in the AdS background. We will now couple this gravity theory to matter CFT_2 with central charge c. This matter CFT_2 is taken to be the Hawking radiation in our context.

1.10.3 Black hole solution

Solving the equations of motion 1.55, we will get a solution of the black hole at some non-zero inverse temperature β. The solution for the dilaton ϕ and the background spacetime for a two-sided eternal black hole in AdS is given by

$$ds^2 = \frac{1}{(\sinh r)^2}\left(dr^2 - dt^2\right) = -\left(\frac{\beta}{2\pi}\,\sinh\frac{\pi}{\beta}(r^+ - r^-)\right)^{-2} dr^+\, dr^-\,, \tag{1.56}$$

$$\Omega = \frac{\beta}{2\pi}\,\sinh\frac{2\pi(-r)}{\beta}\,, \quad r \in (-\infty, 0)\,, \tag{1.57}$$

$$\phi(r) = \phi_{const}\,\frac{2\pi}{\beta}\,\coth\frac{2\pi(-r)}{\beta}\,. \tag{1.58}$$

Here, we define $r^{\pm} = t \pm r$. The black hole entropy becomes

$$S_{\text{BH}}(\beta) = \phi_0 + \phi_r\,\frac{2\pi}{\beta}\,. \tag{1.59}$$

Now, we will couple baths/reservoirs on both sides of the two-sided eternal black hole, as mentioned previously. Here we want to compute the entropy of the radiation region $S'X' \cup SX$ shown in Fig. 1.13.

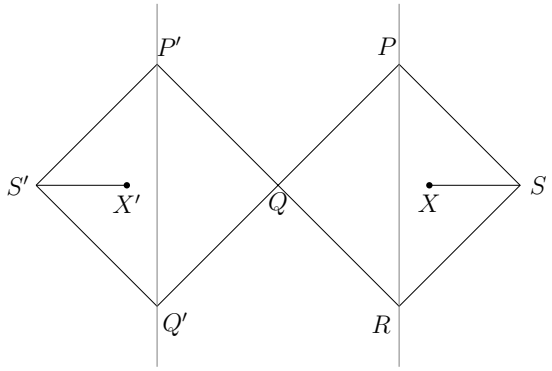

Figure 1.13: We have a two-sided eternal black hole in AdS background and it is coupled with two heat baths along the AdS boundaries. SX and $S'X'$ are the two radiation regions in the heat baths. we want to compute the entropy of these two radiation regions.

1.10.4 Entanglement entropy without island

In this subsection, as shown in the figure, we will compute the entropy of the radiation region $SX \cup S'X'$. Since the combined system is in some pure state at a constant time slice, we just need to compute the entropy of the complementary interval on the same time slice XX'. Here we will directly use the formula 1.21 to compute the entropy of the 2d matter CFT_2 for the interval $XX' = [b_+, b_-]$.

Let us first define a new set of coordinates: $U = e^{t+r}$ and $V = -e^{-t+r}$ for each point.

For point $X(b_+ : (t, r) = (t_b, b))$ the coordinates become

$$b_+ : \quad U_S = e^{t_b+b} \qquad V_S = -e^{-t_b+b} \tag{1.60}$$

For the point X', both of the coordinates $(U_S{}', V_S{}')$ related to the coordinates (U_S, V_S) at X by reflection. Thus the coordinates at $X'(b_- : (t, r) = (t_b, -b))$ are

$$b_- : \quad U_S{}' = -e^{-t_b+b} \qquad V_S{}' = e^{t_b+b} \tag{1.61}$$

The metric becomes

$$dS^2 = -\frac{dU_S dV_S}{\Omega^2} \quad ; \quad \Omega = (-U_S V_S)^{\frac{1}{2}} \tag{1.62}$$

For both the points X and X', the weyl factor remains the same, i.e. $\Omega = (-U_S V_S)^{\frac{1}{2}} = e^b$. The matter entropy 1.21 becomes

$$S_{\text{rad}}(t) = 2 \cdot \frac{c}{6} \log(e^b \cdot 2 \cosh t_b) - \frac{c}{6} \log e^b - \frac{c}{6} \log e^b \tag{1.63}$$

$$= \frac{c}{3} \log(2 \cosh t_b) \approx \frac{c}{3} \frac{2\pi t_b}{\beta}, \tag{1.64}$$

The final expression comes after restoring $\beta = 2\pi$, in the limit $t \gg \beta$. This result shows that the entropy of Hawking radiation increases linearly with time. Now, since the combined system is in a pure state, the entropy of Hawking radiation should have an upper bound, which is the thermodynamic entropy of the two-sided eternal black hole. Therefore, this linear increase of $S_{\rm rad}(t)$ will lead to an information paradox. Including an island-like region, which is the black hole interior, in the entanglement wedge of Hawking radiation will finally resolve the paradox.

1.10.5 Entanglement entropy with island

In this section, we will compute the entanglement entropy of the radiation region while including the black hole interior region in the entanglement wedge of the Hawking radiation. Here we consider some candidate quantum extremal surfaces Y and Y' for the radiation regions SX and $S'X'$ respectively and compute the generalized entropy functional for a region consisting of two intervals $XY = [b_+, a_+]$ and $X'Y' = [b_-, a_-]$. The entropy for these two intervals is identical to each other. Thus, the total entropy will be the sum of these two.

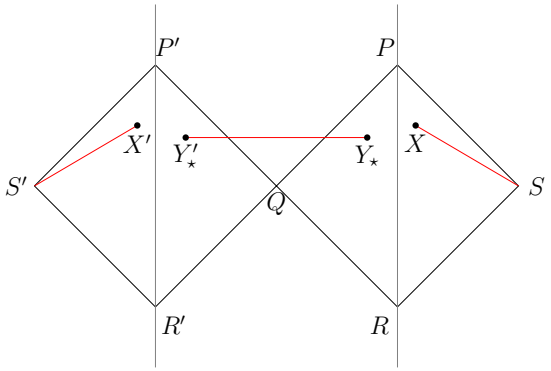

Figure 1.14: We consider some disconnected region, called the island, in the entanglement wedge of the radiation region at later times. The entropy for this radiation plus island region is computed using the island formula, as discussed in Sec. 1.9.7, and it saturates at some upper bound.

Similarly, the new set of coordinates for the point $Y(a_+ : (t, r) = (t_a, -a))$ are

$$a_+ : \qquad U_D = e^{t_a - a} \qquad V_D = -e^{-t_a - a} \tag{1.65}$$

and the coordinates at $Y'(a_- : (t, r) = (t_a, a))$ are

$$a_- : \qquad {U_D}' = -e^{-t_a - a} \qquad {V_D}' = e^{t_a - a} \tag{1.66}$$

We consider the combined system on an equal time slice, i.e. $t_a = t_b$. Thus, the matter entropy for the interval XY is given by

$$\begin{aligned} S(XY) &= \frac{c}{6}\log(-(U_S - U_D)(V_S - V_D)) - \frac{c}{6}\log\Omega(X) - \frac{c}{6}\log\Omega(Y) \\ &= 2\times\frac{c}{6}\log(e^b - e^{-a}) - \frac{c}{6}\log(e^{-a}) - \frac{c}{6}\log(e^b) \\ &= \frac{c}{3}\log\left(2\sinh\frac{b+a}{2}\right). \end{aligned} \tag{1.67}$$

Finally, the generalized entropy function becomes

$$S_{gen}(a) = \phi_{const}\frac{2\pi}{\beta}\coth\frac{2\pi a}{\beta} + \frac{c}{3}\log\left(\frac{\beta}{\pi}\sinh\frac{\pi}{\beta}(b+a)\right) - \frac{c}{6}\log\left(\frac{\beta}{2\pi}\sinh\frac{2\pi a}{\beta}\right). \tag{1.68}$$

The first term is the dilaton term that comes from 1.58, and the third term comes from 1.57.

Similarly, the generalized entropy function for the interval $X'Y'$ becomes the same as 1.68 and the total entropy becomes $S_{rad}(t) = 2S_{gen}(a)$. Now extremizing the total generalized entropy with respect to a, we will get the location of the island boundary.

$$\begin{aligned} &\frac{\partial S_{gen}}{\partial a} = 0 \\ \Rightarrow\ &-\phi_{const}\frac{4\pi^2}{\beta^2}\text{cosech}^2\frac{2\pi a}{\beta} + \frac{c}{3}\frac{\pi}{\beta}\frac{\cosh\frac{\pi}{\beta}(b+a)}{\sinh\frac{\pi}{\beta}(b+a)} - \frac{c}{6}\frac{2\pi}{\beta}\frac{\cosh\frac{2\pi a}{\beta}}{\sinh\frac{2\pi a}{\beta}} = 0 \\ \Rightarrow\ &\phi_{const}\frac{2\pi}{\beta}\frac{1}{\sinh\frac{2\pi a}{\beta}} = \frac{c}{6}\frac{\sinh\frac{\pi}{\beta}(a-b)}{\sinh\frac{\pi}{\beta}(a+b)} \end{aligned} \tag{1.69}$$

solving this equation in the limit $\frac{\phi_r}{\beta} \gg c$, we find that

$$\begin{aligned} \phi_{const}\frac{2\pi}{\beta}2e^{\frac{-2\pi a}{\beta}} &\approx \frac{c}{6}\frac{e^{\frac{\pi}{\beta}(a-b)}}{e^{\frac{\pi}{\beta}(a+b)}} \\ a_\star &\approx \frac{\beta}{2\pi}\log(\phi_{const}\frac{2\pi}{\beta}\frac{12}{c}) + b \end{aligned} \tag{1.70}$$

So the location of the island boundary turns out to be just outside the horizon. Thus at large time, the on-shell entropy value at this extremum becomes

$$S_{rad}(t) \approx 2\phi_{const}\frac{2\pi}{\beta} \tag{1.71}$$

This is equal to the entropy for the two-sided eternal black hole 1.59. Here we have shown how including a disconnected region, which spans the interior of the two-sided eternal black hole, resolves the entropy paradox for a two-sided eternal black hole. The entropy computed

using the island formula shows that the early time linear growth in entropy saturates to an upper bound at later times and it satisfies the general principle of unitary time evolution.

Chapter 2

Timelike QES in Poincare slicing of de Sitter space and FRW universe

In this chapter, we study other cosmological backgrounds, in particular de Sitter space in the Poincaré slicing and FRW universes under certain conditions. This is based on the paper [134]. As we will see (and has been noted previously), the extremal surface structure is rather different in these cases below: in some sense we are simply extending our previous investigations in some formal way to the cosmologies below, with the hope that better understanding will emerge over time.

2.1 de Sitter, Poincare

de Sitter space dS_{d_i+1} in the Poincare slicing and its 2-dim reduction are

$$ds^2 = \frac{R^2}{\tau^2}(-d\tau^2 + dx^2 + dy_i^2) \quad \rightarrow \quad \phi = \frac{R^{d_i}}{(-\tau)^{d_i}}\,, \quad ds^2 = \frac{R^{d_i+1}}{(-\tau)^{d_i+1}}(-d\tau^2 + dx^2)\,. \tag{2.1}$$

We are parametrizing the upper Poincare patch with the future boundary I^+ at $\tau = 0$ and the past horizon at $\tau \to -\infty$, and $-\infty < \tau < 0$ generically so the minus signs are explicitly retained. As τ increases to the future, the dilaton grows. There is a singularity at $\tau \to -\infty$ in the effective 2-dim space: the space is conformally dS_2 (there are some parallels with the discussions of AdS_D reductions in [109]).

In this inflationary patch, we take the observer to be in the ground state, so the bulk entropy is given by the ground state expression. Then the generalized entropy for a bulk observer on

a static worldline at say (x_0, τ_0) is

$$S_{gen} = \frac{\phi_r}{4G}\frac{R^{d_i}}{(-\tau)^{d_i}} + \frac{c}{6}\log\left(\Delta^2\frac{R^{(d_i+1)/2}}{(-\tau)^{(d_i+1)/2}}\right) , \tag{2.2}$$

retaining only terms relevant for extremization. Then extremization gives

$$\frac{c}{3}\frac{\Delta x}{\Delta^2} = 0\,, \qquad -\left(-\frac{d_i\phi_r}{4G}\frac{R^{d_i}}{(-\tau)^{d_i+1}} - \frac{c}{12}\frac{d_i+1}{(-\tau)}\right) - \frac{c}{3}\frac{\tau-\tau_0}{\Delta^2} = 0\ . \tag{2.3}$$

One solution to this is

$$\Delta x = 0\,, \quad \Delta^2 = -(\tau-\tau_0)^2\,; \qquad \frac{d_i\phi_r}{4G}\frac{R^{d_i}}{(-\tau)^{d_i+1}} + \frac{c}{12}\frac{d_i+1}{(-\tau)} + \frac{c}{3}\frac{1}{\tau-\tau_0} = 0\ . \tag{2.4}$$

For a late time observer with $\tau_0 \sim 0$, we have

$$\Delta x = 0\,, \quad \frac{d_i\phi_r}{4G}\frac{R^{d_i}}{(-\tau)^{d_i+1}} + \frac{c}{12}\frac{3-d_i}{\tau} = 0 \quad \to \quad \tau_* = -R\left(\frac{d_i}{3-d_i}\frac{3\phi_r}{Gc}\right)^{1/d_i} \tag{2.5}$$

Note that we are looking for a solution with $\tau < 0$ as per our parametrization: so for $d_i \geq 3$ (*i.e.* dS_5 and higher) the only real QES solution is $\tau \to -\infty$. For $d_i = 1$ this matches the result in [118] ((2.2) matches eq.6.7 there).

Most notably, the above QES solution is timelike-separated from the observer: so $\Delta^2 < 0$ and the generalized entropy (2.2) has an imaginary part from $\log(-1)$. In the spirit of our earlier discussions, it is interesting to look for quantum extremal surfaces that are spacelike-separated from the observer: towards this, note that there is a distinct family of solutions which by construction are spacelike-separated, along the lines of the discussions in the cosmologies earlier with a regulator. Then (2.3) gives

$$\Delta^2 \sim R_c^2\ , \qquad \frac{d_i\phi_r}{4G}\frac{R^{d_i}}{(-\tau)^{d_i+1}} + \frac{c}{12}\frac{d_i+1}{(-\tau)} \sim \frac{c}{3}\frac{\tau-\tau_0}{R_c^2}\ , \tag{2.6}$$

regulating the QES as before with a spatial cutoff R_c. First, note that if we remove the regulator so $R_c \to \infty$, then we obtain (with $t \equiv -\tau > 0$)

$$\frac{d_i\phi_r}{4G}\frac{R^{d_i}}{t^{d_i+1}} + \frac{c}{12}\frac{d_i+1}{t} = 0\ . \tag{2.7}$$

Both terms have the same sign so the only real QES is at $\tau \to -\infty$. This is spacelike separated only if the observer is also localized at sufficiently early times.

With a finite spatial regulator R_c, we see that in general $\tau > \tau_0$, *i.e.* the QES lies on time slices later than the observer. As a first approximation, note that in the classical limit $c \to 0$,

the solution is $\tau \to -\infty$: this is the location where the dilaton is minimized. For early times also, the solution is similar, *i.e.*

$$|\tau_0| \gg R : \qquad \tau \to -\infty \,, \quad \tau \sim \tau_0 \,, \tag{2.8}$$

i.e. the QES is in the far past when the observer is also in the far past. This can be seen to exhibit time-maximization. Let us analyze (2.6) for 4-dim de Sitter upstairs ($d_i = 2$): then

$$\Delta^2 \sim R_c^2 \,, \qquad \frac{\phi_r}{2G}\frac{R^2}{(-\tau)^3} + \frac{c}{12}\frac{3}{(-\tau)} \sim \frac{c}{6}\frac{\tau-\tau_0}{R_c^2} \,. \tag{2.9}$$

With $t \equiv -\tau$, we can rewrite this as

$$\Delta^2 \sim R_c^2 \,, \qquad \frac{6\phi_r}{Gc} R^2 R_c^2 + 3R_c^2 t^2 \sim 2t^3(t_0 - t) \quad \to \quad t^4 - t_0 t^3 + \frac{3R_c^2}{2} t^2 + \frac{3\phi_r}{Gc} R^2 R_c^2 \sim 0 \,. \tag{2.10}$$

Clearly as $t_0 \to 0$, there is no real QES solution since all terms are positive (there appears to be a critical t_0 where the real QES (2.8) stops existing). dS_{d_i+1} can be seen to exhibit similar behaviour.

Overall, in some essential sense, the physical interpretation of the generalized entropy in these cases is not transparent, for instance as holographic entanglement in the dual boundary theory, along the lines of the AdS cases (even from a bulk point of view alone, the timelike separation is unconventional compared with the usual formulations of entanglement on a spatial slice). However our discussion appears to corroborate previous work on classical de Sitter extremal surfaces. Taking the future boundary as a natural anchor in dS, there are either complex extremal surfaces [180, 181, 197] or future-past (timelike) extremal surfaces [182, 136]. The latter future-past surfaces perhaps suggest some new "temporal entanglement" between $I^{\pm}$: taking the area of such surfaces to be real is effectively removing an overall i-factor which would arise from rotating a spatial extremal surface to a timelike one (this is also vindicated by the complex generalized entropy (2.2), (2.4), generalizing [118] for dS_2). Overall perhaps this suggests new interpretations towards entanglement in de Sitter space based on the future boundary and dS/CFT [189, 190, 191]. The dS/CFT dictionary $\Psi_{dS} = Z_{CFT}$ suggests that boundary entanglement is not bulk entanglement (quite unlike $Z_{bulk} = Z_{CFT}$ in AdS). Bulk observables require $|\Psi_{dS}|^2$ suggesting two copies of the dual CFT: this is reflected in the future-past extremal surfaces [182, 136] alluded to above. Other recent perspectives on extremal surfaces anchored on the de Sitter horizon include *e.g.* [133].

2.2 FRW cosmologies, 2-dim gravity and QES

Consider FRW cosmologies with flat spatial sections sourced by a scalar field Ψ (general reviews include *e.g.* [238, 239]): we consider a reduced 2-dim background as

$$ds^2 = -dt^2 + a(t)^2 dx_i^2 \quad \rightarrow \quad \phi = a^{d_i}\,, \quad ds^2 = a^{d_i+1}(-d\tau^2 + dx^2) \tag{2.11}$$

The energy-momentum conservation equation gives $dE + pdV = d(\rho\, a^{d_i+1}) + pd(a^{d_i+1}) = 0$, *i.e.* $\dot{\rho} + (d_i+1)H(\rho+p) = 0$. This along with the Friedmann equation and the equation of state $p = w\rho$ gives FRW cosmologies with

$$p = w\rho\,, \quad a \sim t^k\,, \quad k = \frac{2}{(1+d_i)(1+w)} \qquad \left[\rho = \frac{1}{2}\dot{\Psi}^2 - V\,, \quad p = \frac{1}{2}\dot{\Psi}^2 + V\right] \tag{2.12}$$

Now using conformal time τ gives

$$d\tau = \frac{dt}{a(t)} \quad \rightarrow \quad \tau \sim t^{1-k} \quad \rightarrow \quad a(\tau) \sim \left(\frac{\tau}{\tau_F}\right)^{\frac{k}{1-k}} \equiv \left(\frac{\tau}{\tau_F}\right)^{\nu}\,, \tag{2.13}$$

introducing the FRW scale τ_F so the scale factor becomes dimensionless: τ_F controls the strength of time-dependence in these backgrounds. Note that the above FRW description is slightly different from focussing on the vicinity of the singularity as in [110]: taking dominant time derivatives implies $\dot{\Psi}^2 \gg V$ so $p \sim \rho$, *i.e.* $w \sim 1$, giving $\nu = \frac{1}{d_i}$ so $\phi = a^{d_i} \sim \tau$. More generally the physical bounds on the equation of state parameter w translate to corresponding regimes for ν:

$$\nu = \frac{2}{(1+d_i)(1+w) - 2}\,; \qquad -1 \leq w \leq 1 \quad \Rightarrow \quad \nu > \frac{1}{d_i} \;\text{ or }\; \nu \leq -1\,. \tag{2.14}$$

Now we analyse quantum extremal surfaces here. In general the bulk matter entropy corresponds to some excited state, such as the thermal state. A variety of such studies for FRW cosmologies including entanglement with auxiliary universes appears in [119], revealing islands in various cases. Our discussion here will be limited to simply extending the earlier de Sitter QES solutions to certain FRW cases, which correspond to matter in the ground state (as may arise for pressureless matter with $w = 0$). The generalized entropy for an observer in such a background is

$$S_{gen} = \frac{a^{d_i}}{4G} + \frac{c}{6}\log\left(\Delta^2\, a^{(d_i+1)/2}|_{(\tau,r)}\right)\,, \qquad \Delta^2 = (\Delta x)^2 - (\tau - \tau_0)^2\,, \tag{2.15}$$

where we are using conformal time τ in the 2-dim theory. Now extremization gives

$$\begin{aligned} \partial_x S_{gen} = \frac{c}{6}\frac{\partial_x \Delta^2}{\Delta^2} = 0 \ , \qquad & \partial_\tau S_{gen} = \frac{d_i a^{d_i-1}\,\partial_\tau a}{4G} + \frac{c}{12}\frac{(d_i+1)\partial_\tau a}{a} + \frac{c}{6}\frac{\partial_\tau \Delta^2}{\Delta^2} = 0 \ , \\ \longrightarrow \qquad \frac{c}{3}\frac{\Delta x}{\Delta^2} = 0 \ , \qquad & \frac{d_i \nu}{4G}\frac{\tau^{\nu d_i - 1}}{\tau_F^{\nu d_i}} + \frac{c}{12}\frac{(d_i+1)\nu}{\tau} - \frac{c}{3}\frac{\tau-\tau_0}{\Delta^2} = 0 \ , \end{aligned} \tag{2.16}$$

using (2.13), (2.14). First considering timelike separated QES, we have

$$\Delta x = 0 \ , \quad \Delta^2 = -(\tau-\tau_0)^2 \, ; \qquad \frac{d_i \nu}{4G}\frac{\tau^{\nu d_i - 1}}{\tau_F^{\nu d_i}} + \frac{c}{12}\frac{(d_i+1)\nu}{\tau} + \frac{c}{3}\frac{1}{\tau-\tau_0} = 0 \ , \tag{2.17}$$

analogous to (2.4) in the de Sitter case $\nu = -1$: for $\nu < -1$ the nature of these timelike QES is similar. For $\nu d_i > 1$, taking the first term to be dominant over the second gives

$$\nu > \frac{1}{d_i} \ : \qquad \frac{d_i \nu}{4G}\frac{\tau^{\nu d_i - 1}}{\tau_F^{\nu d_i}} + \frac{c}{3}\frac{1}{\tau-\tau_0} \sim 0 \qquad [\tau \gtrsim \tau_F] \ , \tag{2.18}$$

with corresponding QES solutions (with $\tau_* - \tau_0 < 0$), valid for τ large compared to τ_F. Since these are timelike-separated, the on-shell generalized entropy acquires an imaginary part from $\log(-1)$ in $\Delta^2 < 0$, similar to (2.4).

Alternatively, looking for spacelike separated QES along the lines of (2.6) gives

$$\Delta^2 \sim R_c^2 \ , \qquad \frac{d_i \nu}{4G}\frac{\tau^{\nu d_i - 1}}{\tau_F^{\nu d_i}} + \frac{c}{12}\frac{(d_i+1)\nu}{\tau} \sim \frac{c}{3}\frac{\tau-\tau_0}{R_c^2} \ . \tag{2.19}$$

We are looking in the region of slow time evolution *i.e.* large $\tau \gtrsim \tau_F$ (far from the singularity at $\tau = 0$), towards understanding the evolution of the QES with the observer time τ_0. Then for any $\nu > 0$, we have $\tau^{\nu-1} > \tau^{-1}$ so we can approximate the time extremization equation as

$$\frac{d_i \nu}{4G}\frac{\tau^{\nu d_i - 1}}{\tau_F^{\nu d_i}} \sim \frac{c}{3}\frac{\tau-\tau_0}{R_c^2} \quad \rightarrow \quad \tau^{\nu d_i - 1} \sim \frac{4Gc}{3 d_i \nu}\frac{\tau_F^{\nu d_i}}{R_c^2}\,(\tau-\tau_0). \tag{2.20}$$

This equation while tricky in general does have solutions at least for specific families of ν. For instance pressureless dust has $w = 0$ so using (2.14) we have

$$\begin{aligned} w = 0 \ \ i.e. \ \ \nu = \frac{2}{d_i - 1} \quad & \xrightarrow{d_i=2} \quad \tau^3 \sim \frac{Gc\,\tau_F^4}{3R_c^2}\,(\tau-\tau_0) \ , \\ & \xrightarrow{d_i=3} \quad \tau^2 \sim \frac{4Gc\,\tau_F^3}{9R_c^2}\,(\tau-\tau_0) \ , \end{aligned} \tag{2.21}$$

both of which admit real solutions as long as $\frac{Gc\tau_F^{\nu d_i}}{R_c^2}$ lies in appropriate regimes with regard to τ_0. For instance the $d_i = 3$ case requires $\frac{4Gc\,\tau_F^3}{9R_c^2} > 4\tau_0$ for reality. Since the spatial regulator

$R_c \to \infty$ strictly speaking, it is clear that these solutions only make sense in a limit where we take c small and R_c large holding the above condition fixed: so the existence of these spacelike-separated QES solutions is not generic.

For generic scalar configurations, it is more appropriate to consider bulk entropy contributions that are not those pertaining to the ground state: then $S_{gen} = \frac{a^{d_i}}{4G} + S_b$ gives $\frac{d_i \partial_\tau a}{4G} + \partial_\tau S_b = 0$. Discussions of this sort have previously appeared in *e.g.* [119]. When S_b overpowers the classical area term, the Bekenstein bound is violated and islands can arise if further conditions hold. For S_b representing bulk matter in some mixed state, one might imagine some auxiliary purifying universe "elsewhere" which could then lead to islands.

Chapter 3

Small Schwarzschild de Sitter black holes, Quantum Extremal Surfaces and Islands

The black hole information paradox [1] can be regarded as the tension between the apparent unbounded growth of entanglement entropy of thermal Hawking radiation [2] outside the black hole and the expectation from quantum mechanics that entanglement entropy must become small at late times if purity of the original matter state is to be recovered, *i.e.* it must follow the Page curve [5, 6]. See *e.g.* [3, 4] for discussions of various aspects of the information paradox. Recent exciting discoveries unravelled via the study of entanglement and quantum extremal surfaces [7, 8, 9, 10, 11] have found that including nontrivial "island" contributions does in fact do this job. Quantum extremal surfaces are extrema of the generalized gravitational entropy [12, 13] obtained from the classical area of the entangling RT/HRT surface [14]-[17] after incorporating the bulk entanglement entropy of matter, with explicit calculation possible in effective 2-dimensional models where 2-dim CFT techniques enable detailed analysis of the bulk entanglement entropy. The island, arising as a nontrivial solution to extremization (near the black hole horizon, and only at late times), reflects new replica wormhole saddles [10, 11] and serves to purify the early Hawking radiation thereby leading to the entanglement entropy decreasing. There is a large body of literature on various aspects of these issues, reviewed in *e.g.* [18, 20, 21]: see *e.g.* [22]-[93] for a partial list of investigations on black holes in this regard. Scrutinies of the island formulation and alternative perspectives appear in *e.g.* [94, 95, 96].

In this chapter, we study "small" Schwarzschild de Sitter black holes, *i.e.* the regime where the black hole mass m is small compared with the de Sitter scale l, but large enough that a quasi-static approximation to the geometry is valid. This translates to saying that the

de Sitter temperature is very low compared with that of the black hole. In this regime, we approximate the ambient de Sitter space as a frozen classical background and study the two-sided (eternal) black hole. We can imagine that the black hole has formed from initial matter in a pure state: strictly speaking this can only be an approximation to the bulk CFT at the thermal state at the de Sitter temperature, but it is a reasonable approximation if the de Sitter temperature is very low. We focus on one black hole coordinate patch in the Penrose diagram, Figure 3.1 (which roughly comprises a line of alternating Schwarzschild and de Sitter patches), and consider observers in the static diamond patches far outside the black hole but within the cosmological horizons which bound the black hole patch, Figure 3.2. Then the entanglement entropy of the radiation exhibits an unbounded linear growth in time, which is inconsistent at late times with the entropy of the black hole, and indicative of the information paradox for the black hole. Using the island rule in the extremization of the generalized entropy shows an island emerging at late times a little outside the black hole horizon semiclassically: this then shows finiteness of the entanglement entropy of radiation recovering the expectations on the Page curve. In some essential sense, our analysis (which is purely bulk, with no holography per se) closely mirrors island studies of flat space Schwarzschild black holes in the literature, with the ambient de Sitter space entering only through more complicated coordinates. This is based on the paper [149].

In sec. 3.1, we review 4-dim Schwarzschild de Sitter black holes as required for our purposes, and in sec. 3.2, we describe our setup for the generalized entropy via 2-dim techniques. Sec. 3.2.1 discusses the entanglement entropy in the absence of the island (with details in App. A.1), while sec. 3.3 discusses the island calculation (details in App. A.2; see also App. A.3 for early times). Finally sec. 3.4 contains a Discussion of our approximations and open questions.

3.1 Small Schwarzschild de Sitter black holes $\to$ 2-dim

The Schwarzschild de Sitter black hole spacetime in $3+1$-dimensions has the metric

$$ds^2 = -f(r)dt^2 + \frac{dr^2}{f(r)} + r^2 d\Omega_2^2 \,, \qquad f(r) = 1 - \frac{2m}{r} - \frac{r^2}{l^2} \,. \tag{3.1}$$

This is a Schwarzschild black hole in de Sitter space [97] with an "outer" cosmological (de Sitter) horizon and an "inner" Schwarzschild horizon. The surface gravity at both horizons is generically distinct: Euclidean continuations removing a conical singularity can be defined at each horizon separately but not simultaneously at both [98] (see also [99, 100]). The only (degenerate) exception is in an extremal, or Nariai, limit [101] where both periodicities of

Euclidean time match: the spacetime develops a nearly dS_2 throat in this extremal limit [98]. More on the nearly dS_2 limit and the wavefunction of the universe appears in [102] (see also [103]). Related discussions with some relevance to this chapter also appear in [104].

The general $d+1$-dimensional SdS spacetime is of similar form as (3.1) but with $f(r) = 1-\frac{2m}{l}(\frac{l}{r})^{d-2}-\frac{r^2}{l^2}$, and will have qualitative parallels. We will focus on the 4-dim Schwarzschild de Sitter case in what follows. For SdS_4, the function $f(r)$ is a cubic and the zeroes of $f(r)$, *i.e.* solutions to $f(r)=0$, give the locations of the horizons. We can parametrize this as

$$\begin{aligned} f(r) =& 1-\frac{2m}{r}-\frac{r^2}{l^2} = \frac{1}{l^2\, r}\,(r_D-r)(r-r_S)(r+r_S+r_D), \\ r_D r_S(r_D+r_S) = 2ml^2\,,\ & r_D^2+r_D r_S+r_S^2 = l^2\ ;\ 0\le r_S\le r_D\le l\ ;\ \frac{m}{l}\le\frac{1}{3\sqrt{3}}\ . \end{aligned} \tag{3.2}$$

We will take the roots r_S and r_D to label the Schwarzschild black hole and de Sitter (cosmological) horizons respectively. (The third zero $-(r_D+r_S)$ does not correspond to a physical horizon.) The roots r_S, r_D are constrained as above.

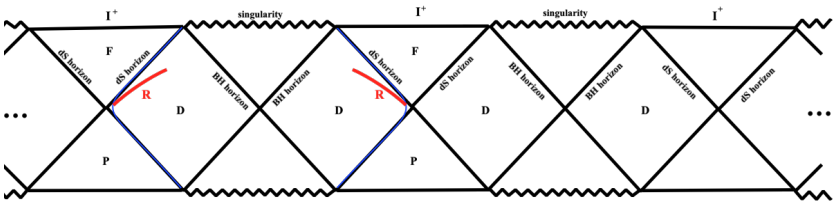

Figure 3.1: The Schwarzschild de Sitter black hole Penrose diagram, with focus on one black hole "patch".

The case with $m=0$, or $r_S=0$, $r_D=l$, is pure de Sitter space, while the flat space Schwarzschild black hole has $l=0$, or $r_S=m$, $r_D=0$. The above structure of horizons is valid for $\frac{m}{l}<\frac{1}{3\sqrt{3}}$, beyond which there are no horizons [97]. The limit $\frac{m}{l}=\frac{1}{3\sqrt{3}}$ corresponds to the cosmological and Schwarzschild horizon values coinciding: here we have $r_S=r_D=r_0=\frac{l}{\sqrt{3}}$ from (3.2). This special value leads to the extremal, or Nariai, limit where the near horizon region (between the horizons) becomes $dS_2\times S^2$. Overall the range of physically interesting r_S, r_D satisfies $0<r_S<r_0<r_D$ for generic values. The fact that $r_S<r_D$ implies that the cosmological horizon is "outside" the Schwarzschild one. The black hole interior has $r<r_S$ with $r\to 0$ the singularity. The region $r_D<r\le\infty$ describes the future and past de Sitter universes, with $r\to\infty$ the future boundary I^+ (or past, I^-). The maximally extended Penrose diagram Figure 3.1 shows an infinitely repeating pattern of Schwarzschild coordinate patches or "unit-cells" containing Schwarzschild black hole horizons cloaking interior regions: these patches are bounded by cosmological horizons on the left and right, with future/past universes beyond the cosmological horizons.

The intermediate static diamond region D is the exterior of the black hole, *i.e.* the static patch with a timelike Killing vector where physical timelike observers can be stationary:

$$D: \qquad r_S < r < r_D \; ; \qquad 0 < f(r) < 1 \; . \tag{3.3}$$

We want to consider the limit of a "small" black hole in de Sitter, *i.e.*

$$m \ll l \, , \qquad l \to \text{large} \qquad \Rightarrow \qquad r_D \gg r_S \; . \tag{3.4}$$

The horizon locations can then be found perturbatively to be $r_S \simeq 2m$, $r_D \simeq l - m \gg r_S$, from (3.2). In this limit (in a sense opposite to the Nariai limit where $r_S \sim r_D$), the black hole is much smaller than the ambient de Sitter scale, *i.e.* we have a small black hole in a large accelerating universe. So we expect that the ambient cosmology can be taken as a frozen classical background while the black hole undergoes Hawking evaporation. This is corroborated by the fact that the black hole Hawking temperature is much larger than the Gibbons-Hawking temperature of the ambient de Sitter horizon: *i.e.* using the surface gravities κ [99, 100] (see also [105]) and $T = \frac{\kappa}{2\pi}$ we obtain[1] in the limit (3.4),

$$T_{BH} \sim \frac{1}{8\pi m} \; , \qquad T_{dS} \sim \frac{1}{2\pi l} \; ; \qquad T_{dS} \ll T_{BH} \; . \tag{3.5}$$

Pushing this to the extreme leads to the flat space limit

$$r_D \sim l \to \infty : \qquad \frac{r_D}{l} \to 1 \; , \qquad r_S \to 2m \; ; \qquad T_{dS} \to 0 \; , \tag{3.6}$$

where the ambient de Sitter background acquires a vanishingly small temperature, approaching asymptotically flat space. Our entire analysis will in fact focus on these limits (3.4), (3.5), with the flat limit (3.6) as a special case to corroborate with.

Towards analysing the generalized entropy, we will require recasting the Schwarzschild de Sitter metric (3.1) in Kruskal coordinates which are regular at the black hole horizon. These are not regular in the vicinity of the de Sitter horizon (where a distinct set of Kruskal variables is more appropriate), but we will find that the black hole Kruskal variables suffices for our considerations. This is consistent with the fact the ambient de Sitter space simply serves as a frozen classical background in our regimes of interest. With this in mind, we define the black hole tortoise coordinate following the discussion in [106]:

$$r^* = \int \frac{1}{f(r)} \, dr = \int \frac{1}{1 - \frac{2m}{r} - \frac{r^2}{l^2}} \, dr = \int \frac{l^2 r}{(r_D - r)(r - r_S)(r + r_S + r_D)} \, dr \; . \tag{3.7}$$

[1] $\kappa_{BH,dS} = \frac{1}{2\sqrt{f(ml^2)}} \left| \frac{df}{dr} \right|_{r_S, r_D}$ which give $\frac{1}{2\beta_{S,D}} \frac{1}{\sqrt{1-3(m/l)^{2/3}}}$, with $\beta_{S,D}$ in (3.9).

Taking $f(r) > 0$ as pertains to the region D in (3.3), this gives

$$e^{r^*} = (r_D - r)^{-\beta_D}(r - r_S)^{\beta_s}(r + r_D + r_S)^{\beta_M} \ , \tag{3.8}$$

with the parameters (which simplify dr^*/dr to $1/f(r)$)

$$\begin{aligned} \beta_D = \frac{l^2 r_D}{(r_D - r_S)(2r_D + r_S)}, \quad \beta_S = \frac{l^2 r_S}{(r_D - r_S)(2r_S + r_D)}, \\ \beta_M = \frac{l^2(r_D + r_S)}{(2r_D + r_S)(2r_S + r_D)}. \end{aligned} \tag{3.9}$$

In the flat limit (3.6), $\beta_S \to r_S$ and $\beta_D \to l$.

The SdS_4 metric (3.1) is recast as $ds^2 = f(r)(-dt^2 + dr^{*2}) + r^2 d\Omega_2^2$. In the neighborhood of the black hole horizon, the Kruskal coordinates are then defined as U_S, V_S, and the Schwarzschild de Sitter metric becomes [106]

$$\begin{aligned} &\alpha_S = \frac{1}{2\beta_S}\,; \qquad U_S V_S = -e^{2\alpha_S r^*} \ , \qquad \frac{U_S}{V_S} = -e^{-2\alpha_S t} \ ; \qquad ds^2 = -\frac{dU_S dV_S}{W^2} + r^2 d\Omega^2, \\ &W = \sqrt{r}\, l\, \alpha_S (r_D - r)^{\frac{-(1+2\alpha_S\beta_D)}{2}} (r - r_S)^{\frac{2\alpha_S\beta_S - 1}{2}} (r + r_S + r_D)^{\frac{2\alpha_S\beta_M - 1}{2}} \ . \end{aligned} \tag{3.10}$$

The value of α_S here ensures regularity at the black hole horizon. (noting $\beta_M + \beta_S = \beta_D$ we see that W has dimensions of inverse length.) The Kruskal coordinates cover both the left and right static diamonds D of the black hole patch: in the right side (containing R_+ in Figure 3.1) we define

$$U_S = -e^{-\alpha_S(t - r^*)} \ , \qquad V_S = e^{\alpha_S(t + r^*)} \ , \tag{3.11}$$

while on the left side (with R_-) there is a relative minus sign, *i.e.* $U_S \to -U_S$, $V_S \to -V_S$.

For our purposes, it is a reasonable approximation to look at the s-wave sector of the black hole and consider the bulk matter as a 2-dim CFT: this enables the use of 2-dim CFT tools to study the entanglement entropy of bulk matter. With this in mind, we consider a reduction ansatz of the form

$$ds^2_{(4)} = g^{(2)}_{\mu\nu} dx^\mu dx^\nu + \lambda^{-2}\phi\, d\Omega_2^2 \ ; \qquad g_{\mu\nu} = \phi^{1/2}\, g^{(2)}_{\mu\nu} \ , \tag{3.12}$$

to obtain 2-dimensional dilaton gravity [107, 108] (see also [109]; applications to certain families of cosmologies appears in [110]). The lengthscale λ^{-1} has been introduced to make the dilaton dimensionless. The dilaton ϕ translates to the 4-dim transverse area of 2-spheres $\frac{4\pi\phi}{\lambda^2}$. The final term represents a Weyl transformation to absorb the dilaton kinetic term giving $\frac{1}{16\pi G_2}\int d^2x\sqrt{-g}\,(\phi\mathcal{R} - \frac{6}{l^2}\phi^{1/2} + 2\lambda^2\phi^{-1/2})$ as the 2-dim action. The 2-dim metric and

dilaton are

$$ds^2 = -\lambda\, r \frac{dU_S dV_S}{W^2} \equiv -\frac{dU_S dV_S}{(W')^2} \ , \qquad \phi = r^2\lambda^2 \ , \tag{3.13}$$

where $W' = \frac{W}{\sqrt{\lambda}\, r}$ and W is the conformal factor given in (3.10). For our discussions of entanglement entropy in these 2-dim theories, λ will be regarded as some fixed length scale independent of the de Sitter scale l so as to not interfere with the flat limit. With $G_{_N}$ the 4-dim Newton constant, $G_2 = \frac{G_N}{V_2}$ and $V_2 = \frac{4\pi}{\lambda^2}$, the area term in the 2-dim theory is $\frac{\phi}{4G_2} = \frac{4\pi\, r^2}{4G_{_N}}$ equivalent to the 4-dim one.

3.2 Black holes in de Sitter and entanglement entropy

In the regimes (3.4), (3.5), that we are considering, we see that there is a version of the information paradox for the black hole that is at play, with some parallels with that for the eternal AdS black hole in [22]. If the black hole forms from initial collapsing matter in a

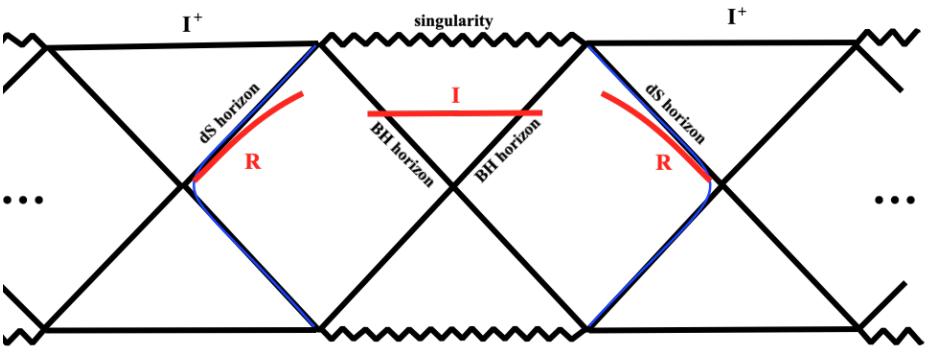

Figure 3.2: The Penrose diagram of a Schwarzschild de Sitter black hole, with focus on one black hole "patch" bounded by cosmological horizons on both sides. Depicted are the radiation regions $R_- \equiv [r_{D-}, b_-]$ and $R_+ \equiv [b_+, r_{D+}]$ and the late time island $I \equiv [a_-, a_+]$.

pure state, then information recovery at late times compared with the black hole timescale requires that the generalized gravitational entropy of the radiation obeys the Page curve. Note that in the current situation, this is only approximate since the ambient de Sitter space is only consistent with bulk CFT matter in a thermal state at the de Sitter temperature. However if the ambient de Sitter temperature is very low, then one might imagine that a pure state approximation is reasonable. This is the limit (3.5) we study to understand the black hole evaporation process here, which we find to be consistent. We will find, as in various previous investigations, that a nontrivial island emerges at late times a little outside the horizon as a nontrivial quantum extremal surface solution to the extremization of the generalized gravitational entropy. Including this and using the island rule shows the late time

entropy to be bounded. Our analysis has close parallels with that of flat space Schwarzschild black holes *e.g.* [58, 59], our expressions showing essential agreement in the flat space limit (3.6).

In our case, we consider distant observers that are stationary, represented by timelike worldlines in the static patch D region (3.3), between the Schwarzschild and de Sitter (cosmological) horizons. Towards simulating the flat space limit, we will consider the far end of the radiation region as asymptoting to the cosmological horizon. The outgoing radiation hits the cosmological horizon and as such is expected to go beyond and eventually hit the future boundary I^+ (future timelike infinity). However we assume that the observers propagating in the static patch D collect this outgoing radiation. So we will focus on the Schwarzschild patch bounded by the cosmological horizons on both sides and ignore the regions beyond: see Figure 3.2.

The island proposal [9] for the fine-grained entropy of the Hawking radiation is

$$S(R) = min \left\{ ext \Big[\frac{Area(\partial I)}{4G_{_N}} + S_{matter}(R \cup I) \Big] \right\} \tag{3.14}$$

where R is a region far from the black hole where the radiation is collected by distant observers and I is a spatially disconnected island around the horizon that is entangled with R. The intuition behind this expression is that after about half the black hole has evaporated, the Hawking radiation going out (roughly I) begins to purify the radiation that was emitted early on (roughly R). This purification of the early radiation by the late Hawking radiation is a reflection of the entanglement between the two parts, and stems from the picture of Hawking radiation as due to production of entangled particle pairs near the horizon (which is taken as vacuum). Thus $R \cup I$ purifies over time and its entanglement thus does not grow: the slowly evaporating black hole has decreasing area, so $S(R)$ decreases in time.

The Hawking process is dominated by s-wave modes. So we calculate the bulk entropy technically using 2-dimensional techniques where we approximate the bulk matter by a 2-dim CFT propagating in the 2-dim background obtained by dimensional reduction. In what follows, we will employ these techniques to calculate the entanglement entropy in the Schwarzschild de Sitter geometry by considering the 2-dim background (3.13) obtained from the reduction of (3.10). There is no holography in our entire discussion here: we are simply calculating the entropy of radiation in the bulk spacetime using the island rule (3.14).

In the absence of the island, the radiation regions are given by the intervals $R_\pm \in D$,

$$R = R_- \cup R_+ \; ; \qquad R_- \equiv [r_{D-}, b_-] \, , \quad R_+ \equiv [b_+, r_{D+}] \, , \tag{3.15}$$

which are the two regions marked in the Figure, one in either asymptotic region of the black hole patch. Since the radiation region is far from the black hole horizon, we have $b_\pm - r_S \gg r_S$. The entropy of the Hawking radiation is

$$S_{matter} = S(R) \ . \tag{3.16}$$

In the 2-dim CFT, the matter entanglement entropy for a single interval $A = [x, y]$ is obtained from the replica formulation [111, 112] after also incorporating in $d[x, y]$ the conformal transformation[2] to a curved space [8], stemming from the W'-factor in the 2-dim metric (3.13),

$$S_A = \frac{c}{3} \log d[x, y] \ = \ \frac{c}{6} \log \left(\frac{-\Delta U_S \Delta V_S}{W'|_x \, W'|_y} \right) \ . \tag{3.17}$$

From (3.13), we see that there is one factor of λ that arises inside the logarithm in each expression of the last form: in addition there is the ultraviolet cutoff ϵ_{UV} as in footnote 2. This factor $\frac{\lambda}{\epsilon_{UV}^2}$ in each such term will not play much role and we will ignore this except where necessary.

The entanglement entropy for multiple disjoint intervals

$$A = [x_1, y_1] \ \cup \ [x_2, y_2] \ \cup \ \ .... \ \ \cup \ [x_N, y_N] \tag{3.18}$$

is more complicated: this arises from the multi-point correlation functions of twist operators and so it depends on not just the central charge but detailed CFT information. In the limit where the intervals are well-separated, one can expand the twist operator products and obtain [111, 112, 113, 114]

$$S_A = \frac{c}{3} \ \log \ \frac{\prod_{i,j} d[x_j, y_i]}{\prod_{i<j} d[x_j, x_i] \ \ \prod_{i<j} d[y_j, y_i]} \tag{3.19}$$

For two intervals $[x_1, y_1] \cup [x_2, y_2]$, this is a limit where the cross ratio x is small, *i.e.*

$$x = \frac{d[x_1, y_1] \, d[x_2, y_2]}{d[x_1, x_2] \, d[y_1, y_2]} \ ; \qquad x \ll 1 \ , \tag{3.20}$$

where we use the Kruskal distances in (3.17) in constructing the cross-ratio. In 2-dim CFTs with a holographic dual, this is the situation where the two intervals A, B are well-separated and their mutual information exhibits a disentangling transition [115] with $I[A, B] = S[A] + S[B] - S[A \cup B] \to 0$, *i.e.* the disconnected surface $S_{dis} = S[A] + S[B]$ has lower area than

[2] Any 2-dim metric is conformally flat so $ds^2 = e^f \eta_{\mu\nu} dx^\mu dx^\nu$. The twist operator 2-point function scales under a conformal transformation as $\langle \sigma(x_1) \, \sigma(x_2) \rangle_{e^f g} = e^{-\Delta_n \, f/2}|_{x_1} \, e^{-\Delta_n \, f/2}|_{x_2} \, \langle \sigma(x_1) \, \sigma(x_2) \rangle_g$ with $\Delta_n = \frac{c}{12} \frac{n^2-1}{n}$. Since the partition function in the presence of twist operators scales as the twist operator 2-point function, the entanglement entropy becomes $S^{12}_{e^f g} = -\lim_{n\to 1} \partial_n \langle \sigma(x_1) \, \sigma(x_2) \rangle_{e^f g} = S^{12}_g + \frac{c}{6} \sum_{endpoints} \log e^{f/2}$, giving for a single interval $S^{12}_g = \frac{c}{6} \log \left(\frac{\Delta^2}{\epsilon^2_{UV}} \right) \ \to \ S^{12}_{e^f g} = \frac{c}{6} \log \left(\frac{\Delta^2}{\epsilon^2_{UV}} \, e^{f/2}|_1 \, e^{f/2}|_2 \right)$.

the connected surface $S_{conn} = S[A \cup B]$. It turns out that the cross-ratio for the points in question becomes small at late times, as we will see later, justifying the use of (3.19) for our purposes.

In what follows, we first calculate the entanglement entropy for the configuration without any island, using 3.16: this shows the entropy of radiation as increasing linearly in time at late times, indicative of the information paradox. Towards resolving this we will include a possible island and calculate the entanglement entropy using the island rule 3.14: this results in a late time entropy that is time-independent.

3.2.1 Entanglement entropy: no island

In this section, we will evaluate the entanglement entropy of the radiation at late times in the absence of any island. Then we have only the radiation regions $R_- \cup R_+$ in Figure 3.2, given by the intervals (3.15), *i.e.* $R_- \equiv [r_{D-}, b_-]$ and $R_+ \equiv [b_+, r_{D+}]$. In the limit (3.4), (3.5), with the de Sitter temperature very low, we can approximate the entire system as a pure state on any slice. Then the bulk matter CFT entropy of R is the same as that of the complementary region $R_c = [b_-, b_+]$, so we obtain

$$S_{matter} = \frac{c}{3} \log \left[d(b_+, b_-) \right] . \tag{3.21}$$

We label the spacetime coordinates in the left and right asymptotic regions in the Schwarzschild patch as

$$b_+ : \quad (t, r) = (t_b, b) , \qquad b_- : \quad (t, r) = (-t_b + \frac{i\beta}{2}, b) ; \qquad \beta = \frac{2\pi}{\alpha_S} . \tag{3.22}$$

This choice of β is simply a convenient way of incorporating the relative minus signs in the Kruskal coordinates (3.10), (3.11), in the left and right regions through $e^{i\beta\alpha_S/2} = e^{i\pi} = -1$. With this parametrization of the left and right time coordinates, we can conveniently use the expressions in (3.11), with β automatically doing the left-right book-keeping.

Then we evaluate the bulk matter entropy in the Schwarzschild de Sitter geometry (3.13) using (3.17) to obtain

$$S_{\text{matter}} = \frac{c}{6} \cdot \log \left(b \, \frac{(U_S(b_-) - U_S(b_+))(V_S(b_+) - V_S(b_-))}{W(b_+) W(b_-)} \right) . \tag{3.23}$$

The total entanglement entropy then becomes

$$S = \frac{c}{6} \log \left[16 \beta_S^2 \, (b - r_S) \, \frac{(r_D - b)(b + r_S + r_D)}{l^2} \, \cosh^2 \left(\frac{t_b}{2\beta_S} \right) \right] . \tag{3.24}$$

The details of the calculation are shown in Appendix A.1. The late time approximation is $t_b \gg b > r_S$, $\frac{t_b}{r_S} \gg 1$: the above result then approximates as

$$S \approx const + \frac{c}{6}\frac{t_b}{\beta_S} \ . \tag{3.25}$$

Now in the flat space limit (3.6), the total entropy at late times becomes $S \approx \frac{c}{6}\frac{t_b}{r_S}$, in agreement with [58, 59]. This linear growth in time means that the entropy of the radiation will eventually be infinitely larger than the Bekenstein-Hawking entropy of the black hole.

3.3 Late time entanglement entropy with island

In this section we will evaluate the entropy of radiation in the presence of an island and show that it saves the entropy bound, recovering the Page curve for the black hole in Schwarzschild de Sitter space at late times $t_a, t_b \gg r_S$. The island is the region marked I in Figure 3.2: the intervals in question are

$$R_- \equiv [r_{D-}, b_-] \, , \qquad R_+ \equiv [b_+, r_{D+}] \ , \qquad I \equiv [a_-, a_+] \ . \tag{3.26}$$

Since we are considering the limit (3.4), (3.5), with the black hole evaporation well-separated from de Sitter physics, we expect the island in question to emerge near the black hole horizon. Then

$$b - r_S \gg a - r_S \sim 0 \ ; \qquad b \gg r_S \ , \tag{3.27}$$

and the last inequality reflects the fact that we are considering distant observers far from the black hole. Since the ambient de Sitter temperature is very low in our considerations as mentioned earlier, we approximate the bulk matter to be in a pure state so the entanglement entropy of $A \equiv R_- \cup I \cup R_+$ is equal to that of the complementary intervals $A_c \equiv [b_-, a_-] \cup [a_+, b_+]$ (see (A.29), for details on the intervals A). The assumptions (3.27) imply that the intervals are well-separated: then we can express the entanglement entropy for A_c using 3.19 as

$$S_{matter} = \frac{c}{3} \log \frac{d[a_+, a_-]\, d[b_+, b_-]\, d[a_+, b_+]\, d[a_-, b_-]}{d[a_+, b_-]\, d[a_-, b_+]} \ . \tag{3.28}$$

For the intervals $[b_-, a_-] \cup [a_+, b_+]$, as the cross-ratio x in (3.20) becomes small, we have $1 - x = \frac{d[a_+,a_-]\, d[b_+,b_-]}{d[a_+,b_-]\, d[a_-,b_+]} \to 1$. Adding the area term $\frac{\phi}{4G_2} = \frac{4\pi a^2}{4G_N}$ for both left and right sides, the total generalized entropy becomes $S_{total} \sim 2\big(\frac{\pi a^2}{G_N} + \frac{c}{3} \log\, d[a_+, b_+]\big)$ since the left and right sides give essentially equal contributions. In detail, using the Kruskal coordinates (3.10), (3.11),

(A.1), we evaluate the total generalized entropy (3.28) obtaining

$$\begin{aligned} S_{total} = \frac{2\pi a^2}{G_{_N}} + \frac{c}{6}\log\Big[&\frac{2^8 r_S^4}{(\frac{r_D-r_S}{l})^4(\frac{2r_S+r_D}{l})^4}(a-r_S)(b-r_S)(\frac{a-r_D}{l})(\frac{b-r_D}{l})\cdot \\ &(\frac{a+r_S+r_D}{l})(\frac{b+r_S+r_D}{l})\cosh^2\frac{t_a}{2\beta_S}\cosh^2\frac{t_b}{2\beta_S}\Big] \\ &+\frac{c}{3}\log\Big[1-2\frac{(a-r_S)^{\alpha_S\beta_S}}{(b-r_S)^{\alpha_S\beta_S}}C(a)\,\cosh\big(\alpha_S(t_a-t_b)\big)\Big] \\ &-\frac{c}{3}\log\Big[1+2\frac{(a-r_S)^{\alpha_S\beta_S}}{(b-r_S)^{\alpha_S\beta_S}}C(a)\,\cosh\big(\alpha_S(t_a+t_b)\big)\Big]\,, \end{aligned} \tag{3.29}$$

with $C(a)$ defined as

$$C(a) = \frac{(r_D-b)^{\alpha_S\beta_D}(a+r_S+r_D)^{\alpha_S\beta_M}}{(r_D-a)^{\alpha_S\beta_D}(b+r_S+r_D)^{\alpha_S\beta_M}}\,. \tag{3.30}$$

See Appendix A.2 for details of this calculation. At late times, $t_a, t_b \gg r_S$, we approximate $\cosh(\alpha_S(t_a+t_b)) \sim 2\cosh(\alpha_S t_a)\cosh(\alpha_S t_b)$ which is large. Then taking into account the expectation $a - r_S \sim 0$ and simplifying, we obtain

$$\begin{aligned} S_{total} = \frac{2\pi a^2}{G_{_N}} + \frac{c}{6}\log\Big[&\frac{16 r_S^4(b-r_S)^2}{(\frac{r_D-r_S}{l})^4(\frac{2r_S+r_D}{l})^4}\frac{(r_D-a)(r_D-b)(a+r_S+r_D)(b+r_S+r_D)}{l^4\ (C(a))^2}\Big] \\ &-\frac{2c}{3}\sqrt{\frac{a-r_S}{b-r_S}}\,C(a)\,\cosh\big(\alpha_S(t_a-t_b)\big)\,. \end{aligned} \tag{3.31}$$

In the flat space limit (3.6), we take r_D large and expand using (3.9) to approximate (3.30) as

$$C(a) \sim \Big(1-\frac{b-a}{r_D}\Big)^{\alpha_S\beta_D}\Big(1-\frac{b-a}{r_D+r_S}\Big)^{\alpha_S\beta_M} \sim 1-\frac{b-a}{2r_S}\,, \tag{3.32}$$

which can further approximated as $e^{-\frac{b-a}{2r_S}}$ in the regime (3.27) to give the total entropy at late times as

$$S_{total} \approx \frac{2\pi a^2}{G_{_N}} + \frac{c}{6}\log\Big[16 r_S^4(b-r_S)^2\, e^{\frac{b-a}{r_S}}\Big] - \frac{2c}{3}\sqrt{\frac{a-r_S}{b-r_S}}\,e^{-\frac{b-a}{2r_S}}\,\cosh\big(\alpha_S(t_a-t_b)\big)\,. \tag{3.33}$$

This is in agreement with *e.g.* [59] upto a factor of ab inside the logarithm, stemming from the fact that we are using the strict 2-dim bulk metric (3.13) after reduction, with the additional conformal factor in W' relative to W in(3.10). This detailed difference (which also arises in other such expressions) does not affect the qualitative behaviour of the generalized entropy in our regime since the s-wave sector is expected to be dominant in the Hawking process.

Now, extremizing (3.31) with respect to the location of the island boundary a gives

$$\begin{aligned}&\frac{\partial S_{total}}{\partial a}=0 \quad \Rightarrow \\ &\frac{4\pi a}{G_{_N}}+\frac{c}{6}\Big[\frac{(1-2\alpha_S\beta_M)(r_D-a)-(1+2\alpha_S\beta_D)(a+r_S+r_D)}{(a+r_S+r_D)(r_D-a)}\Big] \\ &\quad -\frac{2c}{3}\cosh\big(\alpha_S(t_a-t_b)\big)\cdot\sqrt{\frac{a-r_S}{b-r_S}}\,C(a)\,\Big[\frac{\alpha_S\beta_M}{a+r_S+r_D}+\frac{\alpha_S\beta_D}{r_D-a}+\frac{1/2}{a-r_S}\Big]=0\ .\end{aligned} \tag{3.34}$$

Here, since r_D is large in our considerations, the second term scales as $O(\frac{1}{r_D})$ and can thus be ignored: further the $\frac{1}{a+r_S+r_D}$ and $\frac{1}{r_D-a}$ also are suppressed relative to $\frac{1}{a-r_S}$. With these approximations (3.34) becomes

$$a\ \simeq\ \frac{1}{\sqrt{a-r_S}}\,\frac{G_{_N}c}{12\pi}\,\frac{1}{\sqrt{b-r_S}}\,C(a)\,\cosh\big(\alpha_S(t_a-t_b)\big)\ . \tag{3.35}$$

Now we note that we are in the semiclassical regime where

$$0\ll c\ll\frac{1}{G_{_N}}\ , \tag{3.36}$$

so that the classical area term in the generalized entropy is dominant but the bulk matter makes nontrivial subleading contributions (which are not so large as to cause significant backreaction on the classical geometry).

We are looking for an island with boundary $a\sim r_S$ near the black hole horizon: this corroborates with the fact that since the entire right hand side is $O(G_{_N}c)$, in the classical limit $c=0$ we have $a=r_S$. Thus we can solve the above expression in perturbation theory setting $a\sim r_S$ to find the first order correction in $G_{_N}c\ll 1$: then schematically we have

$$a-r_S\simeq\frac{K^2}{r_S^2}\frac{1}{b-r_S}\ ,\qquad K=\frac{G_{_N}c}{12\pi}\cosh\left(\alpha_S(t_a-t_b)\right)C(r_S)\ , \tag{3.37}$$

and we finally obtain (with $C(r_S)$ from (3.30) with $a=r_S$)

$$a\simeq r_S+\frac{(G_{_N}c)^2}{144\pi^2r_S^2(b-r_S)}\,C(r_S)^2\,\cosh^2\big(\alpha_S(t_a-t_b)\big)\ . \tag{3.38}$$

Using (3.32) and the comments there, we obtain in the flat space limit (3.6)

$$a\simeq r_S+\frac{(G_{_N}c)^2}{144\pi^2r_S^2(b-r_S)}\,e^{\frac{r_S-b}{r_S}}\,\cosh^2\big(\alpha_S(t_a-t_b)\big)\ , \tag{3.39}$$

in agreement with [59]. With the value of a in (3.38) the total on-shell entanglement entropy in (3.31) becomes

$$S_{o.s.} = \frac{2\pi r_S^2}{G_{_N}} + \frac{c}{6}\log\Big[\frac{16\beta_s^4(b-r_S)^2}{l^4}\,\frac{(b+r_S+r_D)^{(1+2\alpha_S\beta_M)}}{(2r_S+r_D)^{2\alpha_S\beta_M-1}}\,\frac{(r_D-r_S)^{1+2\alpha_S\beta_D}}{(r_D-b)^{2\alpha_S\beta_D-1}}\Big] - \frac{c^2G_{_N}}{36\pi r_S(b-r_S)}\,C(r_S)^2\,\cosh^2\big(\alpha_S(t_a-t_b)\big)\,. \tag{3.40}$$

Now varying and extremizing the above expression with respect to t_a, we obtain $t_a = t_b$. Using this in (3.40) gives the entanglement entropy (keeping only leading terms) to be

$$S_{o.s.} = \frac{2\pi r_S^2}{G_{_N}} + \frac{c}{6}\log\Big[\frac{16\beta_s^4(b-r_S)^2}{l^4}\,\frac{(b+r_S+r_D)^{(1+2\alpha_S\beta_M)}}{(2r_S+r_D)^{2\alpha_S\beta_M-1}}\,\frac{(r_D-r_S)^{1+2\alpha_S\beta_D}}{(r_D-b)^{2\alpha_S\beta_D-1}}\Big]\,, \tag{3.41}$$

which is time-independent, stemming from the presence of the island. The first term is twice the Bekenstein-Hawking entropy of the black hole and the second term, arising from the bulk entropy of the radiation region purified by the island, is a constant term not growing in time. This recovers the expectations on the Page curve for the evaporating small black hole in de Sitter in the limits we are considering (3.4), (3.5), (3.6). In our discussion which is entirely gravitational, it is natural to take the Planck length as the natural UV scale and set $\lambda^{-1} \sim \epsilon_{UV} \sim l_P$: then putting back the $\frac{\lambda}{\epsilon_{UV}^2}$ factors gives $S_{o.s.} \sim A_s + \frac{c}{3}\log A_S + \frac{c}{3}\log\frac{b}{l_P}$.

Comparison of the late time entanglement entropy without the island (3.25) and that with the island (3.41) enables an estimate of the Page time when the island configuration emerges as the preferred quantum extremal surface with lower area. Making a coarse comparison at the Page time t_P,

$$\frac{c}{6}\frac{t_P}{\beta_S} \sim 2S_{BH} \qquad \Rightarrow \qquad t_P \sim \frac{12\pi\, r_S^2\,\beta_S}{G_{_N}c}\,. \tag{3.42}$$

Beyond this time t_P, the no-island configuration (3.25) has bigger area and we discard it in favour of the island one (3.41) (which is a new saddle stemming from replica wormholes) which does not grow in time. Of course all our analysis is carried out in a quasi-static approximation with $r_S \sim$ fixed, since r_S is decreasing very slowly in time as the black hole evaporates.

It is interesting to note that no such island configuration near the black hole horizon emerges at early times, $t_a, t_b \ll r_S$, when not much Hawking radiation has gone out: see (A.34) in App. A.3, where we consider a coarse approximation with $t_a, t_b \sim 0$. However we might imagine that there arises a "vanishing extremal surface" with the island boundary a far inside the black hole horizon so $a \ll r_S$. Setting up the generalized entropy using Kruskal coordinates in the black hole interior and extremizing in fact reveals such an island in (A.42), with a corresponding generalized entropy that is not significant, vindicating approximate purity in the regimes we are considering.

We have regarded the ambient de Sitter space as a frozen classical background, at very low temperature, with regard to the black hole Hawking process, and found consistency in our island studies and the 2-dim CFT calculations approximating the bulk matter to be in a pure state. The calculation in (A.29) of the entanglement entropy of the complementary intervals alongwith the regularization (A.32) vindicates the approximate purity of the state in this regime. If we keep the de Sitter temperature as nonzero, it would appear that *e.g.* (A.31) would give rise to a growing entanglement in time; see [116] for some related comments.

3.4 Discussion

We focussed on one Kruskal black hole patch in the Penrose diagram Figure 3.1 of eternal Schwarzschild de Sitter (which in the maximal extension comprises a line of alternating black hole and cosmological patches). This single patch (Figure 3.2) is in some sense equivalent to the Penrose diagram of the flat space Schwarzschild black hole embedded in de Sitter, with the cosmological horizons on both sides serving as asymptotic boundaries (akin to null infinity in flat space). Technically we dimensionally reduce the SdS_4 spacetime to 2-dimensions and use 2-dim CFT techniques for calculating the entanglement entropy of bulk matter approximated as a 2-dim CFT. We saw in sec. 3.2.1 that in the absence of the island the bulk entropy for the radiation region exhibits unbounded linear growth, inconsistent at late times when it exceeds the entropy of the black hole. In sec. 3.3 including an appropriate island as in (3.26), upon extremizing the generalized entropy incorporating the island rule, we find an island a little outside the horizon (3.38) semiclassically : the late time entropy (3.31) on-shell becomes (3.40) and is twice the Bekenstein-Hawking entropy of the black hole, plus finite bulk corrections, in the quasi-static approximation. In the flat space limit (3.6), our expressions are in essential agreement with those in [59] (as discussed around (3.33)). This suggests that contributions due to further islands in the other Kruskal patches in our regime are suppressed (if they exist), perhaps consistent with gravity effectively being very weak far from the black hole.

We have restricted to observers propagating within the static patch, with $f(r) < 1$, as appropriate for the physics pertaining to the Hawking evaporation of the black hole. Let us now imagine considering observers near the future boundary I^+ of the de Sitter patch, beyond the cosmological horizon. Various studies on quantum extremal surfaces and cosmologies appear in *e.g.* [117]-[135]. In the present context, one can study the generalized entropy for such I^+ observers as well (see [104] for some discussions on classical RT/HRT surfaces at I^+ in SdS, and [136] and earlier work in dS). This reveals quantum extremal surfaces that are timelike-separated from observers at I^+: there are parallels with studies in the Poincare

patch of de Sitter [118], [134]. In *SdS* however, one might imagine mapping the radiation region R_+ to a corresponding interval at the future boundary *e.g.* by sending out light rays from R_+ to I^+ (see Figure 3.2). This suggests that intervals at I^+ should also be able to access information about black hole evaporation. In particular it might seem possible to find nontrivial island contributions to analyse the generalized entropy for observers at I^+ to access black hole physics in de Sitter. In the next chapter, we will explore these ideas further.

Chapter 4

Small Schwarzschild de Sitter black holes, the future boundary and Islands

This chapter continues the study in [149] of "small" Schwarzschild de Sitter black holes, with the black hole mass m small compared with the de Sitter scale l, but large enough that a quasi-static approximation to the geometry is valid. The de Sitter temperature is very low compared with that of the black hole so the ambient de Sitter space is approximated as a frozen classical background. For calculational purposes, we consider an effective 2-dim dilaton gravity model obtained by dimensional reduction, with the bulk matter representing the black hole Hawking radiation modelled as a 2-dim CFT propagating on this 2-dim space: this is reasonable under the assumption that the s-wave Hawking modes are dominant. We imagine that the black hole has formed from initial matter in a pure state which is a reasonable approximation since the de Sitter temperature is very low (more generally, the bulk matter CFT is in a thermal state at the de Sitter temperature). In [149], we focussed on one black hole coordinate patch in the Penrose diagram (roughly a line of alternating Schwarzschild and de Sitter patches, see Figure 4.1) and considered observers in the static diamond patches far outside the black hole but within the cosmological horizons. While the entanglement entropy of the radiation region exhibits unbounded growth, reflecting the information paradox for the black hole (which has finite entropy), including appropriate island contributions recovers finiteness of entanglement, and thereby expectations on the Page curve. The island emerges at late times a little outside the black hole horizon semiclassically.

The Hawking radiation from the black hole is expected to cross the cosmological horizon and eventually reach the future boundary where it is collected (Figure 4.1). In this chapter, we consider the point of view of these future boundary (meta)observers, and look for semiclassical island resolutions of the black hole information paradox with regard to a radiation region at

the future boundary. The future boundary is in a sense better defined (compared to the static diamond) as a place where gravity is manifestly weak, the space expanding indefinitely.

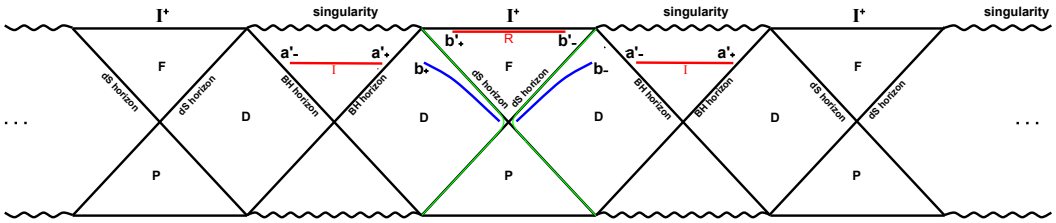

Figure 4.1: The Penrose diagram of a Schwarzschild de Sitter black hole, with radiation region near the future boundary I^+. Depicted are the radiation regions (blue lines) in the static patches, which are analytically continued to the radiation region $R \equiv [b'_+, b'_-]$ at I^+ and the late time island $I \equiv [a'_-, a'_+]$ on both sides.

The radiation region taken as an interval with length labelled by X (alongwith spheres) on the future boundary can be parametrized via Kruskal coordinates T, X, defined by analytic continuation from the static diamond coordinates. We find that the entanglement entropy of Hawking radiation exhibits unbounded growth in the spatial length X along the future boundary, inconsistent with the finiteness of black hole entropy, and reflecting the information paradox. Using the island rule in the extremization of the generalized entropy shows islands emerging for large values of X a little inside the black hole horizon semiclassically: including the island contributions recovers expectations on the Page curve. This future boundary radiation region is entangled with island regions around the horizons of black hole regions on both left and right cosmological horizons (Figure 4.1): this is expected since the future boundary receives Hawking modes from both left and right black holes. Our analysis has some parallels with the island studies in [139] for dS_2 arising under reductions from Nariai limits of higher dim Schwarzschild de Sitter. One might expect timelike separated quantum extremal surfaces for the future boundary resulting in complex-valued entropies as are known in pure de Sitter (see [118] for dS_2, and [134] for reductions of higher dimensional Poincare dS; see also [180], [181], [182], [183], [184] for classical RT/HRT surfaces anchored at the future boundary). However Schwarzschild de Sitter has a "sufficiently wide" Penrose diagram so spacelike separated islands do exist here in accordance with physical expectations for the black hole Page curve (thus we discard timelike separated ones here). This is based on the paper [247].

In sec. 4.1 we discuss parametrizations in various coordinate patches. Sec. 4.2 discusses the entanglement entropy without islands (details in App. B.1), while sec. 4.3 discusses the

island calculation (details in App. B.2). App. B.3.1-B.3.2 discuss inconsistencies in other potential island solutions, while App. B.4 discusses timelike separated quantum extremal surface solutions for future boundary observers. Sec. 4.4 contains a Discussion on various aspects of our study.

4.1 Coordinate parametrizations in various coordinate patches

We will describe various coordinate parametrizations in the various coordinate choices in the Schwarzschild de Sitter spacetime, involving Kruskal variables around the black hole horizon and around the cosmological horizon.

In [149], we considered the radiation region to be in the static diamond bounded by the black hole and cosmological horizons in the Schwarzschild de Sitter background: this static patch is parametrized by certain Kruskal coordinates [106] in the vicinity of the black hole horizon. For our present purposes, we would like to analytically extend the Kruskal coordinates (U_D, V_D) defined in the static patch in the vicinity of the cosmological horizon and (U_S, V_S) near the black hole horizon to a new set of Kruskal coordinates (U'_D, V'_D) lying within the future universe, near the future boundary, and (U'_S, V'_S) in the interior of black hole (inside the horizon) respectively. We will first define the set of coordinates in the static patch and then analytically extend them beyond both horizons.

We will first recast the Schwarzschild de Sitter metric (3.1) in the static patch in terms of the Kruskal coordinates which are regular at the cosmological horizon (but not in the vicinity of the black hole horizon). Towards this, we define the tortoise coordinate following [106]:

$$r^* = \int \frac{1}{f(r)}\, dr = \int \frac{1}{1 - \frac{2m}{r} - \frac{r^2}{l^2}}\, dr = \int \frac{l^2 r}{(r_D - r)(r - r_S)(r + r_S + r_D)}\, dr \ . \tag{4.1}$$

Taking $f(r) > 0$ in the region $r_S < r < r_D$, this gives

$$e^{r^*} = (r_D - r)^{-\beta_D} (r - r_S)^{\beta_s} (r + r_D + r_S)^{\beta_M} \ , \tag{4.2}$$

with the parameters (which simplify dr^*/dr to $1/f(r)$, and satisfy $\beta_M + \beta_S = \beta_D$)

$$\beta_D = \frac{l^2 r_D}{(r_D - r_S)(2r_D + r_S)} \ , \quad \beta_S = \frac{l^2 r_S}{(r_D - r_S)(2r_S + r_D)} \ , \quad \beta_M = \frac{l^2 (r_D + r_S)}{(2r_D + r_S)(2r_S + r_D)} \ . \tag{4.3}$$

The SdS_4 metric (3.1) is recast as $ds^2 = f(r)(-dt^2 + dr^{*2}) + r^2 d\Omega_2^2$. We label the spacetime coordinates in the left and right regions in the vicinity of the cosmological horizon as

$$b_+ : \quad (t, r) = (t_b, b) \ , \qquad b_- : \quad (t, r) = (-t_b + \frac{i\beta}{2}, b) \ ; \qquad \beta = \frac{2\pi}{\alpha_D} \ . \tag{4.4}$$

This choice of β is simply a convenient way of incorporating the relative minus signs in the Kruskal coordinates in the left and right regions through $e^{i\beta\alpha_D/2} = e^{i\pi} = -1$. In the static patch, in the vicinity of the cosmological horizon, these cosmological Kruskal coordinates U_D, V_D, and the Schwarzschild de Sitter metric become

$$\begin{gathered} b_+ : \qquad U_{D_+} = e^{\alpha_D(t_b - r^*)} \ , \quad V_{D_+} = -e^{-\alpha_D(t_b + r^*)} \ , \\ \alpha_D = \frac{1}{2\beta_D} ; \quad U_{D_+} V_{D_+} = -e^{-2\alpha_D r^*} \ , \quad \frac{U_{D_+}}{V_{D_+}} = -e^{2\alpha_D t_b} \ ; \quad ds^2 = -\frac{dU_{D_+} dV_{D_+}}{{W_b}^2} + r^2 d\Omega^2 \ , \\ W_b = \sqrt{r}\, l\, \alpha_D (r_D - r)^{-\frac{(1-2\alpha_D\beta_D)}{2}} (r - r_S)^{-\frac{(1+2\alpha_D\beta_S)}{2}} (r + r_S + r_D)^{-\frac{(1+2\alpha_D\beta_M)}{2}} \end{gathered} \tag{4.5}$$

The value of α_D here ensures regularity at the cosmological horizon. ($\beta_M + \beta_S = \beta_D$ ensures that W has dimensions of inverse length.) With this parametrization of the left and right time coordinates, we conveniently use the expressions in (4.5), with β automatically doing the left-right book-keeping.

We are now considering an interval at the future boundary I^+ where the Hawking radiation from the black hole is expected to be collected. Towards parametrizing this future boundary radiation region, we will analytically continue the cosmological Kruskal coordinates defined above in the static patch to the region beyond the cosmological horizon (*i.e.* the future universe) keeping invariant, as usual, the metric expressed in terms of the new cosmological Kruskal coordinates beyond the cosmological horizon. Let us consider the analytic continuation in $(t_b, {r_b}^*)$ coordinates as

$$(t_b, {r_b}^*) \to \big(X_{b'} = \alpha_D(t_b - \frac{i\pi}{2\alpha_D}), \, T_{b'} = \alpha_D({r_b}^* - \frac{i\pi}{2\alpha_D})\big) \, . \tag{4.6}$$

Thus the new cosmological Kruskal coordinates at both ends b'_+ and b'_- of the future boundary radiation region are defined as (U'_{D_+}, V'_{D_+}) and (U'_{D_-}, V'_{D_-}) respectively and the Schwarzschild

de Sitter metric in terms of $(X_{b'}, T_{b'})$ coordinates becomes

$$
\begin{aligned}
b'_+ : \qquad & U'_{D_+} = e^{(X_{b'}-T_{b'})}\,, \qquad V'_{D_+} = e^{-(X_{b'}+T_{b'})}, \\
b'_- : \qquad & U'_{D_-} = e^{-(X_{b'}+T_{b'})}\,, \qquad V'_{D_-} = e^{(X_{b'}-T_{b'})},
\end{aligned}
$$

$$
U'_{D_\pm} V'_{D_\pm} = e^{-2T_{b'}}\ , \qquad \frac{U'_{D_\pm}}{V'_{D_\pm}} = e^{\pm 2X_{b'}}\ ; \qquad ds^2 = \frac{1}{\alpha_D^2}|f(r)|\left(-dT_{b'}^2 + dX_{b'}^2\right) + r^2 d\Omega^2,
$$

$$
|f(r)| = \frac{1}{l^2 r}(r-r_D)(r-r_S)(r+r_S+r_D)\ . \tag{4.7}
$$

The Schwarzschild de Sitter metric now becomes

$$
ds^2 = -\frac{dU'_{D_\pm} dV'_{D_\pm}}{{W_{b'}}^2} + r^2 d\Omega^2\ ,
$$

$$
W_{b'} = \sqrt{r}\, l\, \alpha_D (r-r_D)^{-\frac{(1-2\alpha_D\beta_D)}{2}} (r-r_S)^{-\frac{(1+2\alpha_D\beta_S)}{2}} (r+r_S+r_D)^{-\frac{(1+2\alpha_D\beta_M)}{2}}\ . \tag{4.8}
$$

For our purposes, it is a reasonable approximation to look at the s-wave sector of the black hole and consider the bulk matter as a 2-dim CFT: this enables the use of 2-dim CFT tools to study the entanglement entropy of bulk matter. So, we will consider the same dimensional reduction of the 4-dim Schwarzschild de Sitter spacetime to a 2-dim background, as in [149] (see the general reviews [107, 108, 51], and [109] for related discussions, as well as [110] for certain families of 2-dim cosmologies).

Recalling from [149], the reduction ansatz $ds^2_{(4)} = g^{(2)}_{\mu\nu} dx^\mu dx^\nu + \lambda^{-2}\phi\, d\Omega_2^2$ alongwith a Weyl transformation $g_{\mu\nu} = \phi^{1/2}\, g^{(2)}_{\mu\nu}$ to absorb the dilaton kinetic term gives the 2-dim dilaton gravity theory $\frac{1}{16\pi G_2}\int d^2x\sqrt{-g}\ (\phi\mathcal{R} - \frac{6}{l^2}\phi^{1/2} + 2\lambda^2\phi^{-1/2})$. The lengthscale λ^{-1} makes the dilaton ϕ dimensionless, which then maps to the 4-dim transverse area of 2-spheres $\frac{4\pi\phi}{\lambda^2}$. With $G_{_N}$ the 4-dim Newton constant, $G_2 = \frac{G_N}{V_2}$ and $V_2 = \frac{4\pi}{\lambda^2}$, the 2-dim theory has area term $\frac{\phi}{4G_2} = \frac{4\pi r^2}{4G_{_N}}$ equivalent to the 4-dim one. Our discussion is entirely gravitational so it is reasonable to take the Planck length as the natural UV scale with $\lambda^{-1} \sim \epsilon_{UV} \sim l_P$. So finally, the dilaton is $\phi = r^2\lambda^2$ and the 2-dim metric is

$$
ds^2 = -\lambda\, r\, \frac{dU'_{D_\pm} dV'_{D_\pm}}{{W_{b'}}^2} \equiv -\frac{dU'_{D_\pm} dV'_{D_\pm}}{(W'_{b'})^2}\ , \tag{4.9}
$$

where $W'_{b'} = \frac{W_{b'}}{\sqrt{\lambda r}} = \frac{\alpha_D e^{-T_{b'}}}{\sqrt{\lambda r|f(r)|}}$ and $W_{b'}$ is the conformal factor given in (4.8).

Next, we define a new set of Kruskal coordinates for the location of the island boundary (the location of the quantum extremal surface): this turns out be in the black hole interior for the future boundary radiation region, so we require coordinate parametrizations within the black

hole horizon. Towards this, we will again first recast the Schwarzschild de Sitter metric (3.1) in the static patch in terms of Kruskal coordinates regular at the black hole horizon. So we define the tortoise coordinate r^* in terms of the parameters β_D, β_S and β_M in the same way as in (4.1), (4.2) and (4.3) in the static patch, in the vicinity of the black hole horizon, with the SdS_4 metric recast as $ds^2 = f(r)(-dt^2 + dr^{*2}) + r^2 d\Omega_2^2$. We label the spacetime coordinates in the left and right regions in the vicinity of the black hole horizon as

$$a_+ : \quad (t,r) = (t_a, a) \ , \qquad a_- : \quad (t,r) = (-t_a + \frac{i\beta}{2}, a) \ ; \qquad \beta = \frac{2\pi}{\alpha_S} \ . \tag{4.10}$$

Here also β takes care of the relative minus signs in the Kruskal coordinates in the left and right regions through $e^{i\beta\alpha_S/2} = e^{i\pi} = -1$. In the static patch around the black hole horizon, the Kruskal coordinates U_S, V_S and the Schwarzschild de Sitter metric become

$$\begin{gathered} a_+ : \qquad U_{S_+} = -e^{-\alpha_S(t_a - r^*)} \ , \quad V_{S_+} = e^{\alpha_S(t_a + r^*)}, \\ \alpha_S = \frac{1}{2\beta_S} ; \quad U_{S_+}V_{S_+} = -e^{2\alpha_S r^*} \ , \quad \frac{U_{S_+}}{V_{S_+}} = -e^{-2\alpha_S t_a} \ ; \quad ds^2 = -\frac{dU_{S_+} dV_{S_+}}{{W_a}^2} + r^2 d\Omega^2 \ , \\ W_a = \sqrt{r}\, l\, \alpha_S (r_D - r)^{-\frac{(1+2\alpha_S\beta_D)}{2}} (r - r_S)^{\frac{(2\alpha_S\beta_S - 1)}{2}} (r + r_S + r_D)^{\frac{(2\alpha_S\beta_M - 1}{2})} \ . \end{gathered} \tag{4.11}$$

The value of α_S here ensures regularity at the black hole horizon. (noting $\beta_M + \beta_S = \beta_D$ we see that W has dimensions of inverse length.) With this parametrization of the left and right time coordinates, we use the expressions in (4.11) with β doing the left-right book-keeping.

Towards parametrizing the island boundary inside the black hole horizon, we will analytically continue the spacetime coordinates defined in the static patch near the black hole horizon keeping invariant the metric in terms of the black hole interior Kruskal coordinates. Let us consider the analytic continuation in $(t_a, {r_a}^*)$ coordinates as

$$(t_a, {r_a}^*) \to \big(X_{a'} = \alpha_S(t_a - \frac{i\pi}{2\alpha_S}),\, T_{a'} = \alpha_S({r_a}^* + \frac{i\pi}{2\alpha_S})\big) \, . \tag{4.12}$$

Thus the new set of Kruskal coordinates at both the island boundaries a'_+ and a'_- are defined as (U'_{S_+}, V'_{S_+}) and (U'_{S_-}, V'_{S_-}) respectively and the Schwarzschild de Sitter metric in terms of

$(X_{a'}, T_{a'})$ coordinates becomes

$$a'_+ : \qquad U'_{S_+} = e^{-(X_{a'}-T_{a'})}\,, \qquad V'_{S_+} = e^{(X_{a'}+T_{a'})},$$
$$a'_- : \qquad U'_{S_-} = e^{(X_{a'}+T_{a'})}\,, \qquad V'_{S_-} = e^{-(X_{a'}-T_{a'})},$$

$$U'_{S_\pm}V'_{S_\pm} = e^{2T_{a'}}\ , \qquad \frac{U'_{S_\pm}}{V'_{S_\pm}} = e^{\mp 2X_{a'}}\ ; \qquad ds^2 = \frac{1}{\alpha_S^2}|f(r)|\left(-dT_{a'}^2 + dX_{a'}^2\right) + r^2 d\Omega^2,$$

$$|f(r)| = \frac{1}{l^2 r}(r_D - r)(r_S - r)(r + r_S + r_D)\ . \tag{4.13}$$

The Schwarzschild de Sitter metric in terms of Kruskal coordinates becomes

$$ds^2 = -\frac{dU'_{S_\pm}dV'_{S_\pm}}{{W_{a'}}^2} + r^2 d\Omega^2\ ,$$
$$W_{a'} = \sqrt{r}\, l\, \alpha_S (r_D - r)^{-\frac{(1+2\alpha_S\beta_D)}{2}}(r_S - r)^{\frac{(2\alpha_S\beta_S - 1)}{2}}(r + r_S + r_D)^{\frac{(2\alpha_S\beta_M - 1}{2})}\ . \tag{4.14}$$

Here also after the same dimensional reduction, as in [149], the 2-dim metric beyond the black hole horizon becomes

$$ds^2 = -\lambda\, r\frac{dU'_{S_\pm}dV'_{S_\pm}}{{W_{a'}}^2} \equiv -\frac{dU'_{S_\pm}dV'_{S_\pm}}{(W'_{a'})^2}\ , \tag{4.15}$$

where $W'_{a'} = \frac{W_{a'}}{\sqrt{\lambda\, r}} = \frac{\alpha_S e^{T_{a'}}}{\sqrt{\lambda\, r|f(r)|}}$ and $W_{a'}$ is the conformal factor given in (4.14).

4.2 Entanglement entropy: no island

In this section, we will evaluate the entanglement entropy of the radiation at late times in the absence of any island. Here we have the radiation region R within the interval b'_+ and b'_- as shown in Figure 4.1. We have chosen the bulk matter to be within the above stated interval in some fixed T slice near the future boundary. The entropy of the Hawking radiation is

$$S_{matter} = S(R)\ . \tag{4.16}$$

We calculate the bulk entropy technically using 2-dimensional techniques where we approximate the bulk matter by a 2-dim CFT propagating in the 2-dim background. In the 2-dim CFT, the matter entanglement entropy for a single interval $A = [x, y]$ is obtained from the replica formulation [111, 112] after also incorporating in $d[x, y]$ the conformal transformation to a curved space [8], stemming from the W'-factor in the 2-dim metric (4.9),

$$S_A = \frac{c}{3}\log d[x, y] \ = \ \frac{c}{6}\log\left(\frac{-\Delta U_S \Delta V_S}{W'|_x\, W'|_y}\right)\ . \tag{4.17}$$

So, we obtain the entropy of the bulk matter CFT of the radiation region as

$$S_{matter} = \frac{c}{3} \log\left[d(b'_+, b'_-)\right] . \tag{4.18}$$

Then we evaluate the bulk matter entropy near the future boundary in the Schwarzschild de Sitter geometry (4.9) to obtain (suppressing $1/\epsilon_{UV}^2$ inside the logarithm, ϵ_{UV} the UV cutoff)

$$S_{\text{matter}} = \frac{c}{6} \log\left(\frac{(U'_{D_-} - U'_{D_+})(V'_{D_+} - V'_{D_-})}{W'_{b'_+} W'_{b'_-}}\right) . \tag{4.19}$$

Using the Kruskal coordinates (4.7), the bulk matter entanglement entropy then becomes

$$S = \frac{c}{6} \log\left[16\lambda\beta_D^2 (b' - r_D) \frac{(b' - r_S)(b' + r_S + r_D)}{l^2} \sinh^2(X_{b'})\right] . \tag{4.20}$$

Alongwith ϵ_{UV}^2 and the discussions around (4.9), it can be seen that the logarithm argument is dimensionless (noting from (4.3) that β_D has dimensions of length). The details of the calculation are shown in Appendix B.1. The late time approximation is done by considering large $X_{b'}$, which means we are considering the entire constant T slice: the above result then approximates as

$$S \approx const + \frac{c}{3} X_{b'} . \tag{4.21}$$

This linear growth of the bulk matter entropy with length $X_{b'}$ means that the entropy of the radiation will eventually be infinitely larger than the Bekenstein-Hawking entropy of the black hole for large $X_{b'}$. This inconsistency is the reflection of the black hole information paradox from the future boundary point of view. See [139] for similar observations in dS_2.

To gain some intuition for this linear growth with "length" at the future boundary relative to linear growth in ordinary time, it is useful to compare the present situation with [149] where we studied the evolution of the entanglement entropy of radiation collected by observers labelled by $b_\pm$ in the left/right static diamond patches (see Fig. 4.1) at late times *i.e.* for large $|t_b|$. In our present context, the future boundary radiation region (b'_+, b'_-) is defined by spacetime coordinates (X'_b, T'_b) obtained by analytic continuation (4.6) of the spacetime coordinates $(t_b, r_b{}^*)$ defined in the static diamond patches. Geometrically, using Fig. 4.1, we see that points in the left and right static diamonds can be mapped to points near the future boundary I^+ by drawing out light rays from b_+ to b'_+ and b_- to b'_-. In the late limit with $|t_b|$ large, the points $b_\pm$ in the left/right static diamonds (left/right ends of the blue radiation regions) move towards the top end of the green lines (observer worldlines just inside the cosmological horizon). The corresponding lightrays map this to points near the

left/right ends of the future boundary, giving large lengths $|X_{b'}|$, consistent with the analytic continuation (4.6). In other words, the points $b'_{\pm}$ approach the ends of the future boundary. This is consistent with the picture of Hawking radiation from the black hole eventually crossing the cosmological horizons and reaching the future boundary, so that late times for static patch observers map to large lengths for future boundary (meta)observers. Our future boundary (meta)observers perspective here is reminiscent of the "census-taker" who looks back into the past and collect data [185]: it would be fascinating to make this precise and develop further.

4.3 Late time entanglement entropy with island

The Hawking radiation from the black hole will eventually cross the cosmological horizon and reach the future boundary (see Figure 4.1), where we imagine it is collected by appropriate (meta)observers. In this section, we will evaluate the entanglement entropy of the bulk matter near the future boundary after including appropriate islands. The island proposal [9] for the fine-grained entropy of the Hawking radiation is

$$S(R) = min\left\{ext\Big[\frac{Area(\partial I)}{4G_{_N}} + S_{matter}(R\cup I)\Big]\right\} \tag{4.22}$$

where R is the region far from the black hole where the radiation is collected by distant observers and I is a spatially disconnected island around the horizon that is entangled with R. The intuition here is that after about half the black hole has evaporated, the outgoing Hawking radiation (roughly I) begins to purify the early radiation (roughly R). This purification by the late Hawking radiation of the early radiation reflects the entanglement between the two parts, stemming from the picture of Hawking radiation as production of entangled particle pairs near the horizon (taken as vacuum). Thus $R\cup I$ purifies over time, its entanglement decreasing. The decreasing area of the slowly evaporating (approximately quasistatic) black hole then leads to $S(R)$ decreasing in time, recovering the falling Page curve expected from unitarity of the original approximately pure state.

In the current case, the future boundary receives Hawking radiation from both the left and right black hole horizons so we expect islands on both left and right. Each island almost entirely covers the corresponding black hole interior: the island boundaries are at a'_{+} and a'_{-} (Figure 4.1). The islands in question turn out to emerge just inside the black hole horizon, so

$$b' - r_D \;\gg\; r_S - a' \;\sim\; 0\ . \tag{4.23}$$

Including an island I at late times *i.e.* for large $X_{b'}$ and $X_{a'}$, the effective radiation region becomes $\Sigma_{rad}\cup I$. Now we make the assumption that the global vacuum state is approximately

pure: this is not strictly true since the bulk matter CFT is expected to be at finite dS temperature in the ambient de Sitter space. However in the limit of a small mass black hole in a very large dS space with correspondingly very low dS temperature, one can take the bulk matter to be at nearly zero temperature and correspondingly in a global pure state. With this assumption, one instead computes the entanglement entropy of the complementary region $(\Sigma_{rad} \cup I)^c$, which comprises the two intervals $[a'_+, b'_+]$ and $[b'_-, a'_-]$, which turns out to be self-consistent.

The entanglement entropy for multiple disjoint intervals

$$A = [x_1, y_1] \ \cup \ [x_2, y_2] \ \cup \ \ .... \ \ \cup \ [x_N, y_N] \tag{4.24}$$

is more complicated, arising from the multi-point correlation functions of twist operators: so it depends on not just the central charge but detailed CFT information. In the limit where the intervals are well-separated, expanding the twist operator products yields [111, 112, 113, 114]

$$S_A = \frac{c}{3} \log \frac{\prod_{i,j} d[x_j, y_i]}{\prod_{i<j} d[x_j, x_i] \ \prod_{i<j} d[y_j, y_i]} \tag{4.25}$$

For two intervals $[x_1, y_1] \cup [x_2, y_2]$, this is a limit where the cross ratio x is small, *i.e.* $x \ll 1$, with $x = \frac{d[x_1,y_1]\, d[x_2,y_2]}{d[x_1,x_2]\, d[y_1,y_2]}$, and we use the Kruskal distances in (4.17) in constructing the cross-ratio. In 2-dim CFTs with a holographic dual, this is the situation where the two intervals A, B are well-separated and their mutual information exhibits a disentangling transition [115] with $I[A, B] = S[A] + S[B] - S[A \cup B] \to 0$, *i.e.* the disconnected surface $S_{dis} = S[A] + S[B]$ has lower area than the connected surface $S_{conn} = S[A \cup B]$. Assuming an approximate global pure state, we are considering the complementary region as the 2-interval region $(\Sigma_{rad} \cup I)^c = [a'_+, b'_+] \cup [b'_-, a'_-]$. When the future boundary interval $[b'_+, b'_-]$ is large approaching the entire future boundary, the two intervals are well-separated (as seen from Figure 4.1), so the cross-ratio above is indeed small, justifying the use of (4.25) for our purposes (we have $1 - x = \frac{d[a'_+,a'_-]\, d[b'_+,b'_-]}{d[a'_+,b'_-]\, d[a'_-,b'_+]} \sim 1$ here). In this limit of approaching the entire future boundary, we have large $b'_\pm$, amounting to the assumption (4.23) here. Note that there is no holography here: we are simply applying the island rule in the 2-dim background obtained from reduction of the SdS_4 geometry and looking for self-consistent island configurations, assuming an approximate global pure state in the very low de Sitter temperature limit. It is also worth noting that while the complementary 2-interval region is unambiguously defined, the 3-interval region is more ambiguous. For instance, in Figure 4.1, one might imagine defining a global Cauchy slice as the spacelike slice passing through the points $\{\frac{(a'_- + a'_+)_L}{2}, a'_+, b'_+, b'_-, a'_-, \frac{(a'_- + a'_+)_R}{2}\}$, where the left/right endpoints are the approximate midpoints of the left/right islands (and this "unit cell" repeats indefinitely along the Penrose diagram). Then the 2-interval subregion $(\Sigma_{rad} \cup I)^c = [a'_+, b'_+] \cup [b'_-, a'_-]$ is complementary to the 3-interval subregion $\Sigma_{rad} \cup I =$

$[\frac{(a'_-+a'_+)_L}{2}, a'_+] \cup [b'_+, b'_-] \cup [a'_-, \frac{(a'_-+a'_+)_R}{2}]$ on this Cauchy slice. It would appear that there is nothing sacrosanct in choosing these midpoints $\frac{(a'_-+a'_+)_{L,R}}{2}$ to define the slice, whereas the 2-interval complement is well-defined via the radiation region and island endpoints. It would be interesting to understand this more elaborately.

In light of the above, the entanglement entropy for the complementary 2-interval region $[a'_+, b'_+] \cup [b'_-, a'_-]$ using (4.25) is

$$S_{matter} = \frac{c}{3} \log \frac{d[a'_+, a'_-]\, d[b'_+, b'_-]\, d[a'_+, b'_+]\, d[a'_-, b'_-]}{d[a'_+, b'_-]\, d[a'_-, b'_+]} \ . \tag{4.26}$$

In detail, using the Kruskal coordinates (4.7), (4.13), the total generalized entropy (4.26) becomes

$$\begin{aligned} S_{total} = \frac{2\pi a'^2}{G_{_N}} + \frac{c}{6} \log \Big[& \frac{2^4 \lambda^2}{\alpha_D^2 \alpha_S^2} (r_S - a')(b' - r_S)(\frac{r_D - a'}{l})(\frac{b' - r_D}{l}) \cdot \\ & (\frac{a' + r_S + r_D}{l})(\frac{b' + r_S + r_D}{l}) \sinh^2 X_{a'} \sinh^2 X_{b'} \Big] \\ & + \frac{c}{3} \log \Big[1 - 2 \frac{(r_S - a')^{\alpha_S \beta_S}}{(b' - r_D)^{\alpha_D \beta_D}} C(a') \cosh (X_{a'} + X_{b'}) \Big] \\ & - \frac{c}{3} \log \Big[1 - 2 \frac{(r_S - a')^{\alpha_S \beta_S}}{(b' - r_D)^{\alpha_D \beta_D}} C(a') \cosh (X_{a'} - X_{b'}) \Big] \ , \end{aligned} \tag{4.27}$$

where we have added the area term, and $C(a')$ is defined as

$$C(a') = \frac{(b' - r_s)^{\alpha_D \beta_S} (a' + r_S + r_D)^{\alpha_S \beta_M} (b' + r_S + r_D)^{\alpha_D \beta_M}}{(r_D - a')^{\alpha_S \beta_D}} \ . \tag{4.28}$$

(Note from (4.3) that $C(a')$ is dimensionless.) See Appendix B.2 for details of this calculation.

Extremizing (4.27) with respect to the location of the island boundary a' as $\frac{\partial S_{total}}{\partial a'} = 0$ gives

$$\begin{aligned} & \frac{4\pi a'}{G_{_N}} + \frac{c}{6} \Big[- \frac{1}{r_S - a'} - \frac{1}{r_D - a'} + \frac{1}{a' + r_S + r_D} \Big] \\ & - \frac{c}{3} \frac{C(a')}{\sqrt{b' - r_D} \sqrt{r_S - a'}} \Big[-1 + 2(r_S - a')(\frac{\alpha_S \beta_M}{a' + r_S + r_D} + \frac{\alpha_S \beta_D}{r_D - a'}) \Big] \cdot \\ & \qquad \Big[\frac{\cosh(X_{a'} + X_{b'})}{1 - 2 \frac{(r_S - a')^{\alpha_S \beta_S}}{(b' - r_D)^{\alpha_D \beta_D}} C(a') \cosh (X_{a'} + X_{b'})} \\ & \qquad\quad - \frac{\cosh(X_{a'} - X_{b'})}{1 - 2 \frac{(r_S - a')^{\alpha_S \beta_S}}{(b' - r_D)^{\alpha_D \beta_D}} C(a') \cosh (X_{a'} - X_{b'})} \Big] = 0 \ . \end{aligned} \tag{4.29}$$

Here, since r_D is large, the terms scaling as $O(\frac{1}{r_D})$ can be ignored: thus the $\frac{1}{a'+r_S+r_D}$ and $\frac{1}{r_D-a'}$ are suppressed relative to $\frac{1}{r_S-a'}$. With these approximations, (4.29) becomes

$$\frac{4\pi a'}{G_N} - \frac{c}{6}\frac{1}{r_S-a'} + \frac{c}{3}\frac{C(a')}{\sqrt{b'-r_D}\sqrt{r_S-a'}} \cdot \Big[\frac{\cosh(X_{a'}+X_{b'})}{1-2\frac{(r_S-a')^{\alpha_S\beta_S}}{(b'-r_D)^{\alpha_D\beta_D}}C(a')\,\cosh\left(X_{a'}+X_{b'}\right)} - \frac{\cosh(X_{a'}-X_{b'})}{1-2\frac{(r_S-a')^{\alpha_S\beta_S}}{(b'-r_D)^{\alpha_D\beta_D}}C(a')\,\cosh\left(X_{a'}-X_{b'}\right)}\Big] = 0\,. \tag{4.30}$$

Next, extremizing (4.27) with respect to $X_{a'}$ as $\frac{\partial S_{total}}{\partial X_{a'}} = 0$ gives

$$\coth X_{a'} = 2\sqrt{\frac{r_S-a'}{b'-r_D}}C(a')\cdot\Big[\frac{\sinh(X_{a'}+X_{b'})}{1-2\frac{(r_S-a')^{\alpha_S\beta_S}}{(b'-r_D)^{\alpha_D\beta_D}}C(a')\,\cosh\left(X_{a'}+X_{b'}\right)} - \frac{\sinh(X_{a'}-X_{b'})}{1-2\frac{(r_S-a')^{\alpha_S\beta_S}}{(b'-r_D)^{\alpha_D\beta_D}}C(a')\,\cosh\left(X_{a'}-X_{b'}\right)}\Big] \tag{4.31}$$

We will consider all possible conditions between $X_{a'}$ and $X_{b'}$ in the extremization equations to look for consistent solutions to the location of island boundary, *i.e.* the value of a' and $X_{a'}$.

We will first consider, $X_{a'} = X_{b'} \Rightarrow X_{a'} - X_{b'} = 0$ and $X_{a'} + X_{b'} = 2X_{a'}$ for large $X_{a'}$ and $X_{b'}$. Then (4.31) becomes

$$1 - 2\sqrt{\frac{r_S-a'}{b'-r_D}}C(a')\cosh 2X_{a'} = 2\sqrt{\frac{r_S-a'}{b'-r_D}}C(a')\frac{\sinh 2X_{a'}}{\coth X_{a'}} \tag{4.32}$$

Putting this condition (4.32) back in (4.30) gives

$$\frac{4\pi a'}{G_N} - \frac{c}{6}\frac{1}{r_S-a'} + \frac{c}{3}\frac{C(a')}{\sqrt{b'-r_D}\sqrt{r_S-a'}}\Big[\frac{\cosh(2X_{a'})}{2\frac{(r_S-a')^{\alpha_S\beta_S}}{(b'-r_D)^{\alpha_D\beta_D}}C(a')\frac{\sinh 2X_{a'}}{\coth X_{a'}}} - 1\Big] = 0$$

$$\Rightarrow \quad \frac{4\pi a'}{G_N} - \frac{c}{3}\frac{C(a')}{\sqrt{b'-r_D}\sqrt{r_S-a'}} - \frac{c}{6}\frac{1}{r_S-a'}\Big(1-\frac{\coth X_{a'}}{\tanh 2X_{a'}}\Big) = 0\,. \tag{4.33}$$

For large $X_{a'}$ and $X_{b'}$, the third term in (4.33) is small compared to the second term. So we can ignore the third term and (4.33) becomes

$$a' \simeq \frac{1}{\sqrt{r_S-a'}}\,\frac{G_N c}{12\pi}\,\frac{1}{\sqrt{b'-r_D}}\,C(a')\,. \tag{4.34}$$

Now we recall that we are in the semiclassical regime where

$$0 \ll c \ll \frac{1}{G_N}\,, \tag{4.35}$$

so that the classical area term in the generalized entropy is dominant but the bulk matter makes nontrivial subleading contributions (which are not so large as to cause significant backreaction on the classical geometry).

We are looking for an island with boundary $a' \sim r_S$ near the black hole horizon: this corroborates with the fact that since the entire right hand side in (4.34) is $O(G_N c)$, in the classical limit $G_N c = 0$ we obtain $a'\sqrt{r_s - a'} \simeq O(G_N c) \sim 0$ giving $a' = r_S$, *i.e.* the quantum extremal surface localizes on the black hole horizon. Thus we can solve the above extremization equation in perturbation theory setting $a' \sim r_S$ at leading order to find the first order correction in $G_N c \ll 1$: then schematically we have

$$r_S - a' \simeq \frac{K^2}{r_S^2}\frac{1}{b' - r_D} \ , \qquad K = \frac{G_N c}{12\pi} C(r_S) \ , \tag{4.36}$$

Thus, we finally obtain (with $C(r_S)$ from (4.28) setting $a' = r_S$)

$$a' \simeq r_S - \frac{(G_N c)^2}{144\pi^2 r_S^2 (b' - r_D)} C(r_S)^2. \tag{4.37}$$

Solving now for $X_{a'}$ from (4.31), we obtain

$$\cosh 2X_{a'} = \frac{6\pi}{G_N c}\frac{r_S(b' - r_D)}{C(r_S)^2}\frac{\coth X_{a'}}{\tanh 2X_{a'} + \coth X_{a'}} \ . \tag{4.38}$$

This is a large $X_{a'}$ value with $e^{2X_{a'}}$ scaling approximately as $O(\frac{1}{G_N c})$. Considering $X_{a'} \sim -X_{b'}$ does not yield consistent island solutions: see App. B.3.2. Further, considering potential island solutions just outside the horizon turns out to be inconsistent: see App. B.3.1. Thus (4.37), (4.38), with $X_{a'} \sim X_{b'}$, encode the correct island solution for the future boundary radiation region. The condition $X_{a'} = X_{b'}$ is consistent with the expectation that the island location lies on the same Cauchy slice as the radiation region location (along the same lines as the condition $t_a = t_b$ within the static diamond in [149])). This amounts to the requirement of spacelike separation in considering the island and radiation as an effectively single entity which purifies so the fact that we recover this is not surprising. The fact that islands outside the horizon are inconsistent is due to causality: the entanglement wedge cannot lie within the causal wedge (we explain this further in the Discussion sec. 4.4).

With the value of a' in (4.37) and $X_{a'}$ in (4.38), the total on-shell entanglement entropy in (4.27) becomes

$$S_{o.s} = \frac{2\pi r_S^2}{G_N} - \frac{c^2 G_N}{36\pi r_S (b' - r_D)} C(r_S)^2 \qquad (4.39)$$
$$+ \frac{c}{6} \log \left[\frac{16\lambda^2 \beta_s^2 \beta_D^2 (b' - r_D)^2}{l^4} \frac{(r_D - r_S)^{1+2\alpha_S \beta_D}}{(b' - r_S)^{2\alpha_S \beta_D - 1} (2r_S + r_D)^{2\alpha_S \beta_M - 1} (b' + r_S + r_D)^{2\alpha_S \beta_M - 1}} \right].$$

which is independent of length $X_{a'}$ and $X_{b'}$, stemming from the presence of the island. The leading first (area) term is twice the Bekenstein-Hawking entropy of the black hole, while the subleading second and third terms arising from the bulk entropy of the radiation region purified by the island are constant terms not growing in length. This recovers the expectations on the Page curve for the entropy of the bulk matter or Hawking radiation considered near the future boundary. The bulk matter at the future boundary radiation region is entangled with the island-like region located just inside the black hole interior in these semiclassical approximations at very low ambient de Sitter temperature.

Comparing the entanglement entropy without the island (4.21) and that with the island (4.39) provides the critical length X_{Page} at which the island transition occurs: we obtain

$$\frac{c}{3} X_{Page} \sim 2 S_{BH} \qquad \Rightarrow \qquad X_{Page} \sim \frac{6\pi {r_S}^2}{G_N c} . \qquad (4.40)$$

The entropy with the island alongwith the associated purification is lower and dominates over the no-island configuration beyond this critical length X_{Page}. Note that here the critical Page length X_{Page} is a dimensionless quantity, using (4.6). This then corresponds to a Page time $t_P \sim \beta_D X_{Page}$ which using (4.3) and the approximations (3.4) gives the large value $t_P \sim l S_{BH}$ (note that this uses the cosmological Kruskal coordinates, distinct from the black hole Kruskal coordinates in [149]). It is however important to note that this Page length is much smaller than another potentially relevant quantity $X_P^{dS} \sim S_{dS}$ controlled by the entropy S_{dS} of the cosmological horizon. In the small black hole limit (3.4) we are considering, $S_{dS} \sim \frac{l^2}{G_N} \gg S_{BH} \sim \frac{r_S^2}{G_N}$, and we do not see any effects above, stemming from the ambient de Sitter space which is just a frozen background. So our critical Page length (4.40) controlled by black hole entropy alone is consistent with the separation of scales in the limit (3.4). Away from this limit, the black hole horizon shrinks while the cosmological horizon absorbs and grows, resulting in a nontrivial nonequilibrium system. It would of course be interesting to understand de Sitter horizon physics, but this appears substantially more challenging within our framework.

Finally, it is worth noting that there are also timelike separated quantum extremal surface solutions following from the extremization of the generalized entropy with respect to the future

boundary observer: we discuss these solutions in App. B.4. The timelike separation implies that the on-shell generalized entropy becomes complex valued. While complex entropies are known in investigations in pure de Sitter space (which does not have a sufficiently wide Penrose diagram) and suggest new objects [180], [181], [182], [183], [184], it is consistent to ignore them in the Schwarzschild de Sitter context where spacelike separated quantum extremal surfaces do exist in accord with physical Page curve expectations for the black hole information paradox.

4.4 Discussion

We recall that in [149], the radiation region was within the static diamond (with endpoints b_+ or b_- in the left or right static diamond, in Figure 4.1). The late time island location was then found to be within the static diamond, just outside the black hole horizon in that case. As we have seen, the island location we have found currently is just inside the black hole horizon, which at first sight might seem contradictory. However this is in fact consistent in the current case. First, the future boundary interval (b'_+, b'_-) in the present case receives Hawking radiation from both the left and right black hole patches, propagating past the left and right cosmological horizons bounding the left and right static diamonds. So this setup is physically distinct from the previous case of a single static diamond. Secondly, in obtaining the island locations we have been considering the limit of large $X_{a'}, X_{b'}$, in the extremization equations. In this limit the future boundary interval (b'_+, b'_-) approaches the entire future boundary, *i.e.* the points $b'_\pm$ approach the endpoints of I^+. Note that the left and right static diamonds are now within the causal wedge of this interval. It would then be causally inconsistent for the entanglement wedge to be within the causal wedge of the radiation interval. The entanglement wedge of the radiation region is the domain of dependence, or bulk causal diamond of the spacelike surface between the boundary of the radiation region and the island boundary (location of quantum extremal surface). As it stands, the island boundary is just inside the black hole horizon so it lies outside the causal wedge, nicely avoiding inconsistency.

The black hole interior island solution is ultimately supported by the calculational fact that other possibilities lead to inconsistencies: for instance, blindly looking for island solutions outside the horizon in the present case exhibits inconsistency in the extremization equations. We carried out this exercise by performing the calculation of sec. 4.3 using static diamond Kruskal coordinates for the potential island lying just outside the black hole horizon in the static diamond ($a' \gtrsim r_s$ in this case, somewhat akin to the parametrizations in [149]). The analog of (4.27) in this case leads to extremization equations similar to (4.29) and (4.31): however there are subtle differences which ensure that the analogs of (4.32) and (4.33) together

do not give consistent island solutions (see App. B.3.1). Further, as we also noted after (4.38), potential island solutions with $X_{a'} = -X_{b'}$ (instead of $X_{a'} = X_{b'}$) also lead to inconsistencies (App. B.3.2). Thus overall, our semiclassical island solution in (4.37) and (4.38) should be regarded as nontrivial. Perhaps the self-consistency of these calculations (in particular using the complementary 2-interval bulk matter entropy) also vindicates the assumption of approximate purity of the initial matter that made the black hole in this very low temperature de Sitter ambience. It would be interesting to explore this in more detail, as discussed around (4.25).

The Schwarzschild de Sitter (SdS) black hole is unstable and thus somewhat different from the AdS black hole. In our small black hole limit (3.4) the ambient de Sitter space effectively remains a frozen background reservoir. In a quasistatic approximation, the black hole evaporates away slowly, and our analysis using the eternal SdS black hole shows the radiation entanglement entropy including the island becoming saturated at some finite value (4.39), approximately $2S_{BH}$ (so the Page curve saturates rather than falls). As the black hole evaporates, its entropy decreases so the saturation value of the radiation entropy decreases leading to the black hole Page curve falling slowly in accord with the approximately pure state that the black hole formed from. Strictly speaking, the ambient de Sitter space temperature (albeit much lower than that of the black hole) implies that the pure state consideration is just an approximation. It would be interesting to study the SdS black hole modelling the bulk matter CFT in the thermal state at finite de Sitter temperature.

The separation of scales in the small black hole limit (3.4) ensures that black holes can be regarded as localized subsystems analyzable by distinct classes of observers (or metaobservers). Then, abstracting away from our technical analysis in Schwarzschild de Sitter black holes vindicates some general lessons for the black hole information paradox here as well. Islands appear to emerge self-consistently evading paradoxes with (i) unitarity as encapsulated by the Page curve (late static patch times and large future boundary lengths), (ii) causality (the island boundary does not lie within the causal wedge), (iii) overcounting (the purifying island is spacelike separated from the radiation, lying on the same Cauchy slice). In this light, de Sitter space itself and cosmological horizons appear exotic: extremal surfaces anchored at the future boundary involve timelike separations (*e.g.* [118], [134], for quantum extremal surfaces, and [180], [181], [182], [183], [184] for classical RT/HRT surfaces). So de Sitter space, and perhaps cosmology more generally, require new insights.

Chapter 5

Study of black hole information paradox: Conclusions

In the chapters 3 and 4 of this thesis, we have focused on the study of the evolution of the entanglement entropy of Hawking radiation for both the radiation regions in the static diamond and close to the future boundary, respectively, for a small Schwarzschild de Sitter black hole geometry. This study leads to the black hole information problem. We have shown that this information problem is a paradox. A Partial resolution of this paradox can be achieved by preserving unitarity, followed by the study of the quantum extremal surface and island in the semiclassical analysis of the black hole evaporation. The reason we are calling the resolution partial is that the semiclassical description of the gravity theory can only tell us about the entropy of the Hawking radiation; we still do not know the precise quantum state of the Hawking radiation, for which we are computing the entropy. In other words, the entire semiclassical analysis we have shown here cannot provide the microscopic details of the black hole evaporation from the gravity description. So we should emphasize that this important aspect of the black hole information problem remains unresolved. In this chapter, we summarize our investigations and key results, presented in the earlier chapters, and also mention Some possible future directions.

In chapter 3, we have studied 4-dim "small" Schwarzschild de Sitter black holes (3.1) with mass m and de Sitter scale l in the limit $m \ll l$ where the de Sitter temperature is very low compared with that of the black hole (3.4), (3.5). In this regime which has qualitative parallels with a flat space limit (3.6), the black hole evaporation process is well-separated from any physics of de Sitter space which can be regarded as a frozen background. Strictly speaking the pure state input can only be approximately true in de Sitter where it is consistent to have bulk matter in a thermal state at the de Sitter temperature. However in the limit of very

low de Sitter temperature, the ambient de Sitter space is behaving approximately like a zero temperature bath. In this regime then, we recover the expectations on the Page curve for the Hawking radiation in the black hole evaporation process, incorporating appropriate island contributions, as we have seen. We are simply regarding this as a gravitational system of a black hole in de Sitter space, with no explicit recourse to holography or string theory (although one might generically expect gravity to be intrinsically holographic): this is consistent with the island rule via replica wormholes which does not rely on holography. It is unclear if we can shed light on questions about microstates here: however perhaps embedding into some AdS (via a dS bubble with a black hole) may be a way to approach this in principle.

In chapter 4, we have studied small 4-dim Schwarzschild de Sitter black holes in the limit of very low de Sitter temperature, building further on previous work [149] for observers within the static diamond far from the black hole horizon. In the present work, we have been considering the black hole Hawking radiation in a radiation region interval at the future boundary (see Figure 4.1). The black hole mass is adequately large that quasistatic approximations to the evaporating black hole in semiclassical gravity are valid. We assume the black hole radiation approximated as a 2-dim CFT at nearly zero temperature propagating in a 2-dim dilaton gravity background (4.9) obtained by dimensional reduction of the 4-dim spacetime. Including appropriate island contributions, we find that the generalized entropy satisfies expectations from the Page curve for the evolution of bulk matter near the future boundary. Our analysis has parallels with [139] which studied island resolutions for dS_2 JT gravity with regard to the future boundary. Our setup here is somewhat more complicated since the assumption of an approximate global pure state is only reasonable, if at all, at very low de Sitter temperature. The fact that these approximate calculations vindicate the island paradigm perhaps suggests the existence of better, more fundamental ways to formulate the information paradox in such nontrivial gravitational backgrounds and of deeper insights into replica wormholes in these sorts of quasistatic gravitational backgrounds.

More broadly, in our entire analysis, de Sitter space plays very little role, although the black hole Kruskal coordinates we employed do encode detailed aspects of the de Sitter space. Strictly speaking an intermediate regime where the black hole temperature is comparable to the de Sitter temperature will require a more detailed analysis of bulk CFT matter in a mixed state corresponding to the thermal state at the de Sitter temperature, and would be interesting to study as a nontrivial nonequilibrium situation. The regions in Schwarzschild de Sitter parameter space we have explored are very far from the Nariai (extremal) limit where a dS_2 throat emerges: see *e.g.* [137, 138, 139, 140] for some recent investigations on the latter. Our island solution (3.38) emerges as a self-consistent solution near the black hole horizon in the regime of very low de Sitter temperature: it would seem that the extremization equation (3.34) has other solutions as well, pertaining to other regimes of more cosmological relevance,

worth exploring. These might dovetail with various studies on quantum extremal surfaces and cosmologies *e.g.* [117]-[135], and perhaps broader issues with de Sitter space *e.g.* [141].

Our discussions of Schwarzschild de Sitter are entirely within the bulk framework of semiclassical gravity, with no holography per se (except in the broad sense of gravity being intrinsically holographic). The future boundary is well-defined as a place where gravity is manifestly weak: however we have simply applied the island formulation in these relatively complicated higher dimensional models under various assumptions and approximations without rigorous justification. So this appears to stretch the regimes of validity of the original island proposals, although it corroborates the general expectations laid out in [18]. It would be nice to better understand in more fundamental ways the deeper underpinnings of semiclassical gravity that encode these self-consistent island formulations of the black hole information paradox. In this regard it might be interesting to understand the interplay between the generalized entropy and its extremization and gravity actions (see *e.g.* [186], [187], [188], [139]) in the context of the general 2-dim dilaton gravity theories (4.9) we consider here arising from reduction of SdS_4.

Especially [139] has some close parallels with our study of the island for a meta observer at the future boundary described in chapter 4: in [139], the authors have studied islands for a radiation region at the future boundary in dS_2 arising under the dimensional reduction of the four-dimensional Schwarzschild-de Sitter (SdS_4) black hole in the near-Nariai limit. They have shown that in the dS_2 JT gravity, for the radiation collected at the future infinity, non-trivial islands appear a little inside the horizons of the black hole regions on both left and right cosmological horizons. These islands purify the radiation region, and the total entropy of the radiation region, together with these islands, obey the Page curve. Here, the global state of the matter is considered to be pure in the dS_2 JT gravity. However, in our work, we made an important assumption that the global state of the matter in the radiation region, together with islands, is considered to be pure only at a very low de Sitter temperature in generic 2d dilaton gravity. In [122], the author has studied islands for the static patch observer in pure dS_2 reduced from the 3-dimensional pure de Sitter background. Here, while computing the entanglement entropy between the states inside and outside the cosmological horizon, a non-trivial island appears far away from the cosmological horizon and moving backwards in time. Including this island, it turns out that the Page curve can be obtained, and it is bound to a value corresponding to the Gibbons-Hawking entropy. In [119], authors have studied islands in more general spacetimes, in particular 4-dimensional FRW spacetime.

Part II

No-boundary extremal surfaces in slow roll inflation and other cosmologies

Chapter 6

de Sitter Extremal Surfaces

It is of great interest to understand cosmology from the point of view of holography [31, 32, 33]. One of the many fascinating aspects of our understanding of holography in AdS-like spaces is the Ryu-Takayanagi formulation of holographic entanglement entropy [14, 15, 16, 17] and its many ramifications. Towards exploring these quantum information ideas in cosmological contexts, it is fascinating to look at de Sitter space as a idealized example of cosmology. This however already has many new features. Thinking of time as the holographic direction, a natural boundary for de Sitter space is in the far future (or past), leading to dS/CFT [189, 190, 191, 192] (see *e.g.* [193, 194, 195] for reviews on de Sitter space and its entropy [97]).

Certain generalizations of the Ryu-Takayanagi formulation of AdS holographic entanglement to de Sitter space were studied in [180, 196, 181, 197, 182, 198, 136, 183, 184, 199]. These pertain to RT/HRT extremal surfaces anchored at the dS future boundary I^+ and amount to considering the bulk analog of setting up entanglement entropy in the dual CFT at I^+, in part towards understanding if de Sitter entropy [97] can be understood as some sort of holographic entanglement entropy. Analysing the extremization shows that surfaces anchored at I^+ do not return to I^+. In entirely Lorentzian dS, this leads to future-past timelike surfaces stretching between $I^\pm$ with pure imaginary area. With a no-boundary type Hartle-Hawking boundary condition, the top half of these timelike surfaces joins with a spacelike part on the hemisphere giving a complex-valued area [183], [184] (and [200, 201] for dS_3/CFT_2). The real part of the area arises from the hemisphere and is precisely half de Sitter entropy (Figure 6.1). Some of these structures [182, 198, 136] are akin to space-time rotations from AdS (some related discussions appear in [202]). In [199], certain analytic continuations were discussed which in fact amount to space-time rotations from AdS.

Recent investigations suggest that the areas of these extremal surfaces are best interpreted as encoding pseudo-entropy or time-entanglement [183], [184], entanglement-like structures involving timelike separations. Pseudo-entropy [203] is the entropy based on the transition matrix $|f\rangle\langle i|$ regarded as a generalized density operator (see also [204]-[216] for some partially related work). In some sense this is perhaps the natural object here since the absence of $I^+ \to I^+$ returns for extremal surfaces suggests that extra data is required in the interior, somewhat reminiscent of scattering amplitudes (equivalently the time evolution operator), and of [190] viewing de Sitter space as a collection of past-future amplitudes. This is also suggested by the dS/CFT dictionary $Z_{CFT} = \Psi_{dS}$ [191]: boundary "entanglement entropy" formulated via Z_{CFT} translates to a bulk object formulated via the Wavefunction Ψ_{dS} (a single ket, rather than a density matrix), leading (not surprisingly) to non-hermitian structures. In [199], fuelled by the analytic continuation, a heuristic version of the Lewkowycz-Maldacena argument [217, 218, 219, 220] (see also [221]) was constructed for the no-boundary de Sitter extremal surfaces for maximal (IR) subregions. Roughly the boundary replica argument on Z_{CFT} translates now to a bulk replica argument on the Wavefunction Ψ_{dS} which is essentially pseudo-entropy. The area now is interpreted as the amplitude for creation of a cosmic brane that localizes on the part Euclidean, part timelike no-boundary extremal surface.

6.1 Reviewing de Sitter extremal surfaces

In this section, we briefly review [184, 199] and previous work here on generalizations of RT/HRT extremal surfaces to de Sitter space (see also [183]). These involve considering the bulk analog of setting up entanglement entropy in the dual Euclidean CFT on the future boundary [180], restricting to some boundary Euclidean time slice, defining subregions on these, and looking for extremal surfaces anchored at I^+ dipping into the time (holographic) direction. Analysing this shows that there are no spacelike surfaces connecting points on I^+. In entirely Lorentzian dS, there are future-past timelike surfaces stretching between $I^\pm$ [182, 136], akin to rotated analogs of the Hartman-Maldacena surfaces [233] in the eternal AdS black hole [234]: these have pure imaginary area, relative to AdS spacelike RT/HRT surfaces. With a no-boundary type Hartle-Hawking boundary condition, the top half of these timelike surfaces joins with a spacelike part on the hemisphere giving a complex-valued area [183], [184] (and [200, 201] for dS_3/CFT_2). The real part of the area arises from the hemisphere and is precisely half de Sitter entropy. Due to the presence of timelike components in these extremal surfaces, these areas are best interpreted as pseudo-entropy, as we see below. From the dual side, in various toy models of "entanglement entropy" in ghost-like theories, complex-valued entropies arise naturally [235, 236] (see also [237]): the negative norm states here lead to

imaginary components. It is worth noting that the adjoints of states are nontrivial in such ghost-like theories so these are perhaps more correctly thought of as pseudo-entropy.

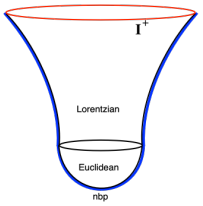

Figure 6.1: No-boundary de Sitter space, with the top Lorentzian region continuing smoothly into the Euclidean hemisphere region ending at the no-boundary point. Also shown are IR no-boundary extremal surfaces (blue) anchored at the future boundary I^+ dipping into the time direction, timelike in the Lorentzian region and going around the hemisphere.

These dS extremal surfaces can also be realized via analytic continuations from AdS (reviewed below). This suggests a natural way to obtain the no-boundary de Sitter extremal surface areas through a heuristic replica argument [199] involving an analytic continuation of the Lewkowycz-Maldacena formulation [217] in AdS to derive RT entanglement entropy (generalized in [218], [219], [220]; see also [221] and the review [17]). The crucial difference here is that since the analytic continuation maps Z_{bulk}^{AdS} to the de Sitter Wavefunction Ψ_{dS}, this is now a replica formulation on Ψ_{dS}, considering the dS/CFT dictionary $Z_{CFT} = \Psi_{dS}$ [191]. With the Wavefunction Ψ_{dS} regarded as an amplitude (or transition matrix from "nothing"), this gives pseudo-entropy. In particular the codim-2 brane that smooths out bulk (orbifold) singularities is now a time-evolving, part Euclidean, part timelike, brane. This gives a complex area semiclassically, with the real part from the Euclidean hemisphere and the timelike part pure imaginary. In this Lewkowycz-Maldacena formulation, the area of these no-boundary dS extremal surfaces arises as the amplitude for cosmic brane creation. So it is important that the divergent pieces of the area arising from near the future boundary are pure imaginary, since otherwise this amplitude would diverge. As it is, there is a finite probability: the real part arises from the maximal hemisphere, with size set by dS entropy.

Overall, directly analysing the bulk extremization and calculating the no-boundary extremal surface areas for the IR (maximal) subregions at the future boundary gives

$$(dS_4) \quad S_{nb} = -i\,\frac{\pi l^2}{2G_4}\frac{R_c}{l} + \frac{\pi l^2}{2G_4}\,; \qquad (dS_3) \quad S_{nb} = -i\frac{l}{2G_3}\log\frac{R_c}{l} + \frac{\pi\, l}{4G_3}\,, \tag{6.1}$$

with the pure imaginary piece from the top Lorentzian part of dS and the real piece (precisely half de Sitter entropy) from the Euclidean hemisphere. These can also be realized via analytic continuations from the AdS RT surfaces which all lie on a constant time slice. Under the $dS \leftrightarrow AdS$ analytic continuation, this AdS constant time slice continues to dS as

$$\begin{aligned} ds^2_{(r>L)} &= \frac{dr^2}{1+\frac{r^2}{L^2}} + r^2 d\Omega^2_{d-1} \quad \xrightarrow{L\to -il} \quad ds^2_{(r>l)} = -\frac{dr^2}{\frac{r^2}{l^2}-1} + r^2 d\Omega^2_{d-1}\,, \\ ds^2_{(r<L)} &= \frac{dr^2}{1+\frac{r^2}{L^2}} + r^2 d\Omega^2_{d-1} \quad \xrightarrow{L\to -il} \quad ds^2_{(r<l)} = \frac{dr^2}{1-\frac{r^2}{l^2}} + r^2 d\Omega^2_{d-1}\,. \end{aligned} \tag{6.2}$$

The AdS boundary at $r \to \infty$ maps to the dS future boundary I^+ at $r \to \infty$, and the AdS region $r \in [L, \infty]$ maps to the dS future universe F parametrized by $r \in [l, \infty]$ (and r is time here). The dS hemisphere is $\tau_E = -it = [0, \frac{\pi}{2}]$ where $-\frac{dr^2}{\frac{r^2}{l^2}-1} > 0$ is Euclidean.

The global dS_{d+1} metric with S^d cross-sections, restricted to any equatorial S^d plane is identical to the $t = const$ slice of the (Lorentzian) dS static coordinatization (6.2), above:

$$ds^2_{global}\Big|_{\theta_d=const} = -d\tau^2 + l^2 \cosh^2 \frac{\tau}{l}\, d\Omega^2_{d-1} \quad = \quad -\frac{dr^2}{\frac{r^2}{l^2}-1} + r^2 d\Omega^2_{d-1} = ds^2_{static}\Big|_{t=const}, \tag{6.3}$$

using $r = l \cosh \frac{\tau}{l}$. Thus a generic equatorial plane in global dS defines the same boundary Euclidean time slice as the $t = const$ slice in the dS static coordinatization, and we will continue to use the parametrization (6.2).

The IR AdS surface space spans the entire AdS boundary sphere. This continues to the IR dS extremal surface (when the subregion becomes the whole space at I^+), going from $r \to \infty$ to $r = l$ as a timelike surface in the Lorentzian dS region and then in the hemisphere from $r = l$ to $r = r_* = 0$ (where it turns around). The turning point r_* only exists in the Euclidean (hemisphere) part of dS.

This IR surface starts at the boundary of the maximal subregion of the S^{d-1} (*i.e.* hemisphere) so it is anchored on the equator of the S^{d-1} (red curve in Figure 6.1) and wraps the equatorial S^{d-2}. From (6.2), it is clear that the IR dS extremal surface becomes a space-time rotation of that in AdS. Its area continues as (with R_c a cutoff at large r)

$$\begin{aligned} \frac{V_{S^{d-2}}}{4G_{d+1}} \int_0^{R_c} \frac{r^{d-2}dr}{\sqrt{1+\frac{r^2}{L^2}}} \quad \xrightarrow{L\to -il} \quad & \frac{V_{S^{d-2}}}{4G_{d+1}} \int_0^{l} \frac{r^{d-2}dr}{\sqrt{1-\frac{r^2}{l^2}}} + \frac{V_{S^{d-2}}}{4G_{d+1}} \int_l^{R_c} r^{d-2} \sqrt{\frac{dr^2}{-(\frac{r^2}{l^2}-1)}}\,, \\ & = \frac{1}{2}\frac{l^{d-1}V_{S^{d-1}}}{4G_{d+1}} - i\#\frac{l^{d-1}}{4G_{d+1}}\frac{R_c^{d-2}}{l^{d-2}} + \dots \end{aligned} \tag{6.4}$$

where the $\dots$ are subleading imaginary terms. For $AdS_4 \to dS_4$ and $AdS_3 \to dS_3$, we obtain

$$\frac{V_{S^1}}{4G_4} \int_0^{R_c} \frac{rdr}{\sqrt{1+\frac{r^2}{L^2}}} = \frac{\pi L^2}{2G_4}\Big(\frac{R_c}{L} - 1\Big) \quad \to \quad -i\frac{\pi l^2}{2G_4}\frac{R_c}{l} + \frac{\pi l^2}{2G_4} = S^{IR}_{dS_4}\,, \tag{6.5}$$

$$\frac{V_{S^0}}{4G_3} \int_0^{R_c} \frac{dr}{\sqrt{1+\frac{r^2}{L^2}}} = \frac{2L}{4G_3} \log \frac{R_c}{L} \quad \to \quad -i\frac{l}{2G_3} \log \frac{R_c}{l} + \frac{\pi l}{4G_3} = S^{IR}_{dS_3}\,. \tag{6.6}$$

These extremal surfaces can also be described explicitly in dS_3 for more general boundary subregions (and for near maximal subregions in dS_{d+1}). Drawing out the extremal surfaces geometrically leads to a natural geometric identification of the bulk subregion dual to a boundary

subregion as an appropriate "pseudo-entanglement" wedge defined as the appropriate domain of dependence bounded by the boundary subregion at I^+ and the extremal surface. However it is *only* for maximal subregions that this leads to consistent disjoint bulk subregions corresponding to disjoint boundary subregions, and thereby a version of subregion-subregion duality. Thus maximal (IR) subregions appear to be the only well-defined subregions geometrically from the perpective of subregion duality.

Chapter 7

No-boundary extremal surfaces in slow-roll inflation and other cosmologies

In this chapter, we study no-boundary extremal surfaces[1] in slow-roll inflation models, with certain inflationary cosmological perturbations to no-boundary de Sitter space which preserve the spatial spherical isometry of dS in global coordinates. These perturbations are described by scalar inflaton perturbations defined imposing regularity at the no-boundary point: this induces corresponding metric perturbations as well (see Figure 7.1). The perturbations have explicit analytic (although still adequately complicated) expressions to $O(\epsilon)$ in the slow-roll parameter ϵ, as described in [223] (and related previous work *e.g.* [222]-[229] that we found useful). This allows us to perform explicit analytic calculations of the no-boundary extremal surface areas and compare them with the Wavefunction. As in de Sitter, we consider maximal (IR) subregions on equatorial plane slices regarded as boundary Euclidean time slices, and look for codim-2 extremal surfaces dipping into the bulk time direction. These are, mostly, entirely timelike in the top Lorentzian part, going around the Euclidean hemisphere. However now the inflationary perturbations induce small wiggles around pure de Sitter, so the metric has various interesting real and imaginary pieces. Thus the no-boundary extremal surface areas now have nontrivial real and imaginary pieces which now arise from both the Euclidean hemisphere and the Lorentzian timelike regions. In general it turns out that the corresponding area integrals must be regarded carefully in the complex time-plane defining appropriate contours (Figure 7.2) that avoid extra poles at the complexification point that arise from

[1]The phrase "no-boundary extremal surface" refers to the Hartle-Hawking type nature of these surfaces in no-boundary de Sitter space [222], not to be confused with the fact that the surfaces are anchored at an asymptotic (future) boundary. Similar comments apply to the no-boundary slow-roll inflation studies here.

the slow-roll perturbations (similar in spirit to calculations of the semiclasical Wavefunction of the Universe). Doing this carefully, we eventually find divergent pure imaginary pieces from near the future boundary as well as real and imaginary finite slow-roll corrections to the leading half de Sitter entropy $\frac{\pi l^2}{2G_4}$ contribution from the hemisphere. For example, we obtain (7.16) in dS_4 slow-roll inflation with the finite parts being $\frac{\pi l^2}{2G_4}\left(1+\epsilon\left(\log 4-\frac{7}{2}+i\pi\right)\right)$. These finite $O(\epsilon)$ corrections precisely match the finite $O(\epsilon)$ corrections in the expansion of the semiclassical Wavefunction of the Universe (equivalently the on-shell action) in slow-roll inflation described in [223]. This is consistent with the Lewkowycz-Maldacena interpretation in [199] of these no-boundary extremal surface areas giving the probability for cosmic brane creation but now in the slow-roll no-boundary geometry.

We do a similar calculation for dS_3 slow-roll inflation as well, with similar spatial spherical symmetry preserving inflaton perturbations and corresponding metric ones. The no-boundary extremal surface areas again have real and imaginary slow-roll corrections. We find that the real finite $O(\epsilon)$ corrections again match those in the expansion of semiclassical Wavefunction (or on-shell action), but the imaginary finite parts do not match. This is likely due to the fact that the boundary reflects a CFT on an even dimensional sphere, with potential extra pure imaginary terms that arise from anomalies. The probabilities, controlled by the real parts, match.

To put this in perspective, it is worth recalling the behaviour of minimal RT surfaces in the AdS black hole [14, 15]. As the boundary subregion size increases, the RT surface dips deeper into the bulk and in the IR limit (maximal subregion), the surface wraps the black hole horizon. The finite part of holographic entanglement entropy then becomes black hole entropy which is the thermal entropy of the dual field theory: this entropy can also be realized from the on-shell action regarded as a partition function [230] (see also [231, 232]). In the de Sitter case with surfaces anchored at the future boundary, the only turning points are in the Euclidean hemisphere which then gives half de Sitter entropy as the real finite part of the no-boundary extremal surface area (in particular for maximal (IR) subregions). This can also be realized by evaluating the on-shell action (semiclassical Wavefunction Ψ_{dS}): the real part then gives the probability $|\Psi_{dS}|^2$ controlled by de Sitter entropy. The underlying reason here in dS stems from the Lewkowycz-Maldacena cosmic brane interpretation in [199]. In the context of slow-roll inflation, the perturbations mix everything but the cosmic brane creation probability controlled by the real finite parts of the no-boundary areas continues to match the probability from the Wavefunction, corroborating the replica arguments near de Sitter. Both probabilities are controlled by de Sitter entropy and its slow-roll corrections, which is the maximum amount of "stuff" in the space.

We also study Schwarzschild de Sitter black holes which in general have conical singularities at the black hole and cosmological horizons which have different time periodicities. In the limit of small mass regarded as a perturbation, we define an appropriate no-boundary geometry at the cosmological horizon whose location is shifted by the black hole mass. Now the no-boundary extremal surface area is similar to that in de Sitter space with a reduced cosmological scale, with the real hemisphere contribution being half the entropy for the modified de Sitter space. This is based on the paper [248].

We review de Sitter extremal surfaces in sec. 6.1. The slow-roll inflation extremal surfaces appear in sec. 7.1 and sec. 7.1.1 for the dS_4 case, and sec. 7.2.1 for the dS_3 case. We then discuss Schwarzschild de Sitter in sec. 7.2.2 and FRW+slowroll cosmologies briefly in sec. 7.2.3. Sec. 7.3 contains a Discussion. Various details appear in the Appendices, in sec. C.1.1 and sec. C.1.2 on the inflation setup broadly, in sec. C.2 and sec. C.3 on the area calculation, and in sec. C.4 on the Wavefunction/action.

7.1 Slow-roll inflation, no-boundary extremal surfaces

We will now describe no-boundary extremal surfaces in slow-roll inflation, with the leading dS_4 area corrected to $O(\epsilon)$ in the slow roll parameter. We first describe the basic setup, which is essentially that described in [223] (and related previous work *e.g.* [222]-[229] that we found useful). The spacetime metric near global dS_{d+1} is

$$ds^2 = -dt^2 + a(t)^2 d\Omega_d^2 \;=\; g_{aa} da^2 + a^2 d\Omega_d^2 \,, \tag{7.1}$$

where we have redefined the time coordinate to be a in the second expression, which turns out to be convenient for our purposes. This form of the metric component g_{aa} applies for both the Euclidean and Lorentzian regions of the spacetime. For pure de Sitter in the above global coordinates, we have in the Lorentzian region $r > 1$,

$$a(t) = l \cosh \tau \equiv l\, r \,, \qquad \tau = \frac{t}{l} \,, \qquad g_{aa} = \frac{1}{1-r^2} < 0 \,. \tag{7.2}$$

The region $r < 1$ gives $g_{aa} > 0$ and describes the Euclidean hemisphere. A global S^d equatorial plane slice as a boundary Euclidean time slice then resembles the $t = const$ slice in dS static coordinatization, as in (6.3). The coordinate r here is essentially α in [223].

We now describe slow-roll inflationary perturbations about de Sitter space (Figure 7.1): the basic setup is in Appendix C.1.1 for the dS_4 case, reviewing the description in [223]. The inflaton scalar field ϕ rolls slowly down the potential $V(\phi)$, with a small slow-roll parameter

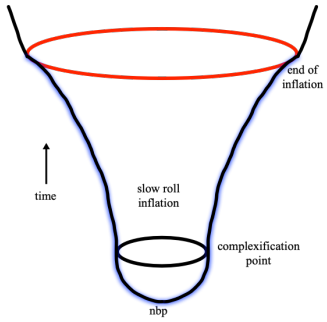

Figure 7.1: Slow-roll inflation as small perturbation wiggles about no-boundary de Sitter space. The Lorentzian region continues smoothly at the "complexification point" into the no-boundary hemisphere region ending at the no-boundary point. Inflation ends at the future boundary (the reheating surface), continuing with standard Big-Bang cosmology at later times. Also shown is the no-boundary extremal surface (blue shadow).

$\epsilon = \frac{V'^2}{2V^2} \ll 1$. We use the Einstein-scalar equations to solve for the inflaton perturbation profile to $O(\epsilon)$ and thereby the metric correction to that order (general useful reviews on inflation include [239, 240]).

Then the metric component g_{rr} to $O(\epsilon)$ in the slow-roll correction has the form

$$g_{aa} = \frac{1}{1-r^2}\big(1 + 2\epsilon\,\beta_>(r)\big)\,, \tag{7.3}$$

where the slow roll correction $\beta_>(r)$ is a function of the rolling inflaton profile: we will describe this in detail later. The no-boundary extremal surfaces we are interested in lie on boundary Euclidean time slices taken as some S^d equatorial plane (*i.e.* S^{d-1}) and extend out from the S^{d-2} boundary of the maximal (hemisphere) subregion on this slice, as in the pure dS case: they thus wrap this S^{d-2} and extend in the time direction, making up the codim-2 surface (blue shadow in Figure 7.1). The metric corrections here have complicated functional form and lead to interesting corrections to the area as we will see. Since the inflationary perturbations here preserve the S^d spherical symmetry, the extremal surfaces on all such equatorial plane slices are equivalent.

The IR no-boundary extremal surface area is given by

$$\begin{aligned} S_{sr_{d+1}} &= S^{r<1}_{d+1} + S^{r>1}_{d+1} \\ &= \frac{V_{S^{d-2}}\, l^{d-1}}{4G_{d+1}} \left(\int_0^1 \frac{r^{d-2}\sqrt{1+2\epsilon\,\beta_<(r)}}{\sqrt{1-r^2}}\, dr \;+\; (-i)\int_1^{R_c/l} \frac{r^{d-2}\sqrt{1+2\epsilon\,\beta_>(r)}}{\sqrt{r^2-1}}\, dr \right) \end{aligned} \tag{7.4}$$

with the leading dS_{d+1} piece and the $O(\epsilon)$ slow roll correction, where $\beta_<(r)$ is to be obtained by analytically continuing $\beta_>(r)$ in the Lorentzian region $r > 1$ to the hemisphere region

where $r < 1$. Expanding to $O(\epsilon)$ we obtain the first slow-roll correction to dS_4 and dS_3 as

$$S_{sr_4} \simeq \frac{\pi\, l^2}{2G_4}\left(-i\int_1^{R_c/l}\frac{1+\epsilon\,\beta_>(r)}{\sqrt{r^2-1}}\,r\,dr+\int_0^1\frac{1+\epsilon\,\beta_<(r)}{\sqrt{1-r^2}}\,r\,dr\right) \tag{7.5}$$

$$S_{sr_3} \simeq \frac{l}{2G_3}\left(-i\int_1^{R_c/l}\frac{1+\epsilon\,\beta_>(r)}{\sqrt{r^2-1}}\,dr+\int_0^1\frac{1+\epsilon\,\beta_<(r)}{\sqrt{1-r^2}}\,dr\right). \tag{7.6}$$

Towards evaluating this, note that the metric (7.3) at leading order $O(\epsilon^0)$ (*i.e.* pure de Sitter) already has a pole at $r = 1$ which is the complexification point where we transit from Lorentzian to Euclidean signature (this is $\tau = 0$, using (7.2)). This does not however lead to any singularities in the extremal surface areas: from (7.5), (7.6), the contribution near $r = 1$ is $\int \frac{dr}{\sqrt{\pm(1-r)}} \sim \sqrt{1-r}$ which is nonsingular, resulting in (6.4), (6.5), (6.6). However, when this pole leads to singularities in calculations, we should go around the pole avoiding it, *i.e.* in the upper half plane: this defines the contour in Figure 7.2 in the τ- or r-variables.

Considering the $O(\epsilon)$ slow-roll corrections, there are indeed extra singular terms in the above expressions (7.5), (7.6), at the complexification point $r = 1$, stemming from the extra $\beta(r)$ terms in the integrand (see (7.13), sourced by the inflaton profile (7.11), using (7.10)). These extra poles lead to divergences, similar technically to those from poles occurring in other calculations in slow-roll inflation: see *e.g.* [223] for some discussions on this (including aspects of earlier numerical studies involving complex contours in the upper half plane avoiding the pole; see *e.g.* [229]). Note that since we are regarding the spacetime background here essentially as a near dS background in the slow-roll phase to $O(\epsilon)$, the details of the full inflationary solution (and the detailed form of the inflaton potential) are not important: thus the pole above necessarily remains in the $O(\epsilon)$ discussions here and must be dealt with.

In the current context, to define the extremal surface areas correctly, we must therefore define these areas as complex integrals in the complex time-plane, with a contour chosen to avoid the pole at $r = 1$, by going around it in the upper half plane, as in Figure 7.2 stated above. As long as we define the complex time-plane integral correctly, normalizing it so that the leading expressions are consistent with the leading de Sitter areas, the details of the contour around the pole are not important as we will see. In pure de Sitter, this time contour essentially encodes the geometric picture of time and correspondingly the shape of the IR extremal surface as in Figure 6.1. In slow-roll, since we are in the semiclassical regime near de Sitter, we expect that the time contour in our $O(\epsilon)$ slow-roll case should retain this semiclassical geometric picture of time and reflect the shape of the slow-roll extremal surface in Figure 7.1 as small wiggles near the de Sitter one.

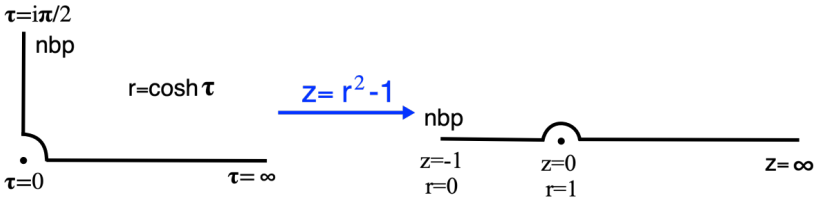

Figure 7.2: The time coordinate τ defines the contour on the left, from the no-boundary point in the Euclidean region at $\tau = i\frac{\pi}{2}$ to the complexification point at $\tau = 0$ and thereon to the Lorentzian region with real τ going to the future boundary $\tau \to \infty$. With the coordinate $r = \cosh\tau$ the nbp is $r = 0$ and the complexification point at $r = 1$. In terms of the coordinate $z = r^2 - 1$ we have the nbp at $z = -1$ and the complexification point at $z = 0$, giving the contour on the right.

Towards describing the leading dS_{d+1} area as well as the $O(\epsilon)$ slow-roll correction, we will find it convenient to use the variable $z = r^2 - 1$, although our analysis can be carried out in the r-variable as well (as we will describe later). The no-boundary point and the complexification point in the r- and z-variables are (Figure 7.2)

$$z = r^2 - 1 \quad \Rightarrow \quad (\text{nbp}) \;\; r = 0 \;\equiv\; z = -1\,; \quad (\text{complexification}) \;\; r = 1 \;\equiv\; z = 0\,. \tag{7.7}$$

The area integral is then recast as a complex contour integral: the contour C in the z-variable, with the pole $z = 0$ regulated to $z = \delta$, is

$$C \;=\; [-1, -\delta] \;\cup\; \left[z = \delta e^{i\theta}\,; \theta = \pi,\; \theta = 0\right] \;\cup\; [\delta, z_c]\;. \tag{7.8}$$

The middle leg is a semicircle of radius δ going around the pole, defined as going from $\theta = \pi$ to $\theta = 0$: then $z = \delta\, e^{i\pi} = -\delta$ at the left end of the semicircle (on the side of the nbp) and $z = \delta$ at its right end, around the complexification point. The details of this regulating semicircle skirting the pole at $r = 1$ or $z = 0$ are not important. In essence, we are evaluating two separate area contributions, from the Lorentzian and hemisphere regions, with regularization at the complexification point.

7.1.1 dS_4 area including $O(\epsilon)$ correction

We will now study the no-boundary extremal surface area (7.5) in 4-dim slow roll inflation: the basic setup here appears in App. C.1.1. The metric is of the form (7.1), (7.2), with $d = 3$, and the overall picture is as depicted in Figure 7.1.

The slow-roll equations of motion (C.2) in the slow-roll approximation become (C.3), *i.e.*

$$3H^2 \sim V(\phi), \qquad 3H\dot{\phi} \sim -V'(\phi)\,. \tag{7.9}$$

The metric component g_{aa} can be shown to take the form (see App. C.4)

$$g_{aa} = \frac{3 - \frac{1}{2}(a\,\partial_a\phi)^2}{3 - V(\phi)\,a^2}\,. \tag{7.10}$$

Expanding to $O(\epsilon)$ in the slow-roll correction with $\phi = \phi_* + \varphi(\tau)$ and $V(\phi) = V_* + V_*{}'\varphi(\tau)$, we solve the inflaton equation of motion (C.5) for the perturbation, imposing regularity at the no-boundary point and matching with the late time expansion (as described in [223]). This finally gives the 4-dim slow-roll inflaton profile in the $r > 1$ Lorentzian region as

$$\epsilon \equiv \frac{V_*{}'^2}{2V_*^2}\,; \qquad \varphi(r) = \sqrt{2\epsilon}\,\tilde{\varphi}(r)\,, \qquad \tilde{\varphi}(r) = \frac{1 + i\sqrt{r^2-1}}{r^2} - \log\left(1 - i\sqrt{r^2-1}\right) - \frac{i\pi}{2}\,, \tag{7.11}$$

and the metric component $g_{rr} = g_{aa}l^2$ in the form (7.3), where in this 4-dim case we have

$$\beta(r) = -\frac{1}{6}\left(r\frac{\partial\tilde{\varphi}}{\partial r}\right)^2 + \frac{\tilde{\varphi}\,r^2}{1-r^2}\,. \tag{7.12}$$

Inputting the inflaton profile (C.7) with $r = \cosh\tau$ gives $\beta(r)$ in the $r > 1$ Lorentzian region,

$$\beta_>(r) = \frac{8 - 9r^4 + 4ir^2\sqrt{r^2-1} + 8i\sqrt{r^2-1} - 6ir^4\sqrt{r^2-1} + r^6\left(6\log\left(1 - i\sqrt{r^2-1}\right) - 1 + 3i\pi\right)}{6r^4\,(r^2-1)}\,. \tag{7.13}$$

To continue this to the $r < 1$ hemisphere region, we note that it is adequate to replace $-i\sqrt{r^2-1}$ by $\sqrt{1-r^2}$ in $\beta_>(r)$: this defines $\beta_<(r)$.

The above recasting gives the dS_4 slow-roll inflation area to $O(\epsilon)$ as

$$S = \frac{\pi\,l^2}{2G_4}\int_C \frac{1 + \epsilon\,\beta_>(r)}{2\sqrt{1-r^2}}\,r\,dr \;\equiv\; \frac{\pi\,l^2}{2G_4}\int_C \frac{1 + \epsilon\,\beta_>(z)}{2\sqrt{-z}}\,dz\,. \tag{7.14}$$

For the leading pure de Sitter piece, there are no singularities and the areas can be evaluated as separate integrals in the Lorentzian and Euclidean regions, as in (6.4). However for the $O(\epsilon)$ contribution to the area, it turns out that there are extra pole pieces at the complexification point $r = 1$ ($z = 0$). Thus it is important to define these as a contour integral in the complex time plane, defining a contour to avoid the pole at $r = 1$, as shown in Figure 7.2. We describe the detailed calculation in Appendix C.2, in both the z- and r-coordinates.

Adding up all the contributions along the full contour C keeping the leading order and $O(\epsilon)$ pieces in (7.14), we obtain

$$\begin{aligned} S &= \frac{\pi l^2}{2G_4}\Bigg[1-\sqrt{\delta} \;+\; \epsilon\left[\left(\log 4-\frac{7}{6}+i\pi\right)-\left(-\frac{2-3i\pi}{6\sqrt{\delta}}+\frac{5}{3}\right)\right] \\ &\quad +\sqrt{\delta}(-i+1) \;+\; \epsilon\left[\frac{2-3i\pi}{6i\sqrt{\delta}}-\frac{2-3i\pi}{6\sqrt{\delta}}\right] \\ &\quad +\frac{1}{i}(\sqrt{z_c}-\sqrt{\delta}) \;+\; \epsilon\left[\left(1+i\frac{7}{6}\sqrt{z_c}-i\sqrt{z_c}\log\sqrt{z_c}\right)-\left(\frac{2-3i\pi}{6i\sqrt{\delta}}+\frac{5}{3}\right)\right]\Bigg]. \end{aligned} \tag{7.15}$$

Finally, note that although we have expressed the area as a single complex-time-plane integral, we have evaluated it as separate integrals in the top timelike part and the hemisphere part, with the semicircle contour only serving to avoid the $r=1$ ($z=0$) pole. Note that all the singular pieces near the pole cancel as they should, so the details of the contour around the pole are unimportant. We obtain finally

$$S_{sr_4}=\frac{\pi l^2}{2G_4}\left(-i\frac{R_c}{l}+1\right) \;+\; \epsilon\,\frac{\pi l^2}{2G_4}\left(-i\frac{R_c}{l}\log\frac{R_c}{l} \;+i\frac{7}{6}\frac{R_c}{l} \;+\; \log 4-\frac{7}{2}+i\pi\right), \tag{7.16}$$

to $O(\epsilon)$ in the slow-roll corrections. Note that the various finite pieces conspire to give the finite value above: the real part of this finite value is negative.

Unlike in the pure de Sitter case, where there was a clean separation between the real part of the area arising from the hemisphere and the imaginary part from the top timelike Lorentzian region, the slow-roll corrections contain real and imaginary parts from both the timelike and hemisphere regions. The finite terms in $S^{\epsilon}_{sr_4}$ in particular arise from the entire surface, both timelike and hemisphere parts.

Recalling the comments after (7.5), (7.6), the minimal time contour (Figure 7.2) we have employed is natural given that the slow-roll case is near de Sitter: it faithfully dovetails with the geometric picture of time in the semiclassical near dS regime here, and encodes the shape (Figure 7.1) of the slow-roll IR extremal surface which is expected to be near that in pure dS (Figure 6.1). Dramatically changing the contour would deviate substantially from the semiclassical geometry here (also the Cauchy theorem cannot apply given the non-analytic expressions here).

It is now interesting to note that this finite value above matches precisely with the finite part in (C.48) of the $O(\epsilon)$ slow-roll correction in the Wavefunction of the Universe $\Psi\sim e^{iI}$ in slow-roll inflation, given in [223]: we review the details of this calculation in App. C.4. But

to summarize, the on-shell dS_4 action with $O(\epsilon)$ slow-roll correction is

$$iI_{sr4} = \frac{\pi\, l^2}{2G_4}\Bigg[1+\epsilon\left(\log 4 - \frac{7}{2} + i\pi\right) \\ -i\left(r_c^3 - \frac{3}{2}r_c\right) + i\epsilon\left(r_c^3\left(\log r_c - \frac{1}{6}\right) + \frac{r_c}{4}\left(6\log r_c - 11\right)\right)\Bigg], \quad (7.17)$$

where $r_c \equiv \frac{R_c}{l}$ is the cutoff near the future boundary. The first line is mostly real while the second line is pure imaginary. We note that $|\Psi|^2 \sim e^{\frac{\pi l^2}{G_4}(1+\epsilon\,\#)}$ is controlled by the the real terms in the first line and is the probability for creation of this universe with slow-roll corrections. The imaginary terms cannot agree since the area corresponds to a codim-2 extremal surface with corresponding divergences while the action corresponds to the full 4-dim space with its corresponding divergences near the future boundary.

The fact that the real terms in S_{sr_4} in (7.16) match those in iI_{sr4} in (7.17) is consistent with and corroborates the heuristic Lewkowycz-Maldacena interpretation in [199] of these no-boundary extremal surface areas as the amplitude for codim-2 cosmic brane creation (reviewed briefly after Figure 6.1). More specifically the probability for this maximal cosmic brane creation matches that for the creation of the Universe. This probability must be finite since it is ultimately dictated by the upper bound set by de Sitter entropy (the maximal amount of "stuff" in this space, controlled by the no-boundary maximal hemisphere): thus the divergent terms near the future boundary cannot contribute and must be pure imaginary. With the slow-roll corrections included, we have seen that the finite terms arise from everywhere. Note that since $\log 4 - \frac{7}{2} < 0$, the no-boundary area or the cosmic brane creation probability has decreased. This is perhaps a reflection of the fact that excitations in de Sitter space decrease its entropy (as for a black hole in de Sitter space).

It is interesting to ask what the analog in AdS is of this matching of the real finite part of the areas and the entropy contribution in the Wavefunction. The AdS Ryu-Takayanagi formulation relies on the existence of a nice optimization: minimal surfaces start at the boundary and turn around in the interior. With regard to the current context, we recall that the RT surface on a constant time slice in the AdS black hole/brane wraps the horizon as the boundary subregion becomes the whole space, *i.e.* the maximal (IR) subregion. The finite part of the area then becomes the bulk entropy (which for the AdS black brane is the thermal entropy in the dual field theory). This entropy can also be realized by the well-known Gibbons-Hawking procedure of regarding the on-shell action as a partition function [230] and evaluating the corresponding entropy: it usefully captures phenomena in AdS/CFT such as the Hawking-Page transition [231, 232]. In the de Sitter case, there are no turning points in the Lorentzian region as we have reviewed: no-boundary extremal surfaces turn around only

in the Euclidean hemisphere and give half dS entropy as the real finite part. This entropy can also be realized from the on-shell action regarded as a partition function: with the slow-roll corrections we obtain the above. The fact that the maximal cosmic brane probability matches the probability from the Wavefunction then corroborates the Lewkowycz-Maldacena arguments in [199].

It is worth noting that the divergent terms in the area (7.16) in the slow-roll corrections exhibit a logarithmic enhancement scaling as $R_c \log R_c$, which might seem surprising considering that the metric component g_{aa} itself (7.3) has only subleading pieces near the future boundary. However we note that the slow-roll correction $\beta_>(r)$ (7.13) part in g_{aa} does have a term scaling as $\log r$ for large r: thus the Lorentzian part of the area (7.5) of this codim-2 surface (which has extra r-factors) for large r scales as $\epsilon \log r$ which leads to the log-enhancement. Similar features appear also in the action (7.17) where the slow-roll correction scales as $\epsilon r_c^3 \log r_c$ while the leading term scales as $V_{S^3} \sim r_c^3$ (as noted in [223]).
(A related point is whether the logarithmic term renders the finite piece ambiguous: in this regard note that rescaling the cutoff as $R_c \to \alpha R_c$ in (7.16) gives an extra $\epsilon \frac{\pi l^2}{2G_4}(-i\frac{R_c}{l}\alpha \log \alpha)$ contribution from the $R_c \log R_c$ term, which modifies only the leading area law divergence term. There is no standalone $\log R_c$ term, so the finite piece is unambiguous.)

To put this enhanced logarithmic scaling in perspective, it is worth recalling similar features in AdS/CFT, especially in the context of nonrelativistic condensed matter-like generalizations and Fermi surfaces. In particular it was noted that certain classes of hyperscaling violating Lifshitz theories exhibit novel holographic entanglement scaling [241, 242, 243]. While these are phenomenological gravitational descriptions, certain gauge-string realizations were found in [244] which precisely recover this logarithmic scaling. For instance, the AdS_5 plane wave $ds^2 = \frac{R^2}{r^2}[-2dx^+dx^- + dx_i^2 + dr^2] + R^2 Q r^2 (dx^+)^2 + R^2 d\Omega_5^2$ is interpreted as a simple anisotropic state in the dual $\mathcal{N} = 4$ Super Yang-Mills CFT_4 with holographic energy momentum density $T_{++} \sim Q$. Under x^+-dimensional reduction this gives $ds^2 = r^{\frac{2\theta}{d_i}}\big(- \frac{dt^2}{r^{2z}} + \frac{\sum_{i=1}^{d_i} dx_i^2 + dr^2}{r^2}\big)$ with $d_i = 2,\ \theta = 1,\ z = 3$ (and $x^- \equiv t$). Holographic entanglement entropy [245] (see also [246]) for a strip subregion along the flux direction then gives the leading divergence $S^{div} \sim N^2 \frac{V_2}{\epsilon^2}$, and the finite part $S^{fin} \sim N^2 V_2 \sqrt{Q} \log(lQ^{1/4})$. Identifying the energy flux Q and the UV cutoff ϵ with the Fermi momentum $k_F \equiv Q^{1/4} \sim \frac{1}{\epsilon}$ recasts the area law divergence as $S^{div} \sim N^2 V_2 k_F^2$ with the finite part resembling the logarithmic enhancement for a Fermi surface $S^{fin} \sim N^2 V_2 k_F^2 \log(l k_F)$. Although the AdS/CMT context is quite different, we see that there are structural similarities with the extremal surface areas (7.16). These complex areas here are expected to encode boundary entanglement entropy in the exotic Euclidean (ghost-like) CFT_3 dual to dS_4 under the slow-roll deformations sourced by the inflaton (although understanding this nontrivial dual in detail is challenging!).

Finally one might ask what the no-boundary slow-roll corrected areas map to in AdS under the analytic continuation $L \to -il$ which for the maximal subregions in $AdS \leftrightarrow dS$ are given by (6.4), (6.5), (6.6). Then the leading term in the area (7.16) is simply the AdS area in (6.5), but the analytic continuation of the slow-roll correction gives imaginary components as well. This suggests that the corresponding perturbations in AdS induce timelike components to the extremal surface. However this blithe continuation needs to be examined more carefully requiring physically reasonable scalar perturbations in AdS that might be analogous to the inflationary no-boundary de Sitter perturbations here.

7.2 Other cosmologies

We will now describe no-boundary extremal surfaces in some other cosmological spacetime backgrounds, including in particular dS_3 slow-roll inflation, and Schwarzschild de Sitter black holes with small mass.

7.2.1 dS_3 area including $O(\epsilon)$ correction

We can generalize the above 4-dim analysis in sec. 7.1.1 to 3-dimensions and study 3-dim slow roll inflation: the basic setup here appears in App. C.1.2. The 3-dim gravity case has no intrinsic dynamics but the inflaton scalar degree of freedom makes it more interesting, even if this is just a toy model of slow-roll inflation. The metric is of the form (7.1), (7.2), with $d = 2$, and the overall picture is as depicted in Figure 7.1.

Here we have the slow-roll equations of motion (C.10), which in the slow-roll approximation become (C.11), *i.e.*

$$H^2 \sim V(\phi), \qquad 2H\dot{\phi} \sim -V'(\phi)\,. \tag{7.18}$$

The inflaton equation of motion (C.12) for the perturbation can be solved as in the dS_4 slow-roll case, imposing regularity at the no-boundary point and matching with the late time expansion. This finally gives the solution as (C.15), *i.e.*

$$\varphi(\tau) = \sqrt{2\epsilon}\left[\left(\frac{i\pi}{4} - \frac{\tau}{2}\right)\tanh\tau + \frac{\log 2}{2} - \frac{i\pi}{4}\right] \equiv \sqrt{2\epsilon}\,\tilde{\varphi}(\tau)\,. \tag{7.19}$$

The slow-roll correction to the metric here, using $r = \cosh\tau$, is

$$g_{rr} = \frac{1 - \frac{1}{2}(r\partial_r\varphi)^2}{1 - Vr^2} \simeq \frac{1}{1 - r^2}\left(1 + 2\epsilon\beta_>(r)\right) \tag{7.20}$$

where

$$2\epsilon\beta_{>}(r) \equiv \frac{V_*'^2}{V_*^2}\left(-\frac{1}{2}(r\partial_r\tilde{\varphi})^2 + \frac{\tilde{\varphi}\, r^2}{1-r^2}\right) \tag{7.21}$$

evaluates to the expression in (C.28).

The slow-roll dS_3 inflation no-boundary extremal surface area in (7.6) is

$$S_{sr_3} \simeq \frac{l}{2G_3}\left(\int_\delta^{z_c} \frac{1+\epsilon\,\beta_{>}(z)}{2i\sqrt{z(1+z)}}\,dz + \int_\delta^{1} \frac{1+\epsilon\,\beta_{<}(z)}{2\sqrt{z(1-z)}}\,dz\right) + \frac{l}{2G_3} I_\epsilon^\theta \tag{7.22}$$

where I_ϵ^θ is the contribution from the semicircle part of the contour, skirting around the pole at $z=0$. We have written this in terms of the variable $z = r^2 - 1$ in (7.7) for $z > 0$ and then continued as $z \to -z$ to the hemisphere region, as in the dS_4 case.

We describe the details of this calculation in Appendix C.3. From there, we obtain

$$\begin{aligned} S \;=\; & \frac{l}{2G_3}\Bigg[\frac{\pi}{2} + \epsilon\Big[\frac{1}{16} i\left(-(\log z_c)^2 + \log z_c + \pi^2 + 4i\pi + 4(\log 2)^2 - 6\log 2\right) \\ & \qquad - \left(-\frac{\pi}{8} + \frac{i\,(8i\pi + \pi^2 - 4\log(16))}{32\sqrt{\delta}}\right)\Big]\Bigg] \;+\; I_\epsilon^\theta \\ & - i\log\sqrt{z_c} + \epsilon\Big[\frac{\pi}{16}(2\pi i - 1 - \log 16) - \left(-\frac{\pi}{8} + \frac{(8i\pi + \pi^2 - 4\log(16))}{32\sqrt{\delta}}\right)\Big]\Bigg] \end{aligned} \tag{7.23}$$

which simplifies to (after rewriting using $z = r^2 - 1$ and expanding at large $r_c = \frac{R_c}{l}$)

$$\begin{aligned} S \;=\; & \frac{l}{2G_3}\Big(\frac{\pi}{2} - i\log\frac{R_c}{l}\Big) \\ & + \epsilon\,\frac{l}{2G_3}\left(-\frac{\pi}{16}(1+\log 16) \;+\; \frac{i}{16}\Big(2\log\frac{R_c}{l} - 4\Big(\log\frac{R_c}{l}\Big)^2 + 3\pi^2 + 4(\log 2)^2 - 6\log 2\Big)\right). \end{aligned} \tag{7.24}$$

The real part of the area including the slow-roll correction here is

$$\mathrm{Re}S = \frac{\pi\, l}{4G_3} - \epsilon\,\frac{l}{2G_3}\frac{\pi}{16}(1+\log 16)\,. \tag{7.25}$$

As in dS_4 inflation, this in fact matches the real parts in (C.51) and (C.53) in App. C.4 obtained to $O(\epsilon)$ from the semiclassical expansion of action or the the logarithm of the Wave-function, *i.e.* $\log\Psi \sim iI_{cl}$. Thus the maximal cosmic brane creation probability matches the probability $|\Psi|^2$ for Universe creation, corroborating the heuristic Lewkowycz-Maldacena interpretation in [199] of these no-boundary extremal surface areas.

The details of this calculation appear in App. C.4. The imaginary finite pieces in (C.51), (C.53) do not agree. The dual here is an even-dimensional CFT and anomaly contributions

of the CFT on a 2-sphere are expected to give further pure imaginary contributions. The CFT anomaly is expected to be proportional to the central charge which in dS_3/CFT_2 is pure imaginary. It would be interesting to understand this breaking of dual conformal invariance by such inflationary perturbations in greater detail.

In this light, it is worth looking more closely at the leading term as well. This in fact contains a subleading finite term near the future boundary: we have the timelike part of the area $-i\frac{l}{2G_3}\int_1^{R_c/l}\frac{dr}{\sqrt{r^2-1}} = -i\frac{l}{2G_3}\log\frac{R_c}{l} - i\frac{l}{2G_3}\log 2$, noting that the indefinite integral is $\log(r+\sqrt{r^2-1})$. This subleading finite term is pure imaginary so the real part of the area controlling the cosmic brane creation probability remains half dS_3 entropy.

7.2.2 Schwarzschild de Sitter black holes with small mass

We will discuss Schwarzschild de Sitter black holes here, but with the black hole mass treated as perturbation: some useful references include [224, 99], as well as our previous work [104, 149, 247]. The metric is

$$ds^2 = -f(r)dt^2 + \frac{dr^2}{f(r)} + r^2 d\Omega_2^2\,, \qquad f(r) = 1 - \frac{2m}{r} - \frac{r^2}{l^2}\,. \tag{7.26}$$

The metric function can be written as

$$f(r) = \frac{1}{l^2\, r}(r_D - r)(r_D + r_S + r)(r - r_S)\,, \qquad r_D r_s(r_D + r_S) = 2ml^2\,, \quad r_D^2 + r_D r_S + r_S^2 = l^2\,. \tag{7.27}$$

The roots r_S and r_D correspond to the black hole and cosmological horizons respectively, and satisfy the constraint relations above, alongwith $0 \le r_S \le r_D \le l$. In addition, we have the condition $\frac{m}{l} \le \frac{1}{3\sqrt{3}}$ for a physical black hole horizon to exist.

In the limit of small mass $m \ll l$, the roots representing the horizon locations can be approximated as

$$r_D \sim l - G_4 m\,, \qquad r_S \sim 2G_4 m\,, \tag{7.28}$$

so that the cosmological horizon at $r_D = l$ shifts a little inward for a nonzero black hole horizon. Since there is a curvature singularity at $r = 0$ inside the black hole horizon, strictly speaking there is no smooth Euclidean instanton that can be extended to a smooth no-boundary geometry. However treating the black hole perturbation to only serve to shift the cosmological horizon, we can look for a no-boundary geometry continuing to take the no-boundary point as $r = 0$. In other words, we disregard the spacetime geometry effects of the black hole (and thus disregard the singularity etc). This amounts to approximating the

metric function as

$$f(r) = \frac{1}{l^2}\left(r_D^2 - r^2 + r_S(r_D - r)\right)\left(1 - \frac{r_S}{r}\right) \xrightarrow{r_S \to 0, \quad l \sim r_D} 1 - \frac{r^2}{r_D^2}\,. \tag{7.29}$$

Now we Euclideanize $t = i\tau_E$, and for $r < r_D$ we glue on a Euclidean hemisphere which is smooth at the no-boundary point $r = 0$, and thus replaces the earlier SdS geometry.

On the $t = const$ slice taken as a boundary Euclidean time slice, we consider the maximal (hemisphere) subregion on the S^2 at the future boundary. Then the no-boundary area becomes

$$S = \frac{V_{S^1}}{4G_4}\int_0^{r_D} \frac{r\,dr}{\sqrt{1 - \frac{r^2}{r_D^2}}} \;+\; \frac{(-i)V_{S^1}}{4G_4}\int_{r_D}^{R_c} \frac{r\,dr}{\sqrt{\frac{r^2}{r_D^2} - 1}}\,. \tag{7.30}$$

This gives

$$S = -i\frac{\pi\, r_D^2}{2G_4}\frac{R_c}{r_D} + \frac{\pi\, r_D^2}{2G_4}\,. \tag{7.31}$$

The real part of this area is half the entropy of the shifted cosmological horizon with size $r_D \sim l - G_4 m$: in other words, treating this as just a modified no-boundary de Sitter space, we obtain the earlier result for pure dS_4. To $O(m)$, this gives

$$\mathrm{Re}S \sim \frac{\pi}{2G_4}(l - G_4 m)^2 \;\sim\; \frac{\pi\, l^2}{2G_4} - \pi\, l\, m\,, \tag{7.32}$$

This matches half the Euclidean action, expanded to $O(m)$, for Schwarzschild de Sitter black holes obtained in [188] by a careful treatment of the conical singularities at the two horizons incorporating δ-function sources there. However it is worth emphasizing that the extremal surface area has been obtained under the approximation (7.29). It would be worth refining this more carefully.

For 3-dim Schwarzschild de Sitter given by

$$ds^2 = -f(r)dt^2 + \frac{dr^2}{f(r)} + r^2 d\phi^2\,, \qquad f(r) = 1 - 8G_3 E - \frac{r^2}{l^2}\,. \tag{7.33}$$

In this case, there is only one horizon at $r_D = l\sqrt{1 - 8G_3 E}$. At sufficiently large E, the space closes up and the entropy $\frac{\pi\, r_D}{2G_3}$ vanishes. As before, for small energy E, we approximate the metric function as $f(r) \sim 1 - \frac{r^2}{r_D^2}$ and evaluate the hemisphere contribution to the no-boundary area as

$$S^h = \frac{2}{4G_3}\int_0^{r_D} \frac{dr}{\sqrt{1 - \frac{r^2}{r_D^2}}} = \frac{\pi\, r_D}{4G_3}\,, \tag{7.34}$$

which is half the entropy of the modified dS_3 space (compare (6.1)). However it is worth noting that the area calculation done exactly instead gives

$$S'^h = \frac{2}{4G_3}\int_0^{r_D} \frac{dr}{\sqrt{1-8G_3E-\frac{r^2}{l^2}}} = \frac{\pi\, l}{4G_3}\,, \tag{7.35}$$

which is half dS_3 entropy independent of the mass E. It is important to note however that in this case, the location $r=0$ is a conical singularity as can be seen from the metric there, *i.e.* $ds^2 \sim -\frac{r_D^2}{l^2}dt^2 + \frac{l^2dr^2}{r_D^2} + r^2d\phi^2 \sim -dt'^2 + dr'^2 + r'^2d\phi'^2$ redefining $t' = \frac{r_D}{l}t\,,\ r' = \frac{lr}{r_D}\,,\ \phi' = \frac{r_D}{l}\phi$ (see *e.g.* [193]). Thus we see that for $r_D < l$, the angle ϕ' is identified modulo $2\pi\frac{r_D}{l}$ reflecting the conical singularity at $r=0$. Thus the area S'^h pertains to this singular space while S^h pertains to the no-boundary space obtained from SdS_3 under the approximations of $f(r)$.

Thus overall, it is important to note that Schwarzschild de Sitter spaces for generic mass have distinct Euclidean periodicities at the black hole and cosmological horizons so they cannot be made regular except at the extremal Nariai point. Thus in evaluating these no-boundary extremal surface areas we are making approximations to construct appropriate no-boundary geometries for small mass perturbations near de Sitter. Perhaps one may better define these areas by more careful treatment of the conical singularities for generic mass.

7.2.2.1 Extremal SdS_4: Nariai

The Nariai or extremal limit of Schwarzschild de Sitter gives a near horizon $dS_2\times S^2$ geometry. This occurs when $r_D = r_S$: then (7.27) gives $r_D = r_S = r_0 = \frac{l}{\sqrt{3}}$ and $\frac{m}{l} = \frac{1}{3\sqrt{3}}$. This is a degenerate limit but regulating near Nariai as $r_D = r_0 - x,\ r_S = r_0 + x$, gives

$$f(r) \sim \frac{3}{l^2}(x^2 - (r-r_0)^2)\,, \tag{7.36}$$

where we approximate $r \sim r_0$ in the $(r_D + r_S + r)$ factor. This amounts to zooming in to the extremal throat region, with the transverse S^2 of size $r_0 = \frac{l}{\sqrt{3}}$. Defining

$$\psi = \int \frac{dr}{\sqrt{f(r)}} = \frac{l}{\sqrt{3}}\sin^{-1}\frac{r-r_0}{x} \equiv \frac{l}{\sqrt{3}}\tilde{\psi}\,, \tag{7.37}$$

the metric on the $t = const$ slice approximates to

$$ds^2 \sim d\psi^2 + \frac{l^2}{3}d\Omega_2^2\,. \tag{7.38}$$

For the no-boundary hemisphere we have $\tilde{\psi} \in [0, \frac{\pi}{2}]$, so the area for a hemispherical cap on an equatorial plane in the S^2 is approximated as

$$S \sim \frac{l^2}{3} \int_0^{\frac{\pi}{2}} d\tilde{\psi} \, \frac{V_{S^1}}{4G_4} = \frac{\pi}{6} \frac{\pi \, l^2}{2G_4} \,, \tag{7.39}$$

which is a factor $\frac{\pi}{6} \sim \frac{1}{2}$ times dS_4 entropy. On the other hand, the Euclidean action for the Nariai limit $dS_2 \times S^2$ is a factor $\frac{2}{3}$ times that for dS_4 [224, 99]. This mismatch is perhaps not surprising since the Nariai limit is far from pure de Sitter, unlike the previous cases we have discussed.

7.2.3 FRW+slow-roll cosmologies

Generic FRW-type cosmologies with spatial S^d slices are of the form

$$ds^2 = -dt^2 + a^2(t) d\Omega_d^2 \,, \qquad a(t) \sim t^\nu \,. \tag{7.40}$$

From the point of view of the slow-roll inflation phase evolving to an FRW cosmology epoch (schematically as in Figure 7.1), we are interested only in regarding this as a Lorentzian FRW space with the timelike part of the slow-roll inflation extremal surfaces joining at the reheating surface (approximately the future boundary) with timelike extremal surfaces in the FRW phase. We restrict to a boundary Euclidean time slice as some S^d equatorial plane and pick maximal (hemisphere) subregions. Then the Lorentzian FRW region gives timelike extremal surfaces with area (suppressing intrinsic FRW lengthscales)

$$S_{FRW} = -i \frac{V_{S^{d-2}}}{4G_{d+1}} \int_{t_0}^{t_l} dt \; a(t)^{d-2} \xrightarrow{4-dim} -i \frac{\pi}{2G_4} \left(t_l^{\nu+1} - t_0^{\nu+1} \right) . \tag{7.41}$$

Appending (7.16), the full extremal surface area for the FRW+inflation cosmology becomes $S_{FRW} + S_{sr4}$. It may be interesting to understand if these sorts of codim-2 area observables can be usefully employed to understand aspects of cosmological observations.

Considering the FRW spaces (7.40) in themselves, in general these will not admit any smooth HH no-boundary Euclidean continuation. Blithely calculating the IR no-boundary extremal surface area gives the Euclidean hemisphere contribution as

$$\begin{aligned} S &= \frac{V_{S^{d-2}}}{4G_{d+1}} \int_0^{\tau_l} d\tau_E \; a(\tau_E)^{d-2} = \frac{V_{S^{d-2}}}{4G_{d+1}} \int_0^{\tau_l} \frac{da \; a(\tau_E)^{d-2}}{(da/d\tau_E)} \\ &\sim \frac{V_{S^{d-2}}}{4G_{d+1}} \int_0^{\tau_l} d\tau_E \, \tau_E^{(d-2)\nu} \xrightarrow{4-dim} \frac{\pi}{2G_4} \frac{\tau_l^{\nu+1}}{\nu+1} \,. \end{aligned} \tag{7.42}$$

where we have taken $a(\tau_E) \sim \tau_E^\nu$, with $\nu > 0$. The sphere S^d shrinks to zero size at the no-boundary point $\tau_E = 0$: however for generic ν, the derivative $\frac{da}{d\tau_E}$ is not smooth so a Big-Bang type singularity persists at $\tau_E = 0$.

7.3 Discussion and conclusions

Building on previous work on de Sitter extremal surfaces anchored at the future boundary, we study no-boundary extremal surfaces in slow-roll inflation models, with perturbations to no-boundary global dS preserving the spatial isometry. While in pure de Sitter space the Euclidean hemisphere gives a real area equalling half de Sitter entropy, the no-boundary extremal surface areas here have nontrivial real and imaginary pieces overall. We evaluate the area integrals in the complex time-plane defining appropriate contours. For the 4-dim case, the real and imaginary finite corrections at leading order in the slow-roll parameter match those in the semiclassical expansion of the Wavefunction (or action), and corroborate the cosmic brane interpretation discussed previously. We also study no-boundary extremal surfaces in other cosmologies including 3-dimensional inflation and Schwarzschild de Sitter spaces with small mass.

Stepping back and looking at a broad-brush level, it is important to understand the connections between the no-boundary extremal surface areas and the Wavefunction of the Universe in greater detail (mirroring connections between boundary entanglement entropy and Z_{CFT} in the exotic duals here): among other things this will shed light on the underlying structure of these extremal surface areas in dS and cosmology more broadly. There is a rich history of such studies in AdS/CFT on extremal surface areas and the bulk partition function (dual to entanglement entropy and the boundary partition function) [14, 15, 16, 17]. One such fact is that for maximal (IR) subregions in the AdS black hole/brane, the RT minimal surface dips all the way into the interior and wraps the horizon so the finite part of entanglement entropy is the black hole/brane entropy. This entropy can also be realized from the action regarded as a partition function. In the current context, a similar observation is that the real finite part of the no-boundary extremal surface in pure de Sitter is half dS entropy, which also arises from the real part of the Wavefunction. It is natural to ask if this correlation [199] between the cosmic brane creation probability (encoded by the real finite parts of the areas) and $|\Psi_{dS}|^2$ continues away from de Sitter. An interesting class of near dS spaces comprises slow-roll inflation. Our studies vindicate this correlation here.

As we have seen, we have found it necessary to define the area integrals in the complex-time plane with appropriate contours required to avoid extra poles at the complexification point. We have done this in the minimal way, by simply evaluating the areas as separate integrals in

the Lorentzian and hemisphere regions, with the regulating time contour Figure 7.2 serving to simply remove the poles (and the details of the regularization are unimportant). The integrals involve non-analytic expressions so one might expect that changing the contour dramatically is not a reasonable thing to do in these complex-valued integrals (and the Cauchy theorem cannot apply). This can be corroborated further in the present case noting that since the slow-roll case is near de Sitter we expect on physical/geometric grounds that the time contour should also be near that in de Sitter. In de Sitter the time contour encodes the IR extremal surface shape in Figure 6.1 so it is natural that the time contour in the slow-roll case encodes the wiggly shape for the IR extremal surface in Figure 7.1: this justifies the minimal time contour Figure 7.2 that we have employed as quite reasonable and natural here. Roughly the time contour dovetails with the geometric picture of time in the semiclassical regimes we have here, near pure de Sitter: indeed any time contour with large deviation from the semiclassical geometry would perhaps be unphysical for the present purposes. In general, these sorts of cosmological perturbations lead to complex metrics that must be treated carefully (the complex nature is not surprising since the no-boundary condition [222] is a regularity condition analogous to positive frequency not reality; see comments in [223] as well as [191]). Thus along the lines of the analysis here, it would be interesting to understand if these sorts of no-boundary extremal surface areas can be evaluated meaningfully and unambiguously for complex metrics appearing in cosmology more generally, and whether they give insights into complex metrics and the KSW criterion [249, 250] (see also [229]).

The classes of de Sitter perturbations we have studied here all preserve the spherical isometry of the S^3 slices in global dS_4. Thus all boundary Euclidean time equatorial plane slices are equivalent, with the corresponding codim-2 no-boundary extremal surface areas all equal. For more general inflationary perturbations with inhomogeneities in particular, we expect that different boundary Euclidean time slices are inequivalent and thus will lead to inequivalent codim-2 extremal surfaces anchored at the future boundary (an example of this inequivalence was already noted in [182], [184] for the extremal surface areas in different slices of dS in the static coordinatization). It would be interesting to explore this further.

The extremal surfaces discussed here and in earlier work have been studied directly and via analytic continuations from AdS but they are the analogs in some sense of the AdS RT minimal surfaces on constant time slices (which map to the boundary Euclidean time slices stretching from the future boundary here). In that light, it is natural to ask for covariant (HRT-like) formulations of these extremal surfaces and the corresponding areas as pseudo-entropy. One might imagine that the corresponding complex-time-plane contour analogs of Figure 7.2 might then be expressed more covariantly.

Finally it would be interesting to understand the analyses here from the point of view of the dual field theory. In a broad sense, dS/CFT [189, 190, 191] is a way to organize de Sitter perturbations in the language of AdS/CFT (and analytic continuations) especially as formulated in [191], and in more recent studies *e.g.* [251, 252, 253]. In this light, it would be interesting to understand the structure of inflationary perturbations and the way they reflect in the no-boundary extremal surface areas regarded as pseudo-entropy. Hopefully quantum information ideas and techniques along these lines will help shed further light on de Sitter holography and the emergence of time.

Appendix A

Appendix to Chapter 3

A.1 Details: entropy in the no-island case

This section contains some details on the calculations of entanglement entropy in the absence of the island in sec. 3.2.1. Using (3.8), (3.10), (3.11), the black hole patch Kruskal coordinates are:

$$U_S = -e^{-\alpha_S t}(r_D - r)^{-\alpha_S\beta_D}(r - r_S)^{\alpha_S\beta_S}(r + r_D + r_S)^{\alpha_S\beta_M}, \tag{A.1}$$

$$V_S = e^{\alpha_S t}(r_D - r)^{-\alpha_S\beta_D}(r - r_S)^{\alpha_S\beta_S}(r + r_D + r_S)^{\alpha_S\beta_M} \ . \tag{A.2}$$

Calculating each part of S_{matter} in equation 3.23 separately gives

$$U_S(b_-) - U_S(b_+) = (r_D - b)^{-\alpha_S\beta_D}(b - r_S)^{\alpha_S\beta_S}(b + r_D + r_S)^{\alpha_S\beta_M}[e^{-\alpha_S t_b} - e^{\alpha_S(t_b - \frac{i\beta}{2})}] \ , \tag{A.3}$$

$$V_S(b_+) - V_S(b_-) = (r_D - b)^{-\alpha_S\beta_D}(b - r_S)^{\alpha_S\beta_S}(b + r_D + r_S)^{\alpha_S\beta_M}[e^{\alpha_S t_b} - e^{-\alpha_S(t_b - \frac{i\beta}{2})}] \ , \tag{A.4}$$

$$W(b_+) = W(b_-) = \sqrt{b}l\alpha_S(r_D - b)^{-\frac{1+2\alpha_S\beta_D}{2}}(b - r_S)^{\frac{2\alpha_S\beta_S - 1}{2}}(b + r_S + r_D)^{\frac{2\alpha_S\beta_M - 1}{2}} \ , \tag{A.5}$$

$$W(b_+)W(b_-) = bl^2\alpha_S^2(r_D - b)^{-(1+2\alpha_S\beta_D)}(b + r_S + r_D)^{(2\alpha_S\beta_M - 1)}(b - r_S)^{(2\alpha_S\beta_S - 1)} \ . \tag{A.6}$$

Plugging all these expressions together in (3.23) gives

$$\begin{aligned} S_{matter} &= \frac{c}{6}\log\Big[b(r_D-b)^{-2\alpha_S\beta_D}(b-r_S)^{2\alpha_S\beta_S}(b+r_D+r_S)^{2\alpha_S\beta_M}(e^{-\alpha_S t_b}-e^{\alpha_S(t_b-\frac{i\alpha_S\beta}{2})})\cdot \\ &\quad (e^{\alpha_S t_b}-e^{-\alpha_S(t_b-\frac{i\alpha_S\beta}{2})})\frac{1}{bl^2\alpha_S^2}(r_D-b)^{(1+2\alpha_S\beta_D)}(b-r_S)^{(1-2\alpha_S\beta_S)}(b+r_S+r_D)^{(1-2\alpha_S\beta_M)}\Big] \\ &= \frac{c}{6}\log\Big[(r_D-b)(b-r_S)(b+r_S+r_D)\frac{1}{l^2\alpha_S^2}\Big(2-(e^{(2\alpha_S t_b-\frac{i\alpha_S\beta}{2})}+e^{-(2\alpha_S t_b-\frac{i\alpha_S\beta}{2})})\Big)\Big] \\ &= \frac{c}{6}\log\Big[(b-r_D)(b-r_S)(b+r_S+r_D)\frac{1}{l^2\alpha_S^2}\Big(e^{(\frac{2t_b}{2\beta_S}-i\pi)}+e^{-(\frac{2t_b}{2\beta_S}-i\pi)}-2\Big)\Big]\,, \end{aligned} \tag{A.7}$$

using $\beta=\frac{2\pi}{\alpha_S}$ from (3.22). From (3.10) we have $\alpha_S=\frac{1}{2\beta_S}$ so this becomes

$$S=\frac{c}{6}\log\Big[(b-r_S)4\beta_S^2\,(\frac{r_D}{l}-\frac{b}{l})(\frac{b}{l}+\frac{r_S}{l}+\frac{r_D}{l})\,4\cosh^2\frac{t_b}{2\beta_S}\Big] \tag{A.8}$$

Thus finally, we obtain (3.24).

A.2 Details: late-time entropy with island

Here we give details on sec. 3.3. We are looking to calculate (3.28), *i.e.*

$$S_{matter}=\frac{c}{3}\log\frac{d(a_+,a_-)d(b_+,b_-)d(a_+,b_+)d(a_-,b_-)}{d(a_+,b_-)d(a_-,b_+)}\,. \tag{A.9}$$

Now calculating each part in S_{matter} separately,

$$\log[d(a_+,a_-)]=\frac{1}{2}\log\frac{[(U_S(a_-)-U_S(a_+))(V_S(a_+)-V_S(a_-))]}{W'(a_+)W'(a_-)} \tag{A.10}$$

with W' as in (3.13). Then we have

$$U_S(a_-)-U_S(a_+)=(r_D-a)^{-\alpha_S\beta_D}(a-r_S)^{\alpha_S-\beta_s}(a+r_S+r_D)^{\alpha_S\beta_M}[e^{-\alpha_S t_a}-e^{\alpha_S t_a}\cdot e^{-\frac{i\alpha_S\beta}{2}}]\,, \tag{A.11}$$

$$V_S(a_+)-V_S(a_-)=(r_D-a)^{-\alpha_S\beta_D}(a-r_S)^{\alpha_S-\beta_S}(a+r_S+r_D)^{\alpha_S\beta_M}[e^{\alpha_S t_a}-e^{-\alpha_S t_a}\cdot e^{\frac{i\alpha_S\beta}{2}}]\,, \tag{A.12}$$

$$W'(a_+)W'(a_-)=l^2\alpha_S^2(r_D-a)^{-(1+2\alpha_S\beta_D)}(a+r_S+r_D)^{(2\alpha_S\beta_M-1)}(a-r_S)^{(2\alpha_S\beta_S-1)}\,. \tag{A.13}$$

Putting all these expressions together in (A.10) gives

$$\log[d(a_+,a_-)]=\frac{1}{2}\log\Big[\frac{1}{l^2\alpha_S^2}(a-r_D)(a-r_S)(a+r_S+r_D)\Big(e^{(2\alpha_S t_a-\frac{i\alpha_S\beta}{2})}+e^{-(2\alpha_S t_a-\frac{i\alpha_S\beta}{2})}-2\Big)\Big] \tag{A.14}$$

Similarly we obtain

$$\log[d(b_+,b_-)] = \frac{1}{2}\log\frac{[(U_S(b_-)-U_S(b_+))(V_S(b_+)-V_S(b_-))]}{W'(b_+)W'(b_-)}$$
$$= \frac{1}{2}\log\Big[\frac{1}{l^2\alpha_S^2}(b-r_D)(b-r_S)(b+r_S+r_D)\Big(e^{(2\alpha_S t_b-\frac{i\alpha_S\beta}{2})}+e^{-(2\alpha_S t_b-\frac{i\alpha_S\beta}{2})}-2\Big)\Big] \tag{A.15}$$

Now, putting (A.14) and (A.15) together gives, using $\beta=\frac{2\pi}{\alpha_S}$,

$$\frac{c}{3}\log[d(a_+,a_-)d(b_+,b_-)] = \frac{c}{6}\log\Big[\frac{2^8 r_S^4}{(\frac{r_D-r_S}{l})^4(\frac{2r_S+r_D}{l})^4}(a-r_S)(b-r_S)(\frac{r_D-a}{l})(\frac{r_D-b}{l})\cdot$$
$$(\frac{a+r_S+r_D}{l})(\frac{b+r_S+r_D}{l})\cosh^2\frac{t_a}{2\beta_S}\cosh^2\frac{t_b}{2\beta_S}\Big]\ . \tag{A.16}$$

We next calculate other relevant contributions:

$$d(a_+,b_+) = \frac{1}{W'(a_+)W'(b_+)}\Big[(U_S(b_+)-U_S(a_+))(V_S(a_+)-V_S(b_+))\Big]^{\frac{1}{2}}$$
$$= \frac{1}{W'(a_+)W'(b_+)}\Bigg[2e^{\alpha_S(r^*(a)+r^*(b))}\cdot$$
$$\Big(\cosh\Big(\alpha_S(r^*(a)-r^*(b))\Big)-\cosh\Big(\alpha_S(t_a-t_b)\Big)\Big)\Bigg]^{\frac{1}{2}} \tag{A.17}$$

$$d(a_-,b_-) = \frac{1}{W'(a_-)W'(b_-)}\Big[(U_S(b_-)-U_S(a_-))(V_S(a_-)-V_S(b_-))\Big]^{\frac{1}{2}}$$
$$= \frac{1}{W'(a_-)W'(b_-)}\Bigg[2e^{\alpha_S(r^*(a)+r^*(b))}\cdot$$
$$\Big(\cosh\Big(\alpha_S(r^*(a)-r^*(b))\Big)-\cosh\Big(\alpha_S(t_a-t_b)\Big)\Big)\Bigg]^{\frac{1}{2}} \tag{A.18}$$

Now, putting (A.17) and (A.18) together

$$d(a_+,b_+)d(a_-,b_-) = \frac{1}{W'(a_+)W'(b_+)W'(a_-)W'(b_-)}\Bigg[2e^{\alpha_S(r^*(a)+r^*(b))}\cdot$$
$$\Big(\cosh\Big(\alpha_S(r^*(a)-r^*(b))\Big)-\cosh\Big(\alpha_S(t_a-t_b)\Big)\Big)\Bigg] \tag{A.19}$$

Similarly

$$d(a_+,b_-) = \frac{1}{W'(a_+)W'(b_-)}\Big[(U_S(b_-)-U_S(a_+))(V_S(a_+)-V_S(b_-))\Big]^{\frac{1}{2}}$$
$$= \frac{1}{W'(a_+)W'(b_-)}\Bigg[2e^{\alpha_S(r^*(a)+r^*(b))}\cdot$$
$$\left(\cosh\Big(\alpha_S(r^*(a)-r^*(b))\Big)-\cosh\Big(\alpha_S(t_a+t_b-\frac{i\beta}{2})\Big)\right)\Bigg]^{\frac{1}{2}} \tag{A.20}$$

$$d(a_-,b_+) = \frac{1}{W'(a_-)W'(b_+)}\Big[(U_S(b_+)-U_S(a_-))(V_S(a_-)-V_S(b_+))\Big]^{\frac{1}{2}}$$
$$= \frac{1}{W'(b_-)W'(a_+)}\Bigg[2e^{\alpha_S(r^*(a)+r^*(b))}\cdot$$
$$\left(\cosh\Big(\alpha_S(r^*(a)-r^*(b))\Big)-\cosh\Big(\alpha_S(t_a+t_b-\frac{i\beta}{2})\Big)\right)\Bigg]^{\frac{1}{2}} \tag{A.21}$$

Now, putting (A.20) and (A.21) together

$$d(a_+,b_-)d(a_-,b_+) = \frac{1}{W'(a_+)W'(b_-)W'(a_-)W'(b_+)}\Bigg[2e^{\alpha_S(r^*(a)+r^*(b))}\cdot$$
$$\left(\cosh\Big(\alpha_S(r^*(a)-r^*(b))\Big)-\cosh\Big(\alpha_S(t_a+t_b-\frac{i\beta}{2})\Big)\right)\Bigg] \tag{A.22}$$

Putting (A.19) and (A.22) together we get

$$\frac{c}{3}\log\frac{d(a_+,b_+)d(a_-,b_-)}{d(a_+,b_-)d(a_-,b_+)} = \frac{c}{3}\log\Bigg[\frac{\cosh\Big(\alpha_S(r^*(a)-r^*(b))\Big)-\cosh\Big(\alpha_S(t_a-t_b)\Big)}{\cosh\Big(\alpha_S(r^*(a)-r^*(b))\Big)-\cosh\Big(\alpha_S(t_a+t_b-\frac{i\beta}{2})\Big)}\Bigg] \tag{A.23}$$

Here

$$\cosh\Big(\alpha_S(t_a+t_b-\frac{i\beta}{2})\Big) = -\cosh\Big(\alpha_S(t_a+t_b)\Big) \tag{A.24}$$

and

$$\cosh\Big(\alpha_S(r^*(a)-r^*(b))\Big) = \frac{1}{2}\Big[\frac{(a-r_S)^{\alpha_S\beta_S}(a+r_D+r_S)^{\alpha_S\beta_M}(r_D-b)^{\alpha_S\beta_D}}{(r_D-a)^{\alpha_S\beta_D}(b+r_D+r_S)^{\alpha_S\beta_M}(b-r_S)^{\alpha_S\beta_S}} + \frac{(r_D-a)^{\alpha_S\beta_D}(b+r_D+r_S)^{\alpha_S\beta_M}(b-r_S)^{\alpha_S\beta_S}}{(a-r_S)^{\alpha_S\beta_S}(a+r_D+r_S)^{\alpha_S\beta_M}(r_D-b)^{\alpha_S\beta_D}}\Big] \sim \frac{1}{2}\frac{(b-r_S)^{\alpha_S\beta_S}}{(a-r_S)^{\alpha_S\beta_S}}\frac{1}{C(a)}\,, \tag{A.25}$$

using the approximations (3.27), and (3.30). Thus we obtain

$$\frac{c}{3}\log\frac{d(a_+,b_+)d(a_-,b_-)}{d(a_+,b_-)d(a_-,b_+)} = \frac{c}{3}\log\Big[1-2\frac{(a-r_S)^{\alpha_S\beta_S}}{(b-r_S)^{\alpha_S\beta_S}}C(a)\,\cosh\Big(\alpha_S(t_a-t_b)\Big)\Big] - \frac{c}{3}\log\Big[1+2\frac{(a-r_S)^{\alpha_S\beta_S}}{(b-r_S)^{\alpha_S\beta_S}}C(a)\,\cosh\Big(\alpha_S(t_a+t_b)\Big)\Big]\,. \tag{A.26}$$

The total bulk matter entanglement entropy thus is (A.16) plus (A.26): along with the area term this gives (3.29). At late times, *i.e.* $t_a, t_b \gg r_S$ the total entanglement entropy S_{total}, after adding the area term, becomes

$$S_{total} \sim \frac{2\pi a^2}{G_N} + \frac{2c}{6}\log\Big[\frac{2^4 r_S^2}{(\frac{r_D-r_S}{l})^2(\frac{2r_S+r_D}{l})^2}\sqrt{(a-r_S)(b-r_S)}\cdot \sqrt{\frac{(r_D-a)}{l}\frac{(r_D-b)}{l}\frac{(a+r_S+r_D)}{l}\frac{(b+r_S+r_D)}{l}}\cosh\frac{t_a}{2\beta_S}\cosh\frac{t_b}{2\beta_S}\Big] + \frac{c}{3}\log\Big[1-2\frac{(a-r_S)^{\alpha_S\beta_S}}{(b-r_S)^{\alpha_S\beta_S}}C(a)\,\cosh\Big(\alpha_S(t_a-t_b)\Big)\Big] - \frac{c}{3}\log\Big[4\frac{(a-r_S)^{\alpha_S\beta_S}}{(b-r_S)^{\alpha_S\beta_S}}C(a)\,\cosh\frac{t_a}{2\beta_S}\cosh\frac{t_b}{2\beta_S}\Big]\,, \tag{A.27}$$

which upon simplifying (taking $a-r_S\sim 0$ so $\log(1-y)\sim -y$) gives (3.31).

Entanglement entropy of the intervals $R_-\cup I\cup R_+$: It is instructive to compare the above late time calculation of the entanglement entropy of the intervals $[b_-,a_-]\cup[a_+,b_+]$ with that of the original three intervals $R_-\cup I\cup R_+\equiv[r_{D-},b_-]\cup[a_-,a_+]\cup[b_+,r_{D+}]$ which are complementary intervals in the black hole Kruskal patch of SdS. Here, r_{D-} and r_{D+} are the boundaries of the entanglement wedge of the Hawking radiation in the left and right universes respectively. We will take these two points r_{D-} and r_{D+} to be very close to the corresponding cosmological (de Sitter) horizons which might be approximated as the effective boundaries of the black hole Kruskal patch in the flat space like limit (3.6) of de Sitter that we are considering here: see Figure 3.2. Thus we define the spacetime coordinates of these

two points as

$$r_{D+}: \quad (t,r) = (t_D, r_D - \delta)\ ; \qquad r_{D-}: \quad (t,r) = (-t_D + \frac{i\beta}{2}, r_D - \delta)\ . \tag{A.28}$$

Under the assumptions (3.27), using (3.19), we approximate the entanglement entropy for $R_- \cup I \cup R_+$ as

$$\begin{aligned} S_{matter} = & \frac{c}{3}\log\Big[d(a_+,a_-)d(b_+,b_-)\Big] + \frac{c}{3}\log\Big[\frac{d(a_+,b_+)d(a_-,b_-)}{d(a_+,b_-)d(a_-,b_+)}\Big] \\ & + \frac{c}{3}\log\Big[\frac{d(a_+,r_{D-})d(a_-,r_{D+})}{d(a_-,r_{D-})d(a_+,r_{D+})}\Big] + \frac{c}{3}\log\Big[\frac{d(b_+,r_{D+})d(b_-,r_{D-})}{d(b_+,r_{D-})d(b_-,r_{D+})}\Big] \\ & + \frac{c}{3}\log\Big[d(r_{D+},r_{D-})\Big]\ . \end{aligned} \tag{A.29}$$

The expressions in the first line are the same as the matter entanglement entropy for the intervals $[b_-,a_-]\cup[a_+,b_+]$ complementary to $R_-\cup I\cup R_+$. Simplifying using the various Kruskal variable distances as described earlier, we obtain for the expressions in the second and third lines

$$\begin{aligned} & \frac{c}{3}\log\Big[1+2\frac{\delta^{\alpha_S\beta_D}(a-r_S)^{\alpha_S\beta_S}(a+r_S+r_D)^{\alpha_S\beta_M}}{(r_D-\delta-r_S)^{\alpha_S\beta_S}(r_D-a)^{\alpha_S\beta_D}(2r_D-\delta+r_S)^{\alpha_S\beta_M}}\cosh\Big(\alpha_S(t_a+t_D)\Big)\Big] \\ & -\frac{c}{3}\log\Big[1-2\frac{\delta^{\alpha_S\beta_D}(a-r_S)^{\alpha_S\beta_S}(a+r_S+r_D)^{\alpha_S\beta_M}}{(r_D-\delta-r_S)^{\alpha_S\beta_S}(r_D-a)^{\alpha_S\beta_D}(2r_D-\delta+r_S)^{\alpha_S\beta_M}}\cosh\Big(\alpha_S(t_a-t_D)\Big)\Big] \\ & +\frac{c}{3}\log\Big[1-2\frac{\delta^{\alpha_S\beta_D}(b-r_S)^{\alpha_S\beta_S}(b+r_S+r_D)^{\alpha_S\beta_M}}{(r_D-\delta-r_S)^{\alpha_S\beta_S}(r_D-b)^{\alpha_S\beta_D}(2r_D-\delta+r_S)^{\alpha_S\beta_M}}\cosh\Big(\alpha_S(t_a-t_D)\Big)\Big] \\ & -\frac{c}{3}\log\Big[1+2\frac{\delta^{\alpha_S\beta_D}(b-r_S)^{\alpha_S\beta_S}(b+r_S+r_D)^{\alpha_S\beta_M}}{(r_D-\delta-r_S)^{\alpha_S\beta_S}(r_D-b)^{\alpha_S\beta_D}(2r_D-\delta+r_S)^{\alpha_S\beta_M}}\cosh\left(\alpha_S(t_a+t_D)\right)\Big] \\ & +\frac{c}{6}\log\Big[\frac{\delta}{\alpha_S^2}\frac{(r_D-r_S-\delta)}{l}\frac{(2r_D+r_S-\delta)}{l}\cosh^2\frac{t_D}{2\beta_S}\Big]\ . \end{aligned} \tag{A.30}$$

Since $\delta \ll r_D$ and the exponent $\alpha_S\beta_D \sim \frac{r_D}{r_S} \gg 1$, we see that the the expressions in the first four lines are of the form $\log(1+\cdots)$ and thus vanishingly small. The last term

$$\frac{c}{3}\log\Big[d(r_{D+},r_{D-})\Big] \sim \frac{c}{6}\log\Big[\frac{(r_D-r_S)}{l}\frac{(2r_D+r_S)}{l}\Big(\frac{\delta}{\alpha_S^2}\cosh^2\frac{t_D}{2\beta_S}\Big)\Big] \tag{A.31}$$

requires a regularization of the cosmological horizon which is akin to spatial infinity ι^0 in the flat space limit. Let us define

$$\frac{(r_D-r_S)}{l}\frac{(2r_D+r_S)}{l}\frac{\delta\,\lambda}{\alpha_S^2\,\epsilon_{UV}^2}\cosh^2\frac{t_D}{2\beta_S} \ \to\ c_D = finite \tag{A.32}$$

where we have reinstated the various lengthscales, as discussed after (3.17), and using (3.13).

With this regularization of the observer near the cosmological horizon r_D, we see that the entanglement entropy of the intervals $[b_-, a_-] \cup [a_+, b_+]$ used in the text and that of the complementary intervals $R_- \cup I \cup R_+$ are essentially equivalent, as expected for bulk matter in a pure state on the entire slice $R_- \cup [b_-, a_-] \cup I \cup [a_+, b_+] \cup R_+$ in the black hole Kruskal patch in Figure 3.2, in the regime of very low de Sitter temperature (3.4), (3.5), (3.6).

A.3 Entanglement entropy with island at early times

In this section, we study the entanglement entropy looking for an island configuration at early times *i.e.* at some small t_a, t_b (with $t_a, t_b \ll r_S$). In this case Hawking quanta have not had time to escape out so we do not expect any island near the black hole horizon of the form (3.38). Indeed, simplifying (3.29) at early times with the coarse approximation $t_a, t_b \sim 0$ gives

$$\begin{aligned} S_{total} = \frac{2\pi a^2}{G_{_N}} + \frac{c}{6}\log\Big[\frac{2^8 r_S^4}{(\frac{r_D-r_S}{l})^4(\frac{2r_S+r_D}{l})^4}(a-r_S)(b-r_S)(\frac{r_D-a}{l})(\frac{r_D-b}{l})\cdot \\ (\frac{a+r_S+r_D}{l})(\frac{b+r_S+r_D}{l})\Big] \\ + \frac{c}{3}\log\Big[1-2\frac{(a-r_S)^{\alpha_S\beta_S}}{(b-r_S)^{\alpha_S\beta_S}}C(a)\Big] - \frac{c}{3}\log\Big[1+2\frac{(a-r_S)^{\alpha_S\beta_S}}{(b-r_S)^{\alpha_S\beta_S}}C(a)\Big]\,. \end{aligned} \tag{A.33}$$

Extremizing with $a - r_S \sim 0$ and simplifying with r_D large (so $C(a) \sim 1$) gives

$$\frac{4\pi a}{G_{_N}} + \frac{c}{6}\frac{1}{a-r_S} - \frac{c}{3}\frac{1}{\sqrt{(a-r_S)(b-r_S)}} \sim 0\,, \tag{A.34}$$

keeping only leading terms. So, since $b \gg r_S$, there is no island solution with $a \gtrsim r_S$.

However we might imagine that there arises a vanishing extremal surface with the island boundary a far inside the black hole horizon so $a \ll r_S$. The boundary b of the entanglement wedge of the Hawking radiation continues to be far away from the horizon *i.e.* $b - r_S \gg r_S - a$. Towards analysing this, we will employ Kruskal coordinates different from those previously used, defined in the black hole interior since $a < r_S$. So we define the tortoise coordinate as

$$r^* = -\int \frac{1}{f(r)}\,dr = -\int \frac{1}{1-\frac{2m}{r}-\frac{r^2}{l^2}}\,dr = \int \frac{l^2 r}{(r_D-r)(r_S-r)(r+r_S+r_D)}\,dr \tag{A.35}$$

This gives

$$e^{r^*} = (r_D-r)^{-\beta_D}(r_S-r)^{\beta_S}(r+r_D+r_S)^{\beta_M} \tag{A.36}$$

where the β-parameters are as in (4.3). The radial null coordinates are $U = t - r^*$, $V = t + r^*$. Then the Kruskal coordinates adapted to the interior are

$$\begin{aligned} U_S &= -e^{-\alpha_S(t-r^*)} = -e^{-\alpha_S t}(r_D - r)^{-\alpha_S\beta_D}(r_S - r)^{\alpha_S\beta_S}(r + r_D + r_S)^{\alpha_S\beta_M} , \\ V_S &= e^{\alpha_S(t+r^*)} = e^{\alpha_S t}(r_D - r)^{-\alpha_S\beta_D}(r_S - r)^{\alpha_S\beta_S}(r + r_D + r_S)^{\alpha_S\beta_M} , \end{aligned} \tag{A.37}$$

with $\alpha_S = \frac{1}{2\beta_S}$. The reduced two dimensional Schwarzschild de Sitter metric is given by

$$ds^2 = -\lambda\, r\, \frac{dU_S dV_S}{W^2} , \qquad W = \sqrt{r} l \alpha_S (r_D - r)^{\frac{-(1+2\alpha_S\beta_D)}{2}} (r_S - r)^{\frac{2\alpha_S\beta_S - 1}{2}} (r + r_S + r_D)^{\frac{2\alpha_S\beta_M - 1}{2}} . \tag{A.38}$$

with W the interior conformal factor.

Towards approximating early times, we will set $t_a, t_b \sim 0$: then assuming $b - r_S \gg r_S - a$ as stated above and calculating as earlier reveals the total entanglement entropy to be

$$\begin{aligned} S_{total} = \frac{2\pi a^2}{G_N} + \frac{c}{6}\log\Big[& \frac{2^8 r_S^4}{(\frac{r_D - r_S}{l})^4 (\frac{2r_S + r_D}{l})^4} (r_S - a)(b - r_S)(\frac{r_D - a}{l})(\frac{r_D - b}{l}) \cdot \\ & (\frac{a + r_S + r_D}{l})(\frac{b + r_S + r_D}{l})\Big] \\ + \frac{c}{3}\log\Big[1 - 2\frac{(r_S - a)^{\alpha_S\beta_S}}{(b - r_S)^{\alpha_S\beta_S}} C(a)\Big] & - \frac{c}{3}\log\Big[1 + 2\frac{(r_S - a)^{\alpha_S\beta_S}}{(b - r_S)^{\alpha_S\beta_S}} C(a)\Big] . \end{aligned} \tag{A.39}$$

The bulk matter entropy is essentially (3.29) with $a - r_S \to r_S - a$ as arises using the interior Kruskal variables in all the distances, and approximating t_a, $t_b \sim 0$.
Extremizing (A.39) with respect to the island boundary a gives

$$\begin{aligned} & \frac{4\pi a}{G_N} + \frac{c}{6}\Big[- \frac{1}{r_S - a} - \frac{1}{r_D - a} + \frac{1}{a + r_S + r_D}\Big] \\ & = \frac{4c}{6} \frac{\sqrt{\frac{r_S - a}{b - r_S}}\, C(a)}{1 - 4\frac{(r_S - a)}{(b - r_S)} C(a)^2} \cdot \Big[- \frac{1/2}{r_S - a} + \frac{\alpha_S\beta_M}{a + r_S + r_D} + \frac{\alpha_S\beta_D}{r_D - a}\Big] . \end{aligned} \tag{A.40}$$

We see that there exists a quantum extremal surface with $0 < a \ll r_S$ and low generalized entropy: approximating (A.40) with $a \ll r_S$ in all $O(c)$ terms gives

$$\frac{4\pi a}{G_N} \sim \frac{c}{6}\Big(\frac{1}{r_S} + \frac{1}{r_D} - \frac{1}{r_S + r_D}\Big) + \frac{c}{3} \frac{\sqrt{\frac{r_S}{b - r_S}}\, C(0)}{1 - \frac{4r_S}{b - r_S} C(0)^2} \Big(- \frac{1}{r_S} + \frac{2\alpha_S\beta_M}{r_S + r_D} + \frac{2\alpha_S\beta_D}{r_D}\Big) . \tag{A.41}$$

With $b \gg r_S$, the second set of terms on the right is subleading to the first so we obtain

$$a \sim \frac{G_N c}{24\pi}\Big(\frac{1}{r_S} + \frac{1}{r_D} - \frac{1}{r_S + r_D}\Big) . \tag{A.42}$$

The quantity in brackets is positive revealing a small quantum extremal surface $a \sim O(G_{_N} c)$ deep in the interior at early times. It is worth noting that we have made a coarse approximation in setting $t_a, t_b \sim 0$: doing this more carefully requires retaining t_a and extremizing, but we expect similar qualitative behaviour at early times.

For this small QES (A.42), the total on-shell entanglement entropy approximates to

$$S_{o.s.} = \frac{c^2 G_{_N}}{288\pi}\Big(\frac{1}{r_S}+\frac{1}{r_D}-\frac{1}{r_S+r_D}\Big)^2 + \frac{c}{3}\log\Big[\frac{2^4 r_S^2\sqrt{r_S(b-r_S)}}{(\frac{r_D-r_S}{l})^2(\frac{2r_S+r_D}{l})^2}\cdot\sqrt{\frac{r_D}{l}\frac{(r_D-b)}{l}\frac{(r_S+r_D)}{l}\frac{(b+r_S+r_D)}{l}}\Big]\,, \tag{A.43}$$

ignoring terms scaling as $r_D^{-\alpha_S\beta_D}$. Thus at early times when Hawking evaporation has not yet kicked in significantly, the generalized entropy is not significant, in accordance with the approximate purity of the early time state.

Appendix B

Appendix to Chapter 4

B.1 Details: entropy in the no-island case

This section contains some details on the calculations of entanglement entropy in the absence of the island in sec. 3.2.1. Using (4.7) and calculating each part of S_{matter} in (4.19) separately gives

$$U'_{D_-} - U'_{D_+} = -e^{-T_{b'}} \cdot 2\sinh X_{b'}\,, \qquad V'_{D_+} - V'_{D_-} = -e^{-T_{b'}} \cdot 2\sinh X_{b'}\,, \tag{B.1}$$

$$W_{b'_+} = W_{b'_-} = \sqrt{b'}\, l\, \alpha_D\, (b' - r_D)^{-\frac{1-2\alpha_D\beta_D}{2}} (b' - r_S)^{-\frac{1+2\alpha_D\beta_S}{2}} (b' + r_S + r_D)^{-\frac{1+2\alpha_D\beta_M}{2}}\,, \tag{B.2}$$

$$\begin{aligned} W_{b'_+} W_{b'_-} &= b'\, l^2\, \alpha_D^2 (b' - r_D)^{-(1-2\alpha_D\beta_D)} (b' + r_S + r_D)^{-(1+2\alpha_D\beta_M)} (b' - r_S)^{-(1+2\alpha_D\beta_S)} \\ &= \frac{\alpha_D^2}{\lambda b' |f(b')|} e^{-2T_{b'}}\,. \end{aligned} \tag{B.3}$$

Plugging all these into (4.19) gives $S_{matter} = \frac{c}{6}\log[\frac{\lambda b'}{\alpha_D^2} e^{2T_{b'}} |f(b')| e^{-2T_{b'}} 4\sinh^2 X_{b'}]$, *i.e.*

$$S_{matter} = \frac{c}{6}\log\left[\frac{\lambda}{l^2\alpha_D^2}(b' - r_S)\,(b' - r_D)(b' + r_S + r_D)\, 4\sinh^2 X_{b'}\right]. \tag{B.4}$$

Thus finally, we obtain (4.20).

B.2 Details: late-time entropy with island

Here we give details on sec. 4.3. We are looking to calculate (4.26), *i.e.*

$$S_{matter} = \frac{c}{3}\log\frac{d(a'_+,a'_-)d(b'_+,b'_-)d(a'_+,b'_+)d(a'_-,b'_-)}{d(a'_+,b'_-)d(a'_-,b'_+)} \ . \tag{B.5}$$

Now calculating each part in S_{matter} separately

$$\log[d(a'_+,a'_-)] = \frac{1}{2}\log\frac{[(U'_{S_-}-U'_{S_+})(V'_{S_+}-V'_{S_-})]}{W'_{a'_+}W'_{a'_-}} \tag{B.6}$$

with $W_{a'}$ as in (4.14). Then we have

$$U'_{S_-}-U'_{S_+} = e^{T_{a'}}\cdot 2\sinh X_{a'}\,, \qquad V'_{S_+}-V'_{S_-} = e^{T_{a'}}\cdot 2\sinh X_{a'}\,, \tag{B.7}$$

$$\begin{aligned} W_{a'_+}W_{a'_-} &= a'l^2\alpha_S^2(r_D-a')^{-(1+2\alpha_S\beta_D)}(a'+r_S+r_D)^{(2\alpha_S\beta_M-1)}(r_S-a')^{(2\alpha_S\beta_S-1)} \\ &= \frac{\alpha_S^2}{\lambda a'|f(a')|}e^{2T_{a'}} \ . \end{aligned} \tag{B.8}$$

Putting all these expressions together in (B.6) gives

$$\begin{aligned} \log[d(a'_+,a'_-)] &= \frac{1}{2}\log\left[\frac{\lambda a'}{\alpha_S^2}e^{-2T_{a'}}|f(a')|e^{2T_{a'}}4\sinh^2 X_{a'}\right] \\ &= \frac{1}{2}\log\left[\frac{\lambda}{l^2\alpha_S^2}(r_D-a')(r_S-a')(a'+r_S+r_D)\cdot 4\sinh^2 X_{a'}\right]. \end{aligned} \tag{B.9}$$

Similarly we obtain

$$\log[d(b'_+,b'_-)] = \frac{1}{2}\log\left[\frac{\lambda}{l^2\alpha_D^2}(b'-r_D)(b'-r_S)(b'+r_S+r_D)\cdot 4\sinh^2 X_{b'}\right]. \tag{B.10}$$

Now, putting (B.9) and (B.10) together gives

$$\begin{aligned} \frac{c}{3}\log[d(a'_+,a'_-)d(b'_+,b'_-)] = \frac{c}{6}\log\Bigg[&\frac{2^4\lambda^2}{\alpha_D^2\alpha_S^2}(r_S-a')(b'-r_S)\left(\frac{r_D-a'}{l}\right)\left(\frac{b'-r_D}{l}\right)\cdot \\ &\left(\frac{a'+r_S+r_D}{l}\right)\left(\frac{b'+r_S+r_D}{l}\right)\sinh^2 X_{a'}\sinh^2 X_{b'}\Bigg] \ . \end{aligned} \tag{B.11}$$

We next calculate other relevant contributions using (4.7) and (4.13): we have

$$U'_{D_+}-U'_{S_+} = e^{(X_{b'}-T_{b'})}-e^{-(X_{a'}-T_{a'})}, \qquad V'_{S_+}-V'_{D_+} = e^{(X_{a'}+T_{a'})}-e^{-(X_{b'}+T_{b'})}\,,$$

$$U'_{D_-}-U'_{S_-} = e^{-(X_{b'}+T_{b'})}-e^{(X_{a'}+T_{a'})}, \qquad V'_{S_-}-V'_{D_-} = e^{-(X_{a'}-T_{a'})}-e^{(X_{b'}-T_{b'})}\,,$$

so

$$d(a'_+, b'_+) = \frac{1}{\sqrt{W'_{a'_+} W'_{b'_+}}} \Big[(U'_{D_+} - U'_{S_+})(V'_{S_+} - V'_{D_+}) \Big]^{\frac{1}{2}}$$
$$= \frac{1}{\sqrt{W'_{a'_+} W'_{b'_+}}} \left[e^{(T_{a'} - T_{b'})} \cdot \Big(2\cosh(X_{a'} + X_{b'}) - 2\cosh(T_{a'} + T_{b'}) \Big) \right]^{\frac{1}{2}}, \qquad \text{(B.12)}$$

$$d(a'_-, b'_-) = \frac{1}{\sqrt{W'_{a'_-} W'_{b'_-}}} \Big[(U'_{D_-} - U'_{S_-})(V'_{S_-} - V'_{D_-}) \Big]^{\frac{1}{2}}$$
$$= \frac{1}{\sqrt{W'_{a'_-} W'_{b'_-}}} \left[e^{(T_{a'} - T_{b'})} \cdot \Big(2\cosh(X_{a'} + X_{b'}) - 2\cosh(T_{a'} + T_{b'}) \Big) \right]^{\frac{1}{2}}. \qquad \text{(B.13)}$$

Now, putting (B.12) and (B.13) together

$$d(a'_+, b'_+)\, d(a'_-, b'_-) = \frac{1}{\sqrt{W'_{a'_+} W'_{b'_+} W'_{a'_-} W'_{b'_-}}} \left[e^{(T_{a'} - T_{b'})} \cdot \Big(2\cosh(X_{a'} + X_{b'}) - 2\cosh(T_{a'} + T_{b'}) \Big) \right]. \qquad \text{(B.14)}$$

Similarly, we have

$$U'_{D_-} - U'_{S_+} = e^{-(X_{b'} + T_{b'})} - e^{-(X_{a'} - T_{a'})}, \qquad V'_{S_+} - V'_{D_-} = e^{(X_{a'} + T_{a'})} - e^{(X_{b'} - T_{b'})},$$
$$U'_{D_+} - U'_{S_-} = e^{(X_{b'} - T_{b'})} - e^{(X_{a'} + T_{a'})}, \qquad V'_{S_-} - V'_{D_+} = e^{-(X_{a'} - T_{a'})} - e^{-(X_{b'} + T_{b'})},$$

so

$$d(a'_+, b'_-) = \frac{1}{\sqrt{W'_{a'_+} W'_{b'_-}}} \Big[(U'_{D_-} - U'_{S_+})(V'_{S_+} - V'_{D_-}) \Big]^{\frac{1}{2}}$$
$$= \frac{1}{\sqrt{W'_{a'_+} W'_{b'_-}}} \left[e^{(T_{a'} - T_{b'})} \cdot \Big(2\cosh(X_{a'} - X_{b'}) - 2\cosh(T_{a'} + T_{b'}) \Big) \right]^{\frac{1}{2}}, \qquad \text{(B.15)}$$

$$d(a'_-, b'_+) = \frac{1}{\sqrt{W'_{a'_-} W'_{b'_+}}} \Big[(U'_{D_+} - U'_{S_-})(V'_{S_-} - V'_{D_+}) \Big]^{\frac{1}{2}}$$
$$= \frac{1}{\sqrt{W'_{a'_-} W'_{b'_+}}} \left[e^{(T_{a'} - T_{b'})} \cdot \Big(2\cosh(X_{a'} - X_{b'}) - 2\cosh(T_{a'} + T_{b'}) \Big) \right]^{\frac{1}{2}}. \qquad \text{(B.16)}$$

Now, putting (B.15) and (B.16) together

$$d(a'_+,b'_-)\,d(a'_-,b'_+)=\frac{1}{\sqrt{W'_{a'_+}W'_{b'_-}W'_{a'_-}W'_{b'_+}}}\left[e^{(T_{a'}-T_{b'})}\cdot\left(2\cosh\left(X_{a'}-X_{b'}\right)-2\cosh\left(T_{a'}+T_{b'}\right)\right)\right]. \tag{B.17}$$

Putting (B.14) and (B.17) together we get

$$\frac{c}{3}\log\frac{d(a'_+,b'_+)d(a'_-,b'_-)}{d(a'_+,b'_-)d(a'_-,b'_+)}=\frac{c}{3}\log\left[\frac{2\cosh\left(T_{a'}+T_{b'}\right)-2\cosh\left(X_{a'}+X_{b'}\right)}{2\cosh\left(T_{a'}+T_{b'}\right)-2\cosh\left(X_{a'}-X_{b'}\right)}\right]. \tag{B.18}$$

Here

$$\begin{aligned}2\cosh\left(T_{a'}+T_{b'}\right)=&\ \frac{1}{2}\left[\frac{(r_S-a')^{\alpha_S\beta_S}(a'+r_D+r_S)^{\alpha_S\beta_M}(b'-r_S)^{\alpha_D\beta_S}(b'+r_D+r_S)^{\alpha_D\beta_M}}{(r_D-a')^{\alpha_S\beta_D}(b'-r_D)^{\alpha_D\beta_D}}\right.\\&\left.+\frac{(r_D-a')^{\alpha_S\beta_D}(b'-r_D)^{\alpha_D\beta_D}}{(b'+r_D+r_S)^{\alpha_D\beta_M}(b'-r_S)^{\alpha_D\beta_S}(r_S-a')^{\alpha_S\beta_S}(a'+r_D+r_S)^{\alpha_S\beta_M}}\right]\\\sim&\ \frac{1}{2}\frac{(b'-r_D)^{\alpha_D\beta_D}}{(r_S-a')^{\alpha_S\beta_S}}\frac{1}{C(a')}\ ,\end{aligned} \tag{B.19}$$

using the approximation (4.23), and (4.28). Thus we obtain

$$\begin{aligned}\frac{c}{3}\log\frac{d(a_+,b'_+)d(a_-,b'_-)}{d(a_+,b'_-)d(a_-,b'_+)}=&\ \frac{c}{3}\log\left[1-2\frac{(r_S-a')^{\alpha_S\beta_S}}{(b'-r_D)^{\alpha_D\beta_D}}C(a')\,\cosh\left(X_{a'}+X_{b'}\right)\right]\\&-\frac{c}{3}\log\left[1-2\frac{(r_S-a')^{\alpha_S\beta_S}}{(b'-r_D)^{\alpha_D\beta_D}}C(a')\,\cosh\left(X_{a'}-X_{b'}\right)\right].\end{aligned} \tag{B.20}$$

The total bulk matter entanglement entropy thus is (B.11) plus (B.20), along with the area term. Thus at large values of X'_a and X'_b, after adding the area term the total entanglement entropy S_{total} becomes (4.27) *i.e.*

$$\begin{aligned}S_{total}\sim&\ \frac{2\pi a'^2}{G_N}+\frac{2c}{6}\log\left[\frac{2^2\lambda}{\alpha_D\alpha_S}\sqrt{(r_S-a')(b'-r_S)}\cdot\right.\\&\left.\sqrt{\frac{(r_D-a')}{l}\frac{(b'-r_D)}{l}\frac{(a'+r_S+r_D)}{l}\frac{(b'+r_S+r_D)}{l}}\sinh X_{a'}\sinh X_{b'}\right]\\&+\frac{c}{3}\log\left[1-2\frac{(r_S-a')^{\alpha_S\beta_S}}{(b'-r_D)^{\alpha_D\beta_D}}C(a')\,\cosh\left(X_{a'}+X_{b'}\right)\right]\\&-\frac{c}{3}\log\left[1-2\frac{(r_S-a')^{\alpha_S\beta_S}}{(b'-r_D)^{\alpha_D\beta_D}}C(a')\,\cosh\left(X_{a'}-X_{b'}\right)\right].\end{aligned} \tag{B.21}$$

B.3 Inconsistencies in other island solutions

In this section, we briefly describe inconsistencies in other potential island solutions.

B.3.1 Island outside the black hole horizon

We discuss a potential island with boundary just outside the black hole horizon *i.e.* in the static diamond, similar to the results in [149]. Here we use the static diamond Kruskal coordinates (4.11) redefined as $X_a = \alpha_S t_a$ and $T_a = \alpha_S r_a^*$ for the location of the island boundary. The calculation now gives the total generalized entropy as

$$\begin{aligned} S_{total} = \frac{2\pi a^2}{G_N} + \frac{c}{6}\log\Big[\frac{2^4\lambda^2}{\alpha_D^2\alpha_S^2}(a-r_S)(b'-r_S)(\frac{r_D-a}{l})(\frac{b'-r_D}{l})\cdot \\ (\frac{a+r_S+r_D}{l})(\frac{b+r_S+r_D}{l})\cosh^2 X_a \sinh^2 X_{b'}\Big] \\ + \frac{c}{3}\log\Big[1+2\frac{(a-r_S)^{\alpha_S\beta_S}}{(b'-r_D)^{\alpha_D\beta_D}}C(a)\,\sinh\left(X_a+X_{b'}\right)\Big] \\ - \frac{c}{3}\log\Big[1+2\frac{(a-r_S)^{\alpha_S\beta_S}}{(b'-r_D)^{\alpha_D\beta_D}}C(a)\,\sinh\left(X_a-X_{b'}\right)\Big]\,, \end{aligned} \tag{B.22}$$

Extremizing (B.22) with the island boundary a as $\frac{\partial S_{total}}{\partial a} = 0$ gives

$$\begin{aligned} \frac{4\pi a}{G_N} + \frac{c}{6}\frac{1}{a-r_S} + \frac{c}{3}\frac{C(a)}{\sqrt{b'-r_D}\sqrt{a-r_S}}\cdot\Big[\frac{\sinh(X_a+X_{b'})}{1+2\frac{(a-r_S)^{\alpha_S\beta_S}}{(b'-r_D)^{\alpha_D\beta_D}}C(a)\,\sinh\left(X_a+X_{b'}\right)} \\ - \frac{\sinh(X_a-X_{b'})}{1+2\frac{(a-r_S)^{\alpha_S\beta_S}}{(b'-r_D)^{\alpha_D\beta_D}}C(a)\,\sinh\left(X_a-X_{b'}\right)}\Big] = 0\,. \end{aligned} \tag{B.23}$$

Next, extremizing (B.22) with respect to X_a as $\frac{\partial S_{total}}{\partial X_a} = 0$ gives

$$\begin{aligned} \tanh X_a = 2\sqrt{\frac{a-r_S}{b'-r_D}}\,C(a)\cdot\Big[\frac{\cosh(X_a-X_{b'})}{1+2\frac{(a-r_S)^{\alpha_S\beta_S}}{(b'-r_D)^{\alpha_D\beta_D}}C(a)\,\sinh\left(X_a-X_{b'}\right)} \\ - \frac{\cosh(X_a+X_{b'})}{1+2\frac{(a-r_S)^{\alpha_S\beta_S}}{(b'-r_D)^{\alpha_D\beta_D}}C(a)\,\sinh\left(X_a+X_{b'}\right)}\Big] \end{aligned} \tag{B.24}$$

Considering $X_a = X_{b'}$, (B.24) becomes

$$\begin{aligned} 1+2\sqrt{\frac{a-r_S}{b'-r_D}}C(a)\sinh 2X_a = 2\sqrt{\frac{a-r_S}{b'-r_D}}C(a)\frac{1}{\tanh X_a} \\ \cdot\left[1+2\sqrt{\frac{a-r_S}{b'-r_D}}C(a)\sinh 2X_a - \cosh 2X_a\right]. \end{aligned} \tag{B.25}$$

Putting this condition (B.25) back in (B.23) for large X_a (with $a - r_S$ small) gives

$$a + \frac{G_N c}{24\pi} \frac{1}{a - r_S} \left(1 - \frac{\tanh X_a}{\coth 2X_a}\right) = 0\,. \tag{B.26}$$

It can be seen that $\frac{\tanh X_a}{\coth 2X_a} < 1$ always so that all terms are positive here: thus there is no solution with $a > r_S$. Thus these extremization equations (B.23) and (B.24) together do not give reasonable island solutions.

Similarly, if we consider $X_a = -X_{b'}$, (B.24) becomes

$$\begin{aligned} 1 + 2\sqrt{\frac{a - r_S}{b' - r_D}} C(a) \sinh 2X_a = 2\sqrt{\frac{a - r_S}{b' - r_D}} C(a) \frac{1}{\tanh X_a} \\ \cdot \left[-1 - 2\sqrt{\frac{a - r_S}{b' - r_D}} C(a) \sinh 2X_a + \cosh 2X_a\right]. \end{aligned} \tag{B.27}$$

Putting this condition (B.27) back in (B.23) for large X_a gives (B.26) again.

B.3.2 Island inside the black hole: another possibility

Recalling sec. 4.3 and the extremization equations (4.30), (4.31). Instead of $X_{a'} = X_{b'}$ considered there, let us consider $X_{a'} = -X_{b'}$: then $X_{a'} + X_{b'} = 0$ and $X_{a'} - X_{b'} = 2X_{a'}$. Then (4.31) gives for large $X_{a'}$ and $X_{b'}$:

$$1 - 2\sqrt{\frac{r_S - a'}{b' - r_D}} C(a') \cosh 2X_{a'} = -2\sqrt{\frac{r_S - a'}{b' - r_D}} C(a') \frac{\sinh 2X_{a'}}{\coth X_{a'}}\,. \tag{B.28}$$

The minus sign on the right hand side leads to trouble when this is put back in (4.30), giving no semiclassical $a' \lesssim r_S$ near horizon island solution.

B.4 Future boundary, timelike separated QES

In this section, we exhibit other quantum extremal surface solutions which are timelike separated from the radiation region near the future boundary. We will use several technical details from [104].

The Schwarzschild de Sitter metric (3.1), after the redefinitions $\tau = \frac{l}{r}$, $\omega = \frac{t}{l}$, becomes

$$ds^2 = \frac{l^2}{\tau^2}\left(-\frac{d\tau^2}{f(\tau)} + f(\tau) d\omega^2 + d\Omega_2^2\right), \qquad f(\tau) = 1 - \tau^2 + \frac{2m}{l}\tau^3 = (1 - a_1\tau)(1 - a_2\tau)(1 + (a_1 + a_2)\tau),$$

$$a_1a_2(a_1+a_2)=\frac{2m}{l}\,,\qquad a_1^2+a_1a_2+a_2^2=1;\qquad 0<a_2<a_1<1\;;\qquad \frac{m}{l}\leq\frac{1}{3\sqrt{3}}.\tag{B.29}$$

In the above, $\tau_c=\frac{1}{a_1}$ and $\tau_s=\frac{1}{a_2}$ are the cosmological (de Sitter) and Schwarzschild horizons. (The third zero does not correspond to a physical horizon.)

For SdS_4 with $f(\tau)$ in (B.29), the tortoise coordinate $y=\int\frac{d\tau}{f(\tau)}$ can be defined as

$$y=\int\frac{d\tau}{1-\tau^2+\frac{2m}{l}\tau^3}=-\beta_1\log(1-a_1\tau)+\beta_2\log(1-a_2\tau)+\beta_3\log(1+(a_1+a_2)\tau)\,.\tag{B.30}$$

With the parameters

$$\beta_1=\frac{a_1}{3a_1^2-1},\qquad \beta_2=-\frac{a_2}{3a_2^2-1},\qquad \beta_3=\frac{a_1+a_2}{3a_1a_2+2}\tag{B.31}$$

the SdS_4 metric becomes

$$ds^2=l^2(\frac{1}{\tau^2}-1+\frac{2m}{l}\tau)(d\omega^2-dy^2)+\frac{l^2}{\tau^2}d\Omega_2^2\,.\tag{B.32}$$

Now, we consider the same reduction ansatz from [149] to perform dimentional reduction of the SdS_4 background to 2-dimensions. The 2-dim metric and dilaton become

$$ds_2^2=\frac{\lambda l^3}{\tau}(\frac{1}{\tau^2}-1+\frac{2m}{l}\tau)(d\omega^2-dy^2),\qquad \phi=\phi_r\frac{\lambda^2l^2}{\tau^2}\,.\tag{B.33}$$

In the reduced 2-dim Schwarzschild de sitter spacetime,the Kruskal coordinates around the cosmological horizon are then defined as U,V and the metric becomes

$$U=e^{\frac{\omega-y}{2\beta_1}},\quad V=-e^{-\frac{\omega+y}{2\beta_1}};\qquad UV=-e^{-\frac{y}{\beta_1}},\quad \frac{U}{V}=-e^{\frac{\omega}{\beta_1}};$$
$$UV=(a_1\tau-1)(1-a_2\tau)^{-\frac{\beta_2}{\beta_1}}(1+(a_1+a_2)\tau)^{-\frac{\beta_3}{\beta_1}}\,,\tag{B.34}$$

$$ds_2^2=\frac{4\beta_1^2g(U,V)}{UV}\,dUdV\,.\tag{B.35}$$

Using (B.33), the generalized entropy for a future boundary observer at $(\omega,\tau)=(\omega_0,\tau_0)$ in the 2-dim SdS_4 spacetime becomes (with $P(\tau_0)=\frac{1}{\tau_0^2}-1+\frac{2m}{l}\tau_0$)

$$S_{gen}=\frac{\phi_r}{4G}\frac{l^2}{\tau^2}+\frac{c}{12}\log[\frac{1}{\epsilon_{uv}^4}((\omega-\omega_0)^2-(y-y_0)^2)^2\frac{\lambda^2l^6}{\tau\tau_0}P(\tau_0)(\frac{1}{\tau^2}-1+\frac{2m}{l}\tau)]\,.\tag{B.36}$$

This expression for S_{gen} should be regarded as a smooth function of U,V, with respect to which we will extremize to find quantum extremal surfaces. However the nature of the QES here can be gleaned by simply noting that the only place the spatial future boundary coordinate ω enters is through the spacetime interval $\Delta^2=(\omega-\omega_0)^2-(y-y_0)^2$ inside the logarithm.

Thus we expect $\frac{\partial S_{gen}}{\partial \omega} = \frac{c}{3}\frac{\omega-\omega_0}{\Delta^2} = 0$, so that $\omega = \omega_0$, *i.e.* the QES is timelike separated from the future boundary observer.

Analysing more carefully, extremizing (B.36) with Kruskal U, V, as

$$\frac{\partial S_{gen}}{\partial U} = \frac{\partial S_{gen}}{\partial \tau}\frac{\partial \tau}{\partial U} + \frac{\partial S_{gen}}{\partial \omega}\frac{\partial \omega}{\partial U} = 0 \quad , \quad \frac{\partial S_{gen}}{\partial V} = \frac{\partial S_{gen}}{\partial \tau}\frac{\partial \tau}{\partial V} + \frac{\partial S_{gen}}{\partial \omega}\frac{\partial \omega}{\partial V} = 0\,, \tag{B.37}$$

and, from (B.36), (B.34), (B.35), noting that

$$\frac{\partial S_{gen}}{\partial \tau} = -\frac{\phi_r}{2G}\frac{l^2}{\tau^3} + \frac{c}{12}\frac{1}{f(\tau)}[-\frac{4(y-y_0)}{\Delta^2} + \tau(1-\frac{3}{\tau^2})], \qquad \frac{\partial S_{gen}}{\partial \omega} = \frac{c}{3}\frac{\omega-\omega_0}{\Delta^2};$$

we find the extremization conditions become

$$[-\frac{\phi_r}{2G}\frac{l^2}{\tau^3} + \frac{c}{12}\frac{1}{f(\tau)}(-\frac{4(y-y_0)}{\Delta^2} + \tau(1-\frac{3}{\tau^2}))]\frac{A(\tau)}{U} + \frac{c}{3}\frac{\omega-\omega_0}{\Delta^2}\frac{\beta_1}{U} = 0\,, \tag{B.38}$$

and

$$[-\frac{\phi_r}{2G}\frac{l^2}{\tau^3} + \frac{c}{12}\frac{1}{f(\tau)}(-\frac{4(y-y_0)}{\Delta^2} + \tau(1-\frac{3}{\tau^2}))]\frac{A(\tau)}{V} + \frac{c}{3}\frac{\omega-\omega_0}{\Delta^2}(-\frac{\beta_1}{V}) = 0\,. \tag{B.39}$$

Subtracting as (B.38)-(B.39) gives $\frac{2c}{3}\frac{\omega-\omega_0}{\Delta^2}\beta_1 = 0$. Thus,

$$\omega = \omega_0\,, \tag{B.40}$$

giving timelike separated QES with respect to the future boundary observer. The timelike separation implies that the generalized entropy becomes complex-valued, with $\log(-|\Delta^2|)$ giving rise to $\log(-1) = i\pi$, as in pure de Sitter.

Now, by putting $\omega = \omega_0$ in (B.38) gives

$$-\frac{\phi_r}{2G}\frac{l^2}{\tau^3} + \frac{c}{12}\frac{1}{f(\tau)}(\frac{4}{y-y_0} + \tau(1-\frac{3}{\tau^2})) = 0 \tag{B.41}$$

The future boundary observer has $r = \infty$ and $\tau_0 = 0$ so $y_0 = 0$. Further considering $\tau = 1-\epsilon$, where $\epsilon \ll 1$, and noting $1 \ll c \ll \frac{1}{G}$, we simplify (B.41) ignoring appropriate terms and obtain

$$\frac{2c}{\log[\frac{(1-a_2(1-\epsilon))^{\beta_2}(1+(a_1+a_2)(1-\epsilon))^{\beta_3}}{(1-a_1(1-\epsilon))^{\beta_1}}]} \approx \frac{3\phi_r}{G}l^2[\frac{\epsilon(2-\epsilon)}{(1-\epsilon)^3} + \frac{2m}{l}] \tag{B.42}$$

Now, considering a_1 and a_2 perturbatively as $a_1 \simeq 1 - \frac{m}{l}$, $a_2 \simeq \frac{2m}{l}$, and $0 < a_2 < a_1 < 1$, we can obtain the parameters $\beta_1, \beta_2, \beta_3$ using (B.31) perturbatively as well. This finally gives

$$c \approx \frac{3\phi_r}{2G} l^2 (\epsilon + \frac{m}{l}) \log(\frac{2}{\epsilon + \frac{m}{l}}) \tag{B.43}$$

which is a consistency condition on the central charge (number of degrees of freedom) of the 2-dim CFT matter for the timelike extremal surface to exist (pure dS corresponds to $m = 0$).

Appendix C

Appendix to Chapter 7

C.1 The basic setup on inflation

C.1.1 dS_4 slow roll

This pertains to sec. 7.1.1 in the main text. We will be brief in our review of pertinent points of inflation: general useful reviews include [239, 240], and [222]-[229]. The action for the 4-dim Einstein scalar theory (with $8\pi G_N = 1$) is

$$I = \int d^4x\sqrt{g}\left(\frac{R}{2} - \frac{1}{2}\left(\nabla\phi\right)^2 - V(\phi)\right) - \int d^3x\sqrt{h}K\,. \tag{C.1}$$

With $ds^2 = -dt^2 + a(t)^2 d\Omega_3^2,\ \phi = \phi(t)$, the equations of motion become

$$\begin{aligned} 3H^2 = 3\left(\frac{\dot{a}}{a}\right)^2 &= -\frac{3}{a^2} + \frac{1}{2}\dot{\phi}^2 + V(\phi), \\ \ddot{\phi} + 3H\dot{\phi} + V'(\phi) &= 0\,. \end{aligned} \tag{C.2}$$

In the slow roll approximation, the inflaton kinetic term is subdominant relative to the potential: for large 3-sphere size a_r near the end of inflation, we ignore the $\frac{3}{a^2}$ curvature term in (C.2), which then gives

$$3H^2 \sim V(\phi), \qquad 3H\dot{\phi} \sim -V'(\phi)\,. \tag{C.3}$$

At "horizon crossing" $\phi = \phi_*$, we have $H_* \equiv H(\phi_*) = \frac{1}{a_*} = \frac{1}{a_r} e^{\mathcal{N}(\phi,\phi_*)}$ and the leading dS metric is (7.1) with radius $H_*^{-1} = l$, and

$$l \equiv \frac{1}{H_*}\,, \qquad H_*^2 \sim \frac{V_*}{3}\,, \qquad \tau = H_* t\,. \tag{C.4}$$

For the inflaton perturbation, the equation of motion alongwith the slow-roll parameter ϵ gives

$$\phi = \phi_* + \varphi\ : \qquad \partial_\tau^2 \varphi + 3\tanh\tau \partial_\tau \varphi + 3\sqrt{2\epsilon} = 0\,, \qquad \epsilon \equiv \frac{{V_*}'^2}{2V_*^2}\,. \tag{C.5}$$

Solving this with $A = \frac{{V_*}'}{H_*^2} = 3\sqrt{2\epsilon}$ gives

$$\varphi(\tau) = -\frac{1}{3}A\log(\cosh\tau) + \frac{1}{6}\mathrm{sech}^2\tau(2A + 3c_1\sinh\tau) + c_1\tan^{-1}\left(\tanh\frac{\tau}{2}\right) + c_2\,. \tag{C.6}$$

Imposing regularity at the no-boundary point $\tau = i\frac{\pi}{2}$ (via the φ-derivative) fixes $c_1 = -\frac{2A}{3i}$. This then gives

$$\varphi(\tau) = \frac{{V_*}'}{V_*}\left(\frac{1 + i\sinh\tau}{\cosh^2\tau} - \log(1 - i\sinh\tau) - i\frac{\pi}{2}\right) = \frac{{V_*}'}{V_*}\tilde{\varphi}(\tau)\,. \tag{C.7}$$

The constant $\tilde{c}_2$ (with $c_2 = \frac{{V_*}'}{V_*}\tilde{c}_2$ in (C.6)) inside the bracket has been fixed to $-i\frac{\pi}{2}$ by expanding at late times (large τ), which gives

$$\varphi(\tau) = \frac{V_*'}{V_*}\tilde{\varphi}(\tau) = \frac{V_*'}{V_*}\left[-\tau + \log 2 + i\frac{\pi}{2} + \tilde{c}_2 + \ldots\right]. \tag{C.8}$$

This gives $\tilde{c}_2 = -i\frac{\pi}{2}$ to match with the slow roll solution expanded around ϕ_* at large τ:

$$\phi = \phi_* - \frac{V_*'}{V_*}\log\left(\frac{a}{a_*}\right) = \phi_* - \frac{V_*'}{V_*}\log\left(\frac{\cosh\tau}{H_* a_*}\right) \sim \phi_* - \frac{V_*'}{V_*}(\tau - \log 2)\ . \tag{C.9}$$

Putting all this together finally gives (7.11). This completes our quick review, following [223].

C.1.2 dS_3 slow roll

The overall setup for inflation is very similar so we will simply list the central expressions used in sec. 7.2.1. The equations of motion (with $8\pi G = 1$) are

$$\begin{aligned} H^2 &= \left(\frac{\dot{a}}{a}\right)^2 = -\frac{1}{a^2} + \frac{1}{2}\dot{\phi}^2 + V(\phi)\,, \\ &\ddot{\phi} + 2H\dot{\phi} + V'(\phi) = 0\,. \end{aligned} \tag{C.10}$$

In the slow roll approximation these give

$$H^2 \sim V(\phi), \qquad 2H\dot{\phi} \sim -V'(\phi)\,, \qquad \rightarrow \qquad H_* \equiv H(\phi_*)\,, \quad H_*^2 \sim V_*\,, \tag{C.11}$$

with the second set of expressions obtained when the 2-sphere size crosses the horizon.

The inflaton equation (C.10) expanding for the perturbation as $\phi = \phi_* + \varphi$ becomes

$$\partial_\tau^2 \varphi + 2\tanh\tau \partial_\tau \varphi + \frac{V_*{}'}{H_*^2} = 0\,. \tag{C.12}$$

With $\sqrt{2\epsilon} = \frac{V_*{}'}{H_*^2} = \frac{V_*{}'}{V_*}$ this has the solution

$$\varphi(\tau) = c_2 + \tanh\tau\left(c_1 - \frac{\sqrt{\epsilon}\,\tau}{\sqrt{2}}\right)\,. \tag{C.13}$$

Regularity at $\tau = i\frac{\pi}{2}$ fixes $c_1 = i\frac{\pi\sqrt{\epsilon}}{2\sqrt{2}}$. The constant c_2 is fixed by matching with the slow roll solution expanded around ϕ_* at late times (large τ),

$$\phi = \phi_* - \frac{V_*'}{V_*}\log\left(\frac{a}{a_*}\right) = \phi_* - \frac{V_*'}{V_*}\left(\frac{\tau}{2} - \frac{\log 2}{2}\right)\,. \tag{C.14}$$

This finally gives the inflaton profile as

$$\varphi(\tau) = \sqrt{2\epsilon}\left[\left(\frac{i\pi}{4} - \frac{\tau}{2}\right)\tanh\tau + \left(\frac{\log 2}{2} - \frac{i\pi}{4}\right)\right]. \tag{C.15}$$

C.2 Details: dS_4 slow-roll area

We describe details of the calculation of the no-boundary extremal surface area for dS_4 slow roll inflation here. The leading contribution to the area (7.14) over the contour (Figure 7.2) is

$$\begin{aligned} S_0 &= \frac{\pi\, l^2}{2G_4}\left(\int_{y=1}^{y=\delta}\frac{d(-y)}{2\sqrt{y}} + \int_{\theta=\pi}^{\theta=0}\frac{d(\delta\, e^{i\theta})}{2\sqrt{-\delta\, e^{i\theta}}} + \frac{1}{i}\int_{\delta}^{z_c}\frac{dz}{2\sqrt{z}}\right) \\ &= \frac{\pi\, l^2}{2G_4}\left(-\sqrt{-z}\Big|_{-1}^{-\delta} + \sqrt{\delta}(-\sqrt{-e^{i\theta}})\Big|_{\theta=\pi}^{\theta=0} + \frac{1}{i}\sqrt{z}\Big|_{\delta}^{z_c}\right) \\ &= \frac{\pi\, l^2}{2G_4}\left(1 - \sqrt{\delta} + \sqrt{\delta}(-i+1) + \frac{1}{i}(\sqrt{z_c} - \sqrt{\delta})\right). \end{aligned} \tag{C.16}$$

On the $[-1, 0]$ leg we have redefined $z = -y$ which makes this piece $\int_\delta^1 \frac{dy}{2\sqrt{y}}$. On the semicircle we have $z = \delta e^{i\theta}$ as stated above and we then integrate in terms of the variable $e^{i\theta}$. Of course

here there is no singularity at $z=0$ but we have written this explicitly above to normalize this calculation with the slow-roll correction to follow. So we obtain simply (with $z_c \sim R_c^2$) $S = \frac{\pi l^2}{2G_4}(1 - i\frac{R_c}{l})$, after reinstating the dimensionful dS_4 scale l.

To calculate the $O(\epsilon)$ slow-roll correction, we first note that the correction to the metric component g_{rr} in (7.13) is recast in the z-variable in (7.7) for $z > 0$ (*i.e.* the Lorentzian region $r > 1$) as

$$\beta_>(z) = \frac{i\left(3\pi(z+1)^3 + \left(z^{3/2} + 9iz - 12\sqrt{z} - 2i\right)\left(-1 - i\sqrt{z}\right)^3\right)}{6z(z+1)^2} + \frac{(z+1)\log\left(1 - i\sqrt{z}\right)}{z}\,, \tag{C.17}$$

and we obtain

$$I_\epsilon^> = \int \frac{\beta_>(z)}{2i\sqrt{z}}\, dz \;=\; \frac{1}{6i\sqrt{z}}\left(2 - 3i\pi(1-z) - 7z - 6(1-z)\log(1 - i\sqrt{z})\right) + \frac{2/3}{1 - i\sqrt{z}}\,, \tag{C.18}$$

with $z > 0$ in this expression. It turns out happily that these integrals can be evaluated in Mathematica (with some care in evaluating them as non-analytic complex objects): the integrated expression can also be cross-checked manually of course. To evaluate the slow-roll correction area integral in the hemisphere region $r < 1$, we continue to $z < 0$: in this regard note that

$$\int_{-1}^{-\delta} \frac{\beta_>(z)}{2\sqrt{-z}} dz = \int_1^{\delta} \frac{\beta_>(-y)}{2\sqrt{y}} d(-y) = \int_\delta^1 \frac{\beta_<(y)}{2\sqrt{y}} dy \equiv I_\epsilon^<(z)\,. \tag{C.19}$$

Thus it is adequate to analytically continue the integrated expression $I_\epsilon^>(z)$ to the hemisphere as $z \to -z$, and we obtain the indefinite integral in the $O(\epsilon)$ piece here as

$$I_\epsilon^<(z) = I_\epsilon^>(-z) = \frac{1}{6\sqrt{z}}\left(-2 + 3i\pi(1+z) - 7z + 6(1+z)\log(1+\sqrt{z})\right) + \frac{2/3}{1+\sqrt{z}}\,, \tag{C.20}$$

with $z > 0$ in this expression now.

Expanding $I_\epsilon^>$ in the $z > 0$ part of the contour, we obtain

$$z = z_c \to \infty: \quad I_\epsilon^> = 1 + i\frac{7}{6}\sqrt{z_c} - i\sqrt{z_c}\log\sqrt{z_c}\,; \qquad z = \delta: \quad I_\epsilon^> = \frac{2 - 3i\pi}{6i\sqrt{\delta}} + \frac{5}{3}\,, \tag{C.21}$$

and we have regulated $z = 0^+$ by $z = \delta > 0$. In obtaining the above, we have expanded $\log(1+z) \sim z$ for small z in the various expressions, and used $\log(-1) = i\pi,\ \log(\pm i) = \pm\frac{i\pi}{2}$. This is important in order to cancel real divergent terms for large z_c: as it stands we see that all the divergent terms for large z_c are pure imaginary.

Expanding $I_\epsilon^<$ in the $z<0$ part of the contour, we obtain near $z=1$ (nbp) and $z=\delta$ (which is near 0^- in the earlier variable)

$$z=1: \quad I_\epsilon^< = \frac{1}{6}(-2+6i\pi-7+12\log 2)+\frac{1}{3}\,, \qquad z=\delta: \quad I_\epsilon^< = \frac{-2+3i\pi}{6\sqrt{\delta}}+\frac{5}{3}\,. \tag{C.22}$$

Along the regulating semicircle around $z=0$ with small $z=\delta$, examining the asymptotics of $I_\epsilon^>$, we obtain

$$I_\epsilon^\theta\Big|_{\theta=\pi}^{\theta=0} = \left(\frac{2-3i\pi}{6\sqrt{-\delta e^{i\theta}}}\right)\Big|_{\theta=\pi}^{\theta=0} = \frac{2-3i\pi}{6i\sqrt{\delta}} - \frac{2-3i\pi}{6\sqrt{\delta}}\,. \tag{C.23}$$

Note that near $z=0$, we have $\beta_>(z)=-\frac{2-3i\pi}{6z}$ as the leading singular behaviour. Integrating this around the semicircle explicitly recovers the above.

Adding up all the above contributions to the area (7.14) finally gives (7.15).

One may question whether the above calculation in the z-variable has introduced subtleties due to the $\sqrt{-z}$ in various places. It turns out that the area can also be calculated directly in the form (7.5) in the r-coordinate (*e.g.* by evaluating in Mathematica). Using $\beta_>(r)$ in (7.13), we obtain below the indefinite integrals $I^>(r)$ and $I^<(r)$ respectively:

$$\begin{aligned}-i\int \frac{1+\epsilon\,\beta_>(r)}{\sqrt{r^2-1}}\,r\,dr \;=\; & -i\sqrt{r^2-1}-i\epsilon\,\frac{1}{6r^2\sqrt{r^2-1}}\Big[\Big(3i\pi r^4-7r^4-6i\pi r^2+5r^2\\ & +4\big(1+i\sqrt{r^2-1}\big)+6r^2(r^2-2)\log\big(1-i\sqrt{r^2-1}\big)\Big)\Big]\end{aligned} \tag{C.24}$$

$$\begin{aligned}\int \frac{1+\epsilon\,\beta_<(r)}{\sqrt{1-r^2}}\,r\,dr \;=\; & -\sqrt{1-r^2}+\epsilon\frac{1}{6r^2\sqrt{1-r^2}}\Big[\Big(3i\pi r^4-7r^4-6i\pi r^2+5r^2\\ & +4\big(1-\sqrt{1-r^2}\big)+6r^2(r^2-2)\log\big(1+\sqrt{1-r^2}\big)\Big)\Big]\,.\end{aligned} \tag{C.25}$$

In the second integral ($r<1$) above, we have obtained $\beta_<(r)$ by continuing $\beta_>(r)$ to $r<1$, which amounts to simply replacing $-i\sqrt{r^2-1}$ by $\sqrt{1-r^2}$ in its four occurrences in the expression (7.13). Then we fix the overall sign of the full integral so that the leading term matches the sign of the leading term $\int_0^1 \frac{r\,dr}{\sqrt{1-r^2}}$ in (7.5) which is the pure dS_4 hemisphere area in (6.4), (6.5). This is the form of the area integral in (7.14) in the r-coordinate. Evaluating these at the various limiting points gives

$$\begin{aligned} I^>(r)\Big|_1^{R_c/l} &= -i\frac{R_c}{l}+\epsilon\left(1-i\frac{R_c}{l}\log\frac{R_c}{l}+i\frac{7}{6}\frac{R_c}{l}\right)-\frac{5}{3}\epsilon\,,\\ I^<(r)\Big|_0^1 &= -\frac{5}{3}\epsilon-\Big[-1+\epsilon\left(\frac{7}{6}-i\pi-\log 4\right)\Big], \end{aligned} \tag{C.26}$$

apart from singular terms at $r = 1$ which can be removed by the contour integral $I^{\theta}_{\epsilon}(r)$ around the regulating semicircle. The above pieces alongwith the overall $\frac{\pi l^2}{2G_4}$ factor add up to give (7.15).

C.3 Details: dS_3 slow-roll area

In this dS_3 case we have

$$\beta(r) = -\frac{1}{2}\left(r\frac{\partial\varphi}{\partial r}\right)^2 + \frac{\varphi\, r^2}{1-r^2}\,. \tag{C.27}$$

Inputting the scalar profile (C.15) in this case and using $r = \cosh\tau$ gives

$$\begin{aligned}\beta_{>}(r) \;=\; \frac{1}{32r^2\,(r^2-1)}\Big[&-4r^4(1+\log 16)+4r^2-4\log^2\left(r+\sqrt{r^2-1}\right)\\ &+4\big(2r\sqrt{r^2-1}\,\left(2r^2-1\right)+i\pi\big)\log\left(r+\sqrt{r^2-1}\right)\\ &-4i\pi\big(-2r^4-r\sqrt{r^2-1}+2r^3\sqrt{r^2-1}\big)+\pi^2\Big]\,.\end{aligned} \tag{C.28}$$

In terms of the variable $z = r^2 - 1$ in (7.7), this becomes

$$\begin{aligned}\beta_{>}(z) \;=\; \frac{1}{32z(z+1)}\Big[&-4(z+1)^2(1+\log 16)+4(z+1)-4\log^2\left(\sqrt{z}+\sqrt{z+1}\right)\\ &+4\left(2\sqrt{z}\sqrt{z+1}(2(z+1)-1)+i\pi\right)\log\left(\sqrt{z}+\sqrt{z+1}\right)\\ &-4i\pi\left(2\sqrt{z}(z+1)^{3/2}-2(z+1)^2-\sqrt{z}\sqrt{z+1}\right)+\pi^2\Big]\,.\end{aligned} \tag{C.29}$$

Integrating gives

$$\begin{aligned}I^{>}_{\epsilon} = \int\frac{\beta_{>}(z)}{2i\sqrt{z(1+z)}}dz \;=\; \frac{1}{32\sqrt{z(z+1)}}\Big[&i\Big(8i\pi(z+1)-4(2z+1)\log^2\left(\sqrt{z}+\sqrt{z+1}\right)\\ &+\pi^2(2z+1)+4i(2\pi z+\pi)\log\left(\sqrt{z}+\sqrt{z+1}\right)-4(z+1)\log 16\Big)\\ &+4\sqrt{z}\sqrt{z+1}(2\pi+i(1+\log 16))\log\left(\sqrt{z}+\sqrt{z+1}\right)\Big]\,.\end{aligned} \tag{C.30}$$

Along the lines of the arguments in (C.19) in the dS_4 case, we have

$$\int_{-1}^{-\delta}\frac{\beta_{>}(z)}{2\sqrt{-z(1+z)}}dz = \int_{1}^{\delta}\frac{\beta_{>}(-y)}{2\sqrt{y(1-y)}}d(-y) = \int_{\delta}^{1}\frac{\beta_{<}(y)}{2\sqrt{y(1-y)}}dy \equiv I^{<}_{\epsilon}(z)\,. \tag{C.31}$$

Thus, analytically continuing the integrated expression $I_\epsilon^>$ to the hemisphere region ($r < 1$) as $z \to -z$ gives

$$\begin{aligned} I_\epsilon^<(z) = I_\epsilon^>(-z) \;\; = \;\; & \frac{1}{32\sqrt{z(1-z)}}\Big[\Big(8i\pi(1-z) - 4(-2z+1)\log^2\left(i\sqrt{z}+\sqrt{1-z}\right) \\ & + \pi^2(-2z+1) + 4i(-2\pi z+\pi)\log\left(i\sqrt{z}+\sqrt{1-z}\right) - 4(1-z)\log 16\Big) \\ & + 4\sqrt{z}\sqrt{1-z}(2\pi + i(1+\log 16))\log\left(i\sqrt{z}+\sqrt{1-z}\right)\Big]\,. \end{aligned} \tag{C.32}$$

Evaluating this at the various limiting points gives

$$\begin{aligned} z = z_c \to \infty : \qquad & I_\epsilon^> = \frac{1}{16} i\left(-(\log z_c)^2 + \log z_c + \pi^2 + 4i\pi + 4(\log 2)^2 - 6\log 2\right), \\ z = \delta : \qquad & I_\epsilon^> = -\frac{\pi}{8} + \frac{i\left(8i\pi + \pi^2 - 4\log 16\right)}{32\sqrt{\delta}}\,. \end{aligned} \tag{C.33}$$

Evaluating this now at $z = 1$ (nbp) and $z = \delta$ (which is 0^- in the earlier variable) gives

$$z = 1 : I_\epsilon^< = \frac{\pi}{16}(2\pi i - 1 - \log 16)\,; \qquad z = \delta : I_\epsilon^< = -\frac{\pi}{8} + \frac{(8i\pi + \pi^2 - 4\log(16))}{32\sqrt{\delta}}\,. \tag{C.34}$$

The contribution on the regulating semicircle is similar to that in the dS_4 case and serves to cancel the singular pieces near $z = 0$: we obtain

$$I_\epsilon^\theta = -\frac{(8i\pi + \pi^2 - 4\log 16)}{32\sqrt{-\delta\, e^{i\theta}}}\Big|_{\theta=\pi}^{\theta=0} = -\frac{(8i\pi + \pi^2 - 4\log 16)}{32\sqrt{\delta}}\left(\frac{1}{i} - 1\right). \tag{C.35}$$

Adding all these above contributions leads to (7.23). As in the dS_4 case, this area calculation can be done in the r-coordinate also, using (C.28), and its continuation to the hemisphere.

C.4 Inflation: on-shell action etc

We review aspects of evaluating the action for spaces with a boundary: besides [222, 224, 99], and [223], some useful references include [191, 225, 226, 227, 102, 228] We consider the $d+1$-dim Einstein-scalar action

$$I = \frac{1}{16\pi G_{d+1}}\int d^{d+1}x\sqrt{g}\left(R - (\partial\phi)^2 - 2V(\phi)\right) - \frac{1}{8\pi G_{d+1}}\int d^3x\sqrt{h}K\,. \tag{C.36}$$

With a minisuperspace-type metric ansatz as required for our analysis here

$$ds^2 = -N^2(t)dt^2 + a^2(t)d\Omega_d^2\,, \tag{C.37}$$

and a $d+1$-split in the ADM formulation, we obtain the spatial curvature and the extrinsic curvature as

$$R^{(d)} = \frac{d(d-1)}{a^2}\,, \qquad K_{ij} = \frac{1}{2N}\dot{h}_{ij} = \frac{1}{2N}\,2a\dot{a}\,s_{ij}\,, \quad K = s^{ij}K_{ij} = \frac{d\,\dot{a}}{aN}\,, \tag{C.38}$$

where s_{ij} is the unit S^d metric. Alongwith cancellations between the bulk and boundary terms above, this gives the Lorentzian action

$$\begin{aligned} iI &= \frac{i}{16\pi G_{d+1}}\int dt\,\Omega_d\,N\,a^d\left(K_{ij}K^{ij} - K^2 + R^{(d)} - 2V + \frac{1}{N^2}\dot{\phi}^2\right) \\ &= \frac{i\,\Omega_d}{16\pi G_{d+1}}\int dt\,N\,a^d\left(-d(d-1)\frac{\dot{a}^2}{a^2N^2} + d(d-1)\frac{1}{a^2} - 2V + \frac{1}{N^2}\dot{\phi}^2\right)\,. \end{aligned} \tag{C.39}$$

Varying with N leads to the Hamiltonian constraint with Lorentzian signature:

$$R^{(d)} - 2V - \frac{1}{N^2}K_{ij}K^{ij} + \frac{1}{N^2}K^2 - \frac{1}{N^2}\dot{\phi}^2 \;=\; 0 \;=\; \frac{d(d-1)}{a^2} + d(d-1)\frac{\dot{a}^2}{a^2N^2} - 2V - \frac{1}{N^2}\dot{\phi}^2\,. \tag{C.40}$$

To go Euclidean, we either take $N \to iN$ or $t \to it$ so $-N^2dt^2 \to N^2dt^2$. This gives

$$-I_E = \frac{\Omega_d}{16\pi G_{d+1}}\int dt\,N\,a^d\left(d(d-1)\frac{\dot{a}^2}{a^2N^2} + d(d-1)\frac{1}{a^2} - 2V - \frac{1}{N^2}\dot{\phi}^2\right)\,, \tag{C.41}$$

as the Euclidean action and the Hamiltonian constraint becomes

$$\frac{d(d-1)}{a^2} - 2V - d(d-1)\frac{\dot{a}^2}{a^2N^2} + \frac{1}{N^2}\dot{\phi}^2 = 0\,. \tag{C.42}$$

For the metric in the Euclidean form on the right in (7.1), with a taken as the time coordinate so $\dot{a} = 1$, we then obtain

$$g_{aa} \equiv N^2 \;=\; \frac{\frac{d(d-1)}{2} - \frac{1}{2}(a\partial_a\phi)^2}{\frac{d(d-1)}{2} - V\,a^2}\,. \tag{C.43}$$

Inputting the Hamiltonian constraint, we can evaluate the on-shell action with the time coordinate taken as $a = t$. We will now evaluate this for dS_4 and dS_3 slow-roll inflation to $O(\epsilon)$ in the slow-roll parameter.

dS_4 **slow-roll:**

With $d = 3$, inputting the Hamiltonian constraint, we obtain the on-shell action

$$-I_E = \frac{6\Omega_3}{16\pi G_4}\int da\,N\,a\left(\frac{1}{N^2} + 1 - \frac{a^2\dot{\phi}^2}{6N^2} - \frac{a^2V}{3}\right) = \frac{3\pi}{2G_4}\int da\,N\,a\left(1 - \frac{a^2V}{3}\right)\,. \tag{C.44}$$

Thus the Lorentzian action taking $N^2 \to -N^2$ can be written with the minus sign inside one radical and becomes

$$iI = -\frac{i\pi}{2G_4}\int da\, a\sqrt{3-\frac{1}{2}(a\partial_a\phi)^2}\,\sqrt{a^2V-3}\,. \tag{C.45}$$

For pure dS_4, we have $V \equiv \Lambda = \frac{3}{l^2}$ and $\phi = const$, giving the real part of the action as $\mathrm{Re}(iI) = -\frac{3i\pi\, l^2}{2G_4}\int_0^1 dr\, r\sqrt{r^2-1} = \frac{\pi\, l^2}{2G_4}$, *i.e.* half dS_4 entropy as expected.

Incorporating the slow-roll correction and expanding to $O(\epsilon)$, we obtain

$$iI = -\frac{3i\pi\, l^2}{2G_4}\int_0^{r_c} dr\, r\,\sqrt{r^2-1}\left[1+\epsilon\left(-\frac{1}{6}\left(r\partial_r\tilde{\varphi}(r)\right)^2+\frac{r^2\tilde{\varphi}(r)}{r^2-1}\right)\right]. \tag{C.46}$$

Breaking up the integral into the Euclidean part over $r \in [0,1]$ and the Lorentzian part $r \in [1, r_c]$ with $r_c \equiv \frac{R_c}{l}$, the leading pure de Sitter term gives

$$iI_0 = \frac{\pi\, l^2}{2G_4}\left[1-i\left(r_c^3-\frac{3}{2}r_c+O\left(\frac{1}{r_c}\right)\right)\right]. \tag{C.47}$$

For the $O(\epsilon)$ correction, we use the explicit expressions for the inflaton profile and evaluate (*e.g.* by defining an appropriate contour to avoid the pole at $r=1$). Simplifying finally gives

$$iI_\epsilon = \frac{\pi\, l^2}{2G_4}\,\epsilon\left[ir_c^3\left(\log r_c-\frac{1}{6}\right)+\frac{ir_c}{4}\left(6\log r_c-11\right)+\left(\log 4-\frac{7}{2}+i\pi\right)+O\left(\frac{1}{r_c}\right)\right]. \tag{C.48}$$

This recovers the expressions in [223] (see App.C.1 for the $O(\epsilon)$ terms), after noting $\frac{V_*}{3} = l^2$ and reinstating $8\pi G_4$.

dS_3 slow-roll:

With $d=2$, inputting the Hamiltonian constraint gives $I_E = -\frac{2\Omega_2}{8\pi G_4}\int da\, N\,(1-a^2V)$, so the on-shell Lorentzian action becomes

$$iI = -\frac{i}{G_3}\int da\, a\sqrt{1-\frac{1}{2}(a\partial_a\phi)^2}\,\sqrt{a^2V-1}\,. \tag{C.49}$$

Expanding to $O(\epsilon)$ and simplifying gives

$$iI = -\frac{il}{G_3}\int_0^{r_c} dr\,\sqrt{r^2-1}\left[1+\epsilon\left(-\frac{1}{2}\left(r\partial_r\tilde{\varphi}(r)\right)^2+\frac{r^2\tilde{\varphi}(r)}{r^2-1}\right)\right]. \tag{C.50}$$

The leading term is the pure dS_3 action

$$\begin{aligned} iI_0 &= -\frac{il}{G_3}\left[\frac{i\pi}{4}+\frac{1}{2}\left(r_c\sqrt{r_c^2-1}-\log\left(r_c+\sqrt{r_c^2-1}\right)\right)\right] \\ &= \frac{\pi\, l}{4G_3}-\frac{il}{G_3}\left(\frac{r_c^2}{2}-\frac{1}{2}\log r_c-\frac{1}{2}\log 2-\frac{1}{4}\right)+O\Big(\frac{1}{r_c}\Big)\,. \end{aligned} \tag{C.51}$$

The subleading $O(\epsilon)$ terms can be evaluated as in the dS_4 case (*e.g.* by an appropriate contour in the complex r-plane, avoiding the pole at $r=1$). Simplifying, this finally gives

$$\begin{aligned} iI_\epsilon &= \frac{l}{2G_3}\,\epsilon\left[-\frac{\pi}{16}(1+\log 16)\right. \\ &\quad \left.+\,\frac{i}{16}\left(4z_c\log z_c-2z_c+(\log z_c)^2+\log z_c+\pi^2+1-4(\log 2)^2-2\log 2\right)\right]. \end{aligned} \tag{C.52}$$

Using $z_c=r_c^2-1$ and expanding gives

$$\begin{aligned} iI_\epsilon &= \frac{l}{2G_3}\,\epsilon\left[-\frac{\pi}{16}(1+\log 16)\right. \\ &\quad \left.+\,\frac{i}{16}\left(8r_c^2\log r_c-2r_c^2+4(\log r_c)^2-6\log r_c+\pi^2-1-4(\log 2)^2-2\log 2\right)\right]. \end{aligned} \tag{C.53}$$

Bibliography

[1] S. W. Hawking, "Breakdown of Predictability in Gravitational Collapse," Phys. Rev. D **14**, 2460-2473 (1976) doi:10.1103/PhysRevD.14.2460

[2] S. W. Hawking, Commun. Math. Phys. **43**, 199-220 (1975) [erratum: Commun. Math. Phys. **46**, 206 (1976)] doi:10.1007/BF02345020

[3] S. D. Mathur, "The Information paradox: A Pedagogical introduction," Class. Quant. Grav. **26**, 224001 (2009) doi:10.1088/0264-9381/26/22/224001 [arXiv:0909.1038 [hep-th]].

[4] A. Almheiri, D. Marolf, J. Polchinski and J. Sully, "Black Holes: Complementarity or Firewalls?," JHEP **02**, 062 (2013) doi:10.1007/JHEP02(2013)062 [arXiv:1207.3123 [hep-th]].

[5] D. N. Page, "Information in black hole radiation," Phys. Rev. Lett. **71**, 3743-3746 (1993) doi:10.1103/PhysRevLett.71.3743 [arXiv:hep-th/9306083 [hep-th]].

[6] D. N. Page, "Time Dependence of Hawking Radiation Entropy," JCAP **09**, 028 (2013) doi:10.1088/1475-7516/2013/09/028 [arXiv:1301.4995 [hep-th]].

[7] G. Penington, "Entanglement Wedge Reconstruction and the Information Paradox," JHEP **09**, 002 (2020) doi:10.1007/JHEP09(2020)002 [arXiv:1905.08255 [hep-th]].

[8] A. Almheiri, N. Engelhardt, D. Marolf and H. Maxfield, "The entropy of bulk quantum fields and the entanglement wedge of an evaporating black hole," JHEP **12**, 063 (2019) doi:10.1007/JHEP12(2019)063 [arXiv:1905.08762 [hep-th]].

[9] A. Almheiri, R. Mahajan, J. Maldacena and Y. Zhao, "The Page curve of Hawking radiation from semiclassical geometry," JHEP **03**, 149 (2020) doi:10.1007/JHEP03(2020)149 [arXiv:1908.10996 [hep-th]].

[10] G. Penington, S. H. Shenker, D. Stanford, Z. Yang, "Replica wormholes & the black hole interior," [arXiv:1911.11977[hep-th]].

[11] A. Almheiri, T. Hartman, J. Maldacena, E. Shaghoulian and A. Tajdini, "Replica Wormholes and the Entropy of Hawking Radiation," JHEP **05**, 013 (2020) [arXiv:1911.12333 [hep-th]].

[12] T. Faulkner, A. Lewkowycz and J. Maldacena, "Quantum corrections to holographic entanglement entropy," JHEP **1311**, 074 (2013) doi:10.1007/JHEP11(2013)074 [arXiv:1307.2892 [hep-th]].

[13] N. Engelhardt and A. C. Wall, "Quantum Extremal Surfaces: Holographic Entanglement Entropy beyond the Classical Regime," JHEP **1501**, 073 (2015) doi:10.1007/JHEP01(2015)073 [arXiv:1408.3203 [hep-th]].

[14] S. Ryu and T. Takayanagi, "Holographic derivation of entanglement entropy from AdS/CFT," *Phys. Rev. Lett.* **96** (2006) 181602, hep-th/0603001.

[15] S. Ryu and T. Takayanagi, "Aspects of holographic entanglement entropy," *JHEP* **08** (2006) 045, hep-th/0605073.

[16] V. E. Hubeny, M. Rangamani, and T. Takayanagi, "A Covariant holographic entanglement entropy proposal," *JHEP* **0707** (2007) 062, arXiv:0705.0016 [hep-th].

[17] M. Rangamani and T. Takayanagi, "Holographic Entanglement Entropy," Lect. Notes Phys. **931**, pp.1-246 (2017) Springer, 2017, doi:10.1007/978-3-319-52573-0 [arXiv:1609.01287 [hep-th]].

[18] A. Almheiri, T. Hartman, J. Maldacena, E. Shaghoulian and A. Tajdini, "The entropy of Hawking radiation," [arXiv:2006.06872 [hep-th]].

[19] R. Mahajan, "Lectures on Quantum Extremal Surfaces and the Page Curve," [arXiv:2502.01933 [hep-th]].

[20] S. Raju, "Lessons from the Information Paradox," [arXiv:2012.05770 [hep-th]].

[21] B. Chen, B. Czech and Z. z. Wang, "Quantum Information in Holographic Duality," [arXiv:2108.09188 [hep-th]].

[22] A. Almheiri, R. Mahajan and J. Maldacena, "Islands outside the horizon," [arXiv:1910.11077 [hep-th]].

[23] P. Buividovich and M. Polikarpov, "Entanglement entropy in gauge theories and the holographic principle for electric strings," *Phys.Lett.* **B670** (2008) 141–145, arXiv:0806.3376 [hep-th].

[24] W. Donnelly, "Decomposition of entanglement entropy in lattice gauge theory," *Phys.Rev.* **D85** (2012) 085004, arXiv:1109.0036 [hep-th].

[25] H. Casini, M. Huerta, and J. A. Rosabal, "Remarks on entanglement entropy for gauge fields," *Phys.Rev.* **D89** (2014) 085012, arXiv:1312.1183 [hep-th].

[26] W. Donnelly, "Entanglement entropy and nonabelian gauge symmetry," *Class. Quant. Grav.* **31** (2014) no. 21, 214003, arXiv:1406.7304 [hep-th].

[27] L. Bombelli, R. K. Koul, J. Lee, and R. D. Sorkin, "A Quantum Source of Entropy for Black Holes," *Phys.Rev.* **D34** (1986) 373–383.

[28] M. Srednicki, "Entropy and area," *Phys.Rev.Lett.* **71** (1993) 666–669, arXiv:hep-th/9303048 [hep-th].

[29] M. B. Hastings, "An area law for one-dimensional quantum systems," *Journal of Statistical Mechanics: Theory and Experiment* **8** (Aug., 2007) 08024, arXiv:0705.2024 [quant-ph].

[30] P. H. Ginsparg, [arXiv:hep-th/9108028 [hep-th]].

[31] J. M. Maldacena, Adv. Theor. Math. Phys. **2**, 231-252 (1998) doi:10.4310/ATMP.1998.v2.n2.a1 [arXiv:hep-th/9711200 [hep-th]].

[32] S. S. Gubser, I. R. Klebanov and A. M. Polyakov, "Gauge theory correlators from non-critical string theory," Phys. Lett. B **428**, 105 (1998) doi:10.1016/S0370-2693(98)00377-3 [hep-th/9802109].

[33] E. Witten, "Anti-de Sitter space and holography," Adv. Theor. Math. Phys. **2**, 253 (1998) [hep-th/9802150];

[34] O. Aharony, S. S. Gubser, J. M. Maldacena, H. Ooguri and Y. Oz, "Large N field theories, string theory and gravity," Phys. Rept. **323**, 183 (2000) doi:10.1016/S0370-1573(99)00083-6 [hep-th/9905111].

[35] I. R. Klebanov, "TASI lectures: Introduction to the AdS / CFT correspondence," doi:10.1142/9789812799630_0007 hep-th/0009139.

[36] E. D'Hoker and D. Z. Freedman, "Supersymmetric gauge theories and the AdS / CFT correspondence," hep-th/0201253.

[37] J. M. Maldacena, "TASI 2003 lectures on AdS / CFT," hep-th/0309246.

[38] G. T. Horowitz and J. Polchinski, "Gauge/gravity duality," In *Oriti, D. (ed.): Approaches to quantum gravity* 169-186 [gr-qc/0602037].

[39] J. Polchinski, "Introduction to Gauge/Gravity Duality," doi:10.1142/9789814350525_0001 arXiv:1010.6134 [hep-th].

[40] A. C. Wall, "Maximin Surfaces, and the Strong Subadditivity of the Covariant Holographic Entanglement Entropy," *Class. Quant. Grav.* **31** (2014) no. 22, 225007, arXiv:1211.3494 [hep-th].

[41] J. D. Bekenstein, Phys. Rev. D **7**, 2333-2346 (1973) doi:10.1103/PhysRevD.7.2333

[42] S. W. Hawking, Nature **248**, 30-31 (1974) doi:10.1038/248030a0

[43] J. M. Bardeen, B. Carter and S. W. Hawking, Commun. Math. Phys. **31**, 161-170 (1973) doi:10.1007/BF01645742

[44] A. C. Wall, "A proof of the generalized second law for rapidly changing fields and arbitrary horizon slices," Phys. Rev. D **85**, 104049 (2012) [erratum: Phys. Rev. D **87**, no.6, 069904 (2013)] doi:10.1103/PhysRevD.85.104049 [arXiv:1105.3445 [gr-qc]].

[45] J. Maldacena, D. Stanford and Z. Yang, "Conformal symmetry and its breaking in two dimensional Nearly Anti-de-Sitter space," PTEP **2016**, no.12, 12C104 (2016) doi:10.1093/ptep/ptw124 [arXiv:1606.01857 [hep-th]].

[46] J. Engelsöy, T. G. Mertens and H. Verlinde, "An investigation of AdS_2 backreaction and holography," JHEP **07**, 139 (2016) doi:10.1007/JHEP07(2016)139 [arXiv:1606.03438 [hep-th]].

[47] A. Almheiri and B. Kang, "Conformal Symmetry Breaking and Thermodynamics of Near-Extremal Black Holes," JHEP **10**, 052 (2016) doi:10.1007/JHEP10(2016)052 [arXiv:1606.04108 [hep-th]].

[48] S. Sachdev, "Universal low temperature theory of charged black holes with AdS_2 horizons," J. Math. Phys. **60**, no.5, 052303 (2019) doi:10.1063/1.5092726 [arXiv:1902.04078 [hep-th]].

[49] A. Almheiri and J. Polchinski, "Models of AdS_2 backreaction and holography," JHEP **11**, 014 (2015) doi:10.1007/JHEP11(2015)014 [arXiv:1402.6334 [hep-th]].

[50] K. Jensen, "Chaos in AdS_2 Holography," Phys. Rev. Lett. **117**, no.11, 111601 (2016) doi:10.1103/PhysRevLett.117.111601 [arXiv:1605.06098 [hep-th]].

[51] T. G. Mertens and G. J. Turiaci, "Solvable models of quantum black holes: a review on Jackiw–Teitelboim gravity," Living Rev. Rel. **26**, no.1, 4 (2023) doi:10.1007/s41114-023-00046-1 [arXiv:2210.10846 [hep-th]].

[52] S. D. Mathur, "Fuzzballs and black hole thermodynamics," [arXiv:1401.4097 [hep-th]].

[53] J. Maldacena and L. Susskind, "Cool horizons for entangled black holes," Fortsch. Phys. **61**, 781-811 (2013) doi:10.1002/prop.201300020 [arXiv:1306.0533 [hep-th]].

[54] A. Almheiri, "Holographic Quantum Error Correction and the Projected Black Hole Interior," [arXiv:1810.02055 [hep-th]].

[55] H. Z. Chen, Z. Fisher, J. Hernandez, R. C. Myers and S. M. Ruan, "Information Flow in Black Hole Evaporation," JHEP **03**, 152 (2020) doi:10.1007/JHEP03(2020)152 [arXiv:1911.03402 [hep-th]].

[56] A. Almheiri, R. Mahajan and J. E. Santos, "Entanglement islands in higher dimensions," SciPost Phys. **9**, no.1, 001 (2020) doi:10.21468/SciPostPhys.9.1.001 [arXiv:1911.09666 [hep-th]].

[57] F. F. Gautason, L. Schneiderbauer, W. Sybesma and L. Thorlacius, "Page Curve for an Evaporating Black Hole," JHEP **05**, 091 (2020) doi:10.1007/JHEP05(2020)091 [arXiv:2004.00598 [hep-th]].

[58] T. Anegawa and N. Iizuka, "Notes on islands in asymptotically flat 2d dilaton black holes," JHEP **07**, 036 (2020) doi:10.1007/JHEP07(2020)036 [arXiv:2004.01601 [hep-th]].

[59] K. Hashimoto, N. Iizuka and Y. Matsuo, "Islands in Schwarzschild black holes," JHEP **06**, 085 (2020) doi:10.1007/JHEP06(2020)085 [arXiv:2004.05863 [hep-th]].

[60] T. Hartman, E. Shaghoulian and A. Strominger, "Islands in Asymptotically Flat 2D Gravity," JHEP **07**, 022 (2020) doi:10.1007/JHEP07(2020)022 [arXiv:2004.13857 [hep-th]].

[61] T. J. Hollowood and S. P. Kumar, "Islands and Page Curves for Evaporating Black Holes in JT Gravity," JHEP **08**, 094 (2020) doi:10.1007/JHEP08(2020)094 [arXiv:2004.14944 [hep-th]].

[62] C. Krishnan, V. Patil and J. Pereira, "Page Curve and the Information Paradox in Flat Space," [arXiv:2005.02993 [hep-th]].

[63] M. Alishahiha, A. Faraji Astaneh and A. Naseh, "Island in the presence of higher derivative terms," JHEP **02**, 035 (2021) doi:10.1007/JHEP02(2021)035 [arXiv:2005.08715 [hep-th]].

[64] T. Li, J. Chu and Y. Zhou, "Reflected Entropy for an Evaporating Black Hole," JHEP **11**, 155 (2020) doi:10.1007/JHEP11(2020)155 [arXiv:2006.10846 [hep-th]].

[65] X. Dong, X. L. Qi, Z. Shangnan and Z. Yang, "Effective entropy of quantum fields coupled with gravity," JHEP **10**, 052 (2020) doi:10.1007/JHEP10(2020)052 [arXiv:2007.02987 [hep-th]].

[66] H. Z. Chen, Z. Fisher, J. Hernandez, R. C. Myers and S. M. Ruan, "Evaporating Black Holes Coupled to a Thermal Bath," JHEP **01**, 065 (2021) doi:10.1007/JHEP01(2021)065 [arXiv:2007.11658 [hep-th]].

[67] Y. Ling, Y. Liu and Z. Y. Xian, "Island in Charged Black Holes," JHEP **03**, 251 (2021) doi:10.1007/JHEP03(2021)251 [arXiv:2010.00037 [hep-th]].

[68] Y. Matsuo, "Islands and stretched horizon," JHEP **07**, 051 (2021) doi:10.1007/JHEP07(2021)051 [arXiv:2011.08814 [hep-th]].

[69] K. Goto, T. Hartman and A. Tajdini, "Replica wormholes for an evaporating 2D black hole," JHEP **04**, 289 (2021) doi:10.1007/JHEP04(2021)289 [arXiv:2011.09043 [hep-th]].

[70] I. Akal, Y. Kusuki, N. Shiba, T. Takayanagi and Z. Wei, "Entanglement Entropy in a Holographic Moving Mirror and the Page Curve," Phys. Rev. Lett. **126**, no.6, 061604 (2021) doi:10.1103/PhysRevLett.126.061604 [arXiv:2011.12005 [hep-th]].

[71] F. Deng, J. Chu and Y. Zhou, "Defect extremal surface as the holographic counterpart of Island formula," JHEP **03**, 008 (2021) doi:10.1007/JHEP03(2021)008 [arXiv:2012.07612 [hep-th]].

[72] G. K. Karananas, A. Kehagias and J. Taskas, "Islands in linear dilaton black holes," JHEP **03**, 253 (2021) doi:10.1007/JHEP03(2021)253 [arXiv:2101.00024 [hep-th]].

[73] X. Wang, R. Li and J. Wang, "Islands and Page curves of Reissner-Nordström black holes," JHEP **04**, 103 (2021) doi:10.1007/JHEP04(2021)103 [arXiv:2101.06867 [hep-th]].

[74] E. Verheijden and E. Verlinde, "From the BTZ black hole to JT gravity: geometrizing the island," JHEP **11**, 092 (2021) doi:10.1007/JHEP11(2021)092 [arXiv:2102.00922 [hep-th]].

[75] K. Kawabata, T. Nishioka, Y. Okuyama and K. Watanabe, "Probing Hawking radiation through capacity of entanglement," JHEP **05**, 062 (2021) doi:10.1007/JHEP05(2021)062 [arXiv:2102.02425 [hep-th]].

[76] L. Anderson, O. Parrikar and R. M. Soni, "Islands with gravitating baths: towards ER = EPR," JHEP **21**, 226 (2020) doi:10.1007/JHEP10(2021)226 [arXiv:2103.14746 [hep-th]].

[77] A. Bhattacharya, A. Bhattacharyya, P. Nandy and A. K. Patra, "Islands and complexity of eternal black hole and radiation subsystems for a doubly holographic model," JHEP **05**, 135 (2021) doi:10.1007/JHEP05(2021)135 [arXiv:2103.15852 [hep-th]].

[78] W. Kim and M. Nam, "Entanglement entropy of asymptotically flat non-extremal and extremal black holes with an island," Eur. Phys. J. C **81**, no.10, 869 (2021) doi:10.1140/epjc/s10052-021-09680-x [arXiv:2103.16163 [hep-th]].

[79] K. Ghosh and C. Krishnan, "Dirichlet baths and the not-so-fine-grained Page curve," JHEP **08**, 119 (2021) doi:10.1007/JHEP08(2021)119 [arXiv:2103.17253 [hep-th]].

[80] X. Wang, R. Li and J. Wang, "Page curves for a family of exactly solvable evaporating black holes," Phys. Rev. D **103**, no.12, 126026 (2021) doi:10.1103/PhysRevD.103.126026 [arXiv:2104.00224 [hep-th]].

[81] R. Li, X. Wang and J. Wang, "Island may not save the information paradox of Liouville black holes," Phys. Rev. D **104**, no.10, 106015 (2021) doi:10.1103/PhysRevD.104.106015 [arXiv:2105.03271 [hep-th]].

[82] R. Li and J. Wang, "Hawking radiation and page curves of the black holes in thermal environment," Commun. Theor. Phys. **73**, no.7, 075401 (2021) doi:10.1088/1572-9494/abf823

[83] K. Kawabata, T. Nishioka, Y. Okuyama and K. Watanabe, "Replica wormholes and capacity of entanglement," JHEP **10**, 227 (2021) doi:10.1007/JHEP10(2021)227 [arXiv:2105.08396 [hep-th]].

[84] Y. Lu and J. Lin, "Islands in Kaluza–Klein black holes," Eur. Phys. J. C **82**, no.2, 132 (2022) doi:10.1140/epjc/s10052-022-10074-w [arXiv:2106.07845 [hep-th]].

[85] J. Kruthoff, R. Mahajan and C. Murdia, "Free fermion entanglement with a semitransparent interface: the effect of graybody factors on entanglement islands," SciPost Phys. **11**, 063 (2021) doi:10.21468/SciPostPhys.11.3.063 [arXiv:2106.10287 [hep-th]].

[86] M. H. Yu and X. H. Ge, "Islands and Page curves in charged dilaton black holes," Eur. Phys. J. C **82**, no.1, 14 (2022) doi:10.1140/epjc/s10052-021-09932-w [arXiv:2107.03031 [hep-th]].

[87] B. Ahn, S. E. Bak, H. S. Jeong, K. Y. Kim and Y. W. Sun, "Islands in charged linear dilaton black holes," Phys. Rev. D **105**, no.4, 046012 (2022) doi:10.1103/PhysRevD.105.046012 [arXiv:2107.07444 [hep-th]].

[88] X. Wang, K. Zhang and J. Wang, "What can we learn about islands and state paradox from quantum information theory?," [arXiv:2107.09228 [hep-th]].

[89] N. H. Cao, "Entanglement entropy and Page curve of black holes with island in massive gravity," Eur. Phys. J. C **82**, no.4, 381 (2022) doi:10.1140/epjc/s10052-022-10343-8 [arXiv:2108.10144 [hep-th]].

[90] I. Aref'eva and I. Volovich, "A Note on Islands in Schwarzschild Black Holes," [arXiv:2110.04233 [hep-th]].

[91] S. He, Y. Sun, L. Zhao and Y. X. Zhang, "The universality of islands outside the horizon," JHEP **05**, 047 (2022) doi:10.1007/JHEP05(2022)047 [arXiv:2110.07598 [hep-th]].

[92] Y. Matsuo, "Entanglement entropy and vacuum states in Schwarzschild geometry," JHEP **06**, 109 (2022) doi:10.1007/JHEP06(2022)109 [arXiv:2110.13898 [hep-th]].

[93] J. Tian, "Islands in Generalized Dilaton Theories," [arXiv:2204.08751 [hep-th]].

[94] A. Laddha, S. G. Prabhu, S. Raju and P. Shrivastava, "The Holographic Nature of Null Infinity," SciPost Phys. **10**, no.2, 041 (2021) doi:10.21468/SciPostPhys.10.2.041 [arXiv:2002.02448 [hep-th]].

[95] H. Geng, A. Karch, C. Perez-Pardavila, S. Raju, L. Randall, M. Riojas and S. Shashi, "Inconsistency of Islands in Theories with Long-Range Gravity," [arXiv:2107.03390 [hep-th]].

[96] I. Bena, E. J. Martinec, S. D. Mathur and N. P. Warner, "Fuzzballs and Microstate Geometries: Black-Hole Structure in String Theory," [arXiv:2204.13113 [hep-th]].

[97] G. W. Gibbons and S. W. Hawking, "Cosmological Event Horizons, Thermodynamics, and Particle Creation," Phys. Rev. D **15**, 2738 (1977). doi:10.1103/PhysRevD.15.2738

[98] P. H. Ginsparg and M. J. Perry, "Semiclassical Perdurance of de Sitter Space," Nucl. Phys. B **222**, 245 (1983). doi:10.1016/0550-3213(83)90636-3

[99] R. Bousso and S. W. Hawking, "Pair creation of black holes during inflation," Phys. Rev. D **54**, 6312 (1996) doi:10.1103/PhysRevD.54.6312 [gr-qc/9606052].

[100] R. Bousso and S. W. Hawking, "(Anti)evaporation of Schwarzschild-de Sitter black holes," Phys. Rev. D **57**, 2436-2442 (1998) doi:10.1103/PhysRevD.57.2436 [arXiv:hep-th/9709224 [hep-th]].

[101] H. Nariai, "On some static solutions of Einstein's gravitational field equations in a spherically symmetric case", Sci. Rep. Tohoku Univ. Eighth Ser. 34, 1950.

[102] J. Maldacena, G. J. Turiaci and Z. Yang, "Two dimensional Nearly de Sitter gravity," arXiv:1904.01911 [hep-th].

[103] D. Anninos, F. Denef and D. Harlow, "The Wave Function of Vasiliev's Universe - A Few Slices Thereof," Phys. Rev. D **88**, 084049 (2013) [arXiv:1207.5517 [hep-th]].

[104] K. Fernandes, K. S. Kolekar, K. Narayan and S. Roy, "Schwarzschild de Sitter and extremal surfaces," Eur. Phys. J. C **80**, no.9, 866 (2020) doi:10.1140/epjc/s10052-020-08437-2 [arXiv:1910.11788 [hep-th]].

[105] S. Shankaranarayanan, "Temperature and entropy of Schwarzschild-de Sitter space-time," Phys. Rev. D **67**, 084026 (2003) doi:10.1103/PhysRevD.67.084026 [arXiv:gr-qc/0301090 [gr-qc]].

[106] J. Guven and D. Núñez, "Schwarzschild-de Sitter space and its perturbations," Phys. Rev. D **42**, no.8, 2577-2584 (1990) doi:10.1103/physrevd.42.2577

[107] A. Strominger, "Les Houches lectures on black holes," [arXiv:hep-th/9501071 [hep-th]].

[108] D. Grumiller, W. Kummer and D. V. Vassilevich, "Dilaton gravity in two-dimensions," Phys. Rept. **369**, 327-430 (2002) doi:10.1016/S0370-1573(02)00267-3 [arXiv:hep-th/0204253 [hep-th]].

[109] K. Narayan, "On aspects of two-dimensional dilaton gravity, dimensional reduction, and holography," Phys. Rev. D **104**, no.2, 026007 (2021) doi:10.1103/PhysRevD.104.026007 [arXiv:2010.12955 [hep-th]].

[110] R. Bhattacharya, K. Narayan and P. Paul, "Cosmological singularities and 2-dimensional dilaton gravity," JHEP **08**, 062 (2020) doi:10.1007/JHEP08(2020)062 [arXiv:2006.09470 [hep-th]].

[111] P. Calabrese and J. L. Cardy, "Entanglement entropy and quantum field theory," J. Stat. Mech. **0406**, P06002 (2004) doi:10.1088/1742-5468/2004/06/P06002 [arXiv:hep-th/0405152 [hep-th]].

[112] P. Calabrese and J. Cardy, "Entanglement entropy and conformal field theory," J. Phys. A **42**, 504005 (2009) doi:10.1088/1751-8113/42/50/504005 [arXiv:0905.4013 [cond-mat.stat-mech]].

[113] P. Calabrese, J. Cardy, E. Tonni, "Entanglement entropy of two disjoint intervals in conformal field theory," J. Stat. Mech. **0911**, P11001 (2009) doi:10.1088/1742-5468/2009/11/P11001 [arXiv:0905.2069 [hep-th]].

[114] P. Calabrese, J. Cardy, E. Tonni, "Entanglement entropy of two disjoint intervals in conformal field theory II," J. Stat. Mech. **1101**, P01021 (2011) doi:10.1088/1742-5468/2011/01/P01021 [arXiv:1011.5482 [hep-th]].

[115] M. Headrick, "Entanglement Renyi entropies in holographic theories," Phys. Rev. D **82**, 126010 (2010) [arXiv:1006.0047 [hep-th]].

[116] D. S. Ageev and I. Y. Aref'eva, "Thermal density matrix breaks down the Page curve," [arXiv:2206.04094 [hep-th]].

[117] C. Krishnan, "Critical Islands," JHEP **01**, 179 (2021) doi:10.1007/JHEP01(2021)179 [arXiv:2007.06551 [hep-th]].

[118] Y. Chen, V. Gorbenko and J. Maldacena, "Bra-ket wormholes in gravitationally prepared states," [arXiv:2007.16091 [hep-th]].

[119] T. Hartman, Y. Jiang and E. Shaghoulian, "Islands in cosmology," JHEP **11**, 111 (2020) doi:10.1007/JHEP11(2020)111 [arXiv:2008.01022 [hep-th]].

[120] M. Van Raamsdonk, "Comments on wormholes, ensembles, and cosmology," arXiv:2008.02259[hep-th].

[121] V. Balasubramanian, A. Kar and T. Ugajin, "Islands in de Sitter space," JHEP **02**, 072 (2021) doi:10.1007/JHEP02(2021)072 [arXiv:2008.05275 [hep-th]].

[122] W. Sybesma, "Pure de Sitter space and the island moving back in time," Class. Quant. Grav. **38**, no.14, 145012 (2021) doi:10.1088/1361-6382/abff9a [arXiv:2008.07994 [hep-th]].

[123] A. Manu, K. Narayan and P. Paul, "Cosmological singularities, entanglement and quantum extremal surfaces," JHEP **04**, 200 (2021) doi:10.1007/JHEP04(2021)200 [arXiv:2012.07351 [hep-th]].

[124] S. Choudhury, S. Chowdhury, N. Gupta, A. Mishara, S. P. Selvam, S. Panda, G. D. Pasquino, C. Singha and A. Swain, "Circuit Complexity From Cosmological Islands," Symmetry **13**, 1301 (2021) doi:10.3390/sym13071301 [arXiv:2012.10234 [hep-th]].

[125] R. Bousso and A. Shahbazi-Moghaddam, "Island Finder and Entropy Bound," Phys. Rev. D **103**, no.10, 106005 (2021) doi:10.1103/PhysRevD.103.106005 [arXiv:2101.11648 [hep-th]].

[126] H. Geng, Y. Nomura and H. Y. Sun, "Information paradox and its resolution in de Sitter holography," Phys. Rev. D **103**, no.12, 126004 (2021) doi:10.1103/PhysRevD.103.126004 [arXiv:2103.07477 [hep-th]].

[127] S. Fallows and S. F. Ross, "Islands and mixed states in closed universes," JHEP **07**, 022 (2021) doi:10.1007/JHEP07(2021)022 [arXiv:2103.14364 [hep-th]].

[128] L. Aalsma and W. Sybesma, "The Price of Curiosity: Information Recovery in de Sitter Space," JHEP **05**, 291 (2021) doi:10.1007/JHEP05(2021)291 [arXiv:2104.00006 [hep-th]].

[129] D. Giataganas and N. Tetradis, "Entanglement entropy in FRW backgrounds," Phys. Lett. B **820**, 136493 (2021) doi:10.1016/j.physletb.2021.136493 [arXiv:2105.12614 [hep-th]].

[130] L. Aalsma, A. Cole, E. Morvan, J. P. van der Schaar and G. Shiu, "Shocks and information exchange in de Sitter space," JHEP **10**, 104 (2021) doi:10.1007/JHEP10(2021)104 [arXiv:2105.12737 [hep-th]].

[131] K. Langhoff, C. Murdia and Y. Nomura, "Multiverse in an inverted island," Phys. Rev. D **104**, no.8, 086007 (2021) doi:10.1103/PhysRevD.104.086007 [arXiv:2106.05271 [hep-th]].

[132] S. E. Aguilar-Gutierrez, A. Chatwin-Davies, T. Hertog, N. Pinzani-Fokeeva and B. Robinson, "Islands in Multiverse Models," [arXiv:2108.01278 [hep-th]].

[133] E. Shaghoulian, "The central dogma and cosmological horizons," JHEP **01**, 132 (2022) doi:10.1007/JHEP01(2022)132 [arXiv:2110.13210 [hep-th]].

[134] K. Goswami, K. Narayan and H. K. Saini, "Cosmologies, singularities and quantum extremal surfaces," JHEP **03**, 201 (2022) doi:10.1007/JHEP03(2022)201 [arXiv:2111.14906 [hep-th]].

[135] R. Bousso and E. Wildenhain, "Islands in closed and open universes," Phys. Rev. D **105**, no.8, 086012 (2022) doi:10.1103/PhysRevD.105.086012 [arXiv:2202.05278 [hep-th]].

[136] K. Narayan, "de Sitter future-past extremal surfaces and the entanglement wedge," Phys. Rev. D **101**, no.8, 086014 (2020) doi:10.1103/PhysRevD.101.086014 [arXiv:2002.11950 [hep-th]].

[137] J. Kames-King, E. M. H. Verheijden and E. P. Verlinde, "No Page curves for the de Sitter horizon," JHEP **03**, 040 (2022) doi:10.1007/JHEP03(2022)040 [arXiv:2108.09318 [hep-th]].

[138] U. Moitra, S. K. Sake and S. P. Trivedi, "Aspects of Jackiw-Teitelboim gravity in Anti-de Sitter and de Sitter spacetime," JHEP **06**, 138 (2022) doi:10.1007/JHEP06(2022)138 [arXiv:2202.03130 [hep-th]].

[139] A. Svesko, E. Verheijden, E. P. Verlinde and M. R. Visser, "Quasi-local energy and microcanonical entropy in two-dimensional nearly de Sitter gravity," [arXiv:2203.00700 [hep-th]].

[140] A. Levine and E. Shaghoulian, "Encoding beyond cosmological horizons in de Sitter JT gravity," [arXiv:2204.08503 [hep-th]].

[141] V. Chandrasekaran, R. Longo, G. Penington and E. Witten, "An Algebra of Observables for de Sitter Space," [arXiv:2206.10780 [hep-th]].

[142] H. Geng and A. Karch, "Massive islands," JHEP **09**, 121 (2020) doi:10.1007/JHEP09(2020)121 [arXiv:2006.02438 [hep-th]].

[143] H. Geng, A. Karch, C. Perez-Pardavila, S. Raju, L. Randall, M. Riojas and S. Shashi, "Information Transfer with a Gravitating Bath," SciPost Phys. **10**, no.5, 103 (2021) doi:10.21468/SciPostPhys.10.5.103 [arXiv:2012.04671 [hep-th]].

[144] F. Omidi, "Entropy of Hawking radiation for two-sided hyperscaling violating black branes," JHEP **04**, 022 (2022) doi:10.1007/JHEP04(2022)022 [arXiv:2112.05890 [hep-th]].

[145] R. Espíndola, B. Najian and D. Nikolakopoulou, "Islands in FRW Cosmologies," [arXiv:2203.04433 [hep-th]].

[146] C. F. Uhlemann, "Islands and Page curves in 4d from Type IIB," JHEP **08**, 104 (2021) doi:10.1007/JHEP08(2021)104 [arXiv:2105.00008 [hep-th]].

[147] C. J. Chou, H. B. Lao and Y. Yang, "Page curve of effective Hawking radiation," Phys. Rev. D **106**, no.6, 066008 (2022) doi:10.1103/PhysRevD.106.066008 [arXiv:2111.14551 [hep-th]].

[148] A. Karch, H. Sun and C. F. Uhlemann, "Double holography in string theory," JHEP **10**, 012 (2022) doi:10.1007/JHEP10(2022)012 [arXiv:2206.11292 [hep-th]].

[149] K. Goswami and K. Narayan, "Small Schwarzschild de Sitter black holes, quantum extremal surfaces and islands," JHEP **10**, 031 (2022) doi:10.1007/JHEP10(2022)031 [arXiv:2207.10724 [hep-th]].

[150] A. Roy Chowdhury, A. Saha and S. Gangopadhyay, "Role of mutual information in the Page curve," Phys. Rev. D **106**, no.8, 086019 (2022) [arXiv:2207.13029 [hep-th]].

[151] M. H. Yu and X. H. Ge, "Entanglement islands in generalized two-dimensional dilaton black holes," Phys. Rev. D **107**, no.6, 066020 (2023) [arXiv:2208.01943 [hep-th]].

[152] R. Bousso and G. Penington, "Entanglement wedges for gravitating regions," Phys. Rev. D **107**, no.8, 086002 (2023) doi:10.1103/PhysRevD.107.086002 [arXiv:2208.04993 [hep-th]].

[153] P. J. Hu, D. Li and R. X. Miao, "Island on codimension-two branes in AdS/dCFT," JHEP **11**, 008 (2022) doi:10.1007/JHEP11(2022)008 [arXiv:2208.11982 [hep-th]].

[154] D. S. Ageev, I. Y. Aref'eva, A. I. Belokon, A. V. Ermakov, V. V. Pushkarev, T. A. Rusalev, "Infrared regularization and finite size dynamics of entanglement entropy in Schwarzschild black hole," Phys. Rev. D **108**, no.4, 046005 (2023) [arXiv:2209.00036 [hep-th]].

[155] C. S. Chu, R. X. Miao, "Tunneling of Bell Particles, Page Curve and Black Hole Information," [arXiv:2209.03610 [hep-th]].

[156] G. Yadav and N. Joshi, "Cosmological and black hole islands in multi-event horizon spacetimes," Phys. Rev. D **107**, no.2, 026009 (2023) doi:10.1103/PhysRevD.107.026009 [arXiv:2210.00331 [hep-th]].

[157] L. Aalsma, S. E. Aguilar-Gutierrez and W. Sybesma, "An outsider's perspective on information recovery in de Sitter space," JHEP **01**, 129 (2023) doi:10.1007/JHEP01(2023)129 [arXiv:2210.12176 [hep-th]].

[158] C. Y. Lu, M. H. Yu, X. H. Ge and L. J. Tian, "Page curve and phase transition in deformed Jackiw–Teitelboim gravity," Eur. Phys. J. C **83**, no.3, 215 (2023) doi:10.1140/epjc/s10052-023-11358-5 [arXiv:2210.14750 [hep-th]].

[159] D. Stepanenko and I. Volovich, "Schwarzschild black holes, Islands and Virasoro algebra," Eur. Phys. J. Plus **138**, no.8, 688 (2023) doi:10.1140/epjp/s13360-023-04342-1 [arXiv:2211.03153 [hep-th]].

[160] I. Ben-Dayan, M. Hadad and E. Wildenhain, "Islands in the fluid: islands are common in cosmology," JHEP **03**, 077 (2023) doi:10.1007/JHEP03(2023)077 [arXiv:2211.16600 [hep-th]].

[161] D. Basu, Q. Wen and S. Zhou, "Entanglement Islands from Hilbert Space Reduction," [arXiv:2211.17004 [hep-th]].

[162] J. Kudler-Flam and Y. Kusuki, "On quantum information before the Page time," JHEP **05**, 078 (2023) doi:10.1007/JHEP05(2023)078 [arXiv:2212.06839 [hep-th]].

[163] R. Emparan, R. Luna, R. Suzuki, M. Tomašević and B. Way, "Holographic duals of evaporating black holes," JHEP **05**, 182 (2023) doi:10.1007/JHEP05(2023)182 [arXiv:2301.02587 [hep-th]].

[164] Y. S. Piao, "Implication of the island rule for inflation and primordial perturbations," Phys. Rev. D **107**, no.12, 123509 (2023) doi:10.1103/PhysRevD.107.123509 [arXiv:2301.07403 [hep-th]].

[165] C. Z. Guo, W. C. Gan and F. W. Shu, "Page curves and entanglement islands for the step-function Vaidya model of evaporating black holes," JHEP **05**, 042 (2023) doi:10.1007/JHEP05(2023)042 [arXiv:2302.02379 [hep-th]].

[166] S. Parvizi and M. Shahbazi, "Analogue gravity and the island prescription," Eur. Phys. J. C **83**, no.8, 705 (2023) doi:10.1140/epjc/s10052-023-11874-4 [arXiv:2302.08742 [hep-th]].

[167] T. N. Hung and C. H. Nam, "Compactified extra dimension and entanglement island as clues to quantum gravity," Eur. Phys. J. C **83**, no.6, 472 (2023) doi:10.1140/epjc/s10052-023-11606-8 [arXiv:2303.00348 [hep-th]].

[168] C. H. Wu and J. Xu, "Islands in non-minimal dilaton gravity: exploring effective theories for black hole evaporation," JHEP **10**, 094 (2023) doi:10.1007/JHEP10(2023)094 [arXiv:2303.03410 [hep-th]].

[169] M. Cadoni, M. Oi and A. P. Sanna, "Evaporation and information puzzle for 2D nonsingular asymptotically flat black holes," JHEP **06**, 211 (2023) doi:10.1007/JHEP06(2023)211 [arXiv:2303.05557 [hep-th]].

[170] A. Roy Chowdhury, A. Saha and S. Gangopadhyay, "Mutual information of subsystems and the Page curve for the Schwarzschild–de Sitter black hole," Phys. Rev. D **108**, no.2, 026003 (2023) [arXiv:2303.14062 [hep-th]].

[171] D. S. Ageev, I. Y. Aref'eva, A. I. Belokon, V. V. Pushkarev and T. A. Rusalev, "Entanglement entropy in de Sitter: no pure states for conformal matter," [arXiv:2304.12351 [hep-th]].

[172] D. Basu, J. Lin, Y. Lu and Q. Wen, "Ownerless island and partial entanglement entropy in island phases," [arXiv:2305.04259 [hep-th]].

[173] H. S. Jeong, K. Y. Kim and Y. W. Sun, "Entanglement entropy analysis of dyonic black holes using doubly holographic theory," Phys. Rev. D **108**, no.12, 126016 (2023) doi:10.1103/PhysRevD.108.126016 [arXiv:2305.18122 [hep-th]].

[174] C. W. Tong, D. H. Du and J. R. Sun, "Island of Reissner-Nordström anti-de Sitter black holes in the large d limit," [arXiv:2306.06682 [hep-th]].

[175] M. H. Yu, X. H. Ge and C. Y. Lu, "Page Curves for Accelerating Black Holes," [arXiv:2306.11407 [hep-th]].

[176] C. J. Chou, H. B. Lao and Y. Yang, "Page Curve of AdS-Vaidya Model for Evaporating Black Holes," [arXiv:2306.16744 [hep-th]].

[177] S. E. Aguilar-Gutierrez, R. Espíndola and E. K. Morvan-Benhaim, "A teleportation protocol in Schwarzschild-de Sitter space," [arXiv:2308.13516 [hep-th]].

[178] B. Czech, S. Shuai and H. Tang, "Information recovery in the Hayden-Preskill protocol," [arXiv:2310.16988 [hep-th]].

[179] V. Franken, H. Partouche, F. Rondeau and N. Toumbas, "Closed FRW holography: A time-dependent ER=EPR realization," [arXiv:2310.20652 [hep-th]].

[180] K. Narayan, "Extremal surfaces in de Sitter spacetime," Phys. Rev. D **91**, no.12, 126011 (2015) doi:10.1103/PhysRevD.91.126011 [arXiv:1501.03019 [hep-th]].

[181] Y. Sato, "Comments on Entanglement Entropy in the dS/CFT Correspondence," Phys. Rev. D **91**, no.8, 086009 (2015) doi:10.1103/PhysRevD.91.086009 [arXiv:1501.04903 [hep-th]].

[182] K. Narayan, "On extremal surfaces and de Sitter entropy," Phys. Lett. B **779**, 214-222 (2018) doi:10.1016/j.physletb.2018.02.010 [arXiv:1711.01107 [hep-th]].

[183] K. Doi, J. Harper, A. Mollabashi, T. Takayanagi and Y. Taki, "Pseudoentropy in dS/CFT and Timelike Entanglement Entropy," Phys. Rev. Lett. **130**, no.3, 031601 (2023) doi:10.1103/PhysRevLett.130.031601 [arXiv:2210.09457 [hep-th]].

[184] K. Narayan, "de Sitter space, extremal surfaces, and time entanglement," Phys. Rev. D **107**, no.12, 126004 (2023) doi:10.1103/PhysRevD.107.126004 [arXiv:2210.12963 [hep-th]].

[185] L. Susskind, "The Census taker's hat," [arXiv:0710.1129 [hep-th]].

[186] J. F. Pedraza, A. Svesko, W. Sybesma and M. R. Visser, "Semi-classical thermodynamics of quantum extremal surfaces in Jackiw-Teitelboim gravity," JHEP **12**, 134 (2021) doi:10.1007/JHEP12(2021)134 [arXiv:2107.10358 [hep-th]].

[187] J. F. Pedraza, A. Svesko, W. Sybesma and M. R. Visser, "Microcanonical action and the entropy of Hawking radiation," Phys. Rev. D **105**, no.12, 126010 (2022) doi:10.1103/PhysRevD.105.126010 [arXiv:2111.06912 [hep-th]].

[188] E. K. Morvan, J. P. van der Schaar and M. R. Visser, "On the Euclidean action of de Sitter black holes and constrained instantons," SciPost Phys. **14**, no.2, 022 (2023) doi:10.21468/SciPostPhys.14.2.022 [arXiv:2203.06155 [hep-th]].

[189] A. Strominger, "The dS / CFT correspondence," JHEP **0110**, 034 (2001) [hep-th/0106113].

[190] E. Witten, "Quantum gravity in de Sitter space," [hep-th/0106109].

[191] J. M. Maldacena, "Non-Gaussian features of primordial fluctuations in single field inflationary models," JHEP **0305**, 013 (2003), [astro-ph/0210603].

[192] D. Anninos, T. Hartman and A. Strominger, "Higher Spin Realization of the dS/CFT Correspondence," Class. Quant. Grav. **34**, no. 1, 015009 (2017) doi:10.1088/1361-6382/34/1/015009 [arXiv:1108.5735 [hep-th]].

[193] M. Spradlin, A. Strominger and A. Volovich, "Les Houches lectures on de Sitter space," hep-th/0110007.

[194] D. Anninos, "De Sitter Musings," Int. J. Mod. Phys. A **27**, 1230013 (2012) doi:10.1142/S0217751X1230013X [arXiv:1205.3855 [hep-th]].

[195] D. A. Galante, "Modave lectures on de Sitter space & holography," PoS **Modave2022**, 003 (2023) doi:10.22323/1.435.0003 [arXiv:2306.10141 [hep-th]].

[196] K. Narayan, "de Sitter space and extremal surfaces for spheres," Phys. Lett. B **753**, 308 (2016) [arXiv:1504.07430 [hep-th]].

[197] M. Miyaji and T. Takayanagi, "Surface/State Correspondence as a Generalized Holography," PTEP **2015**, no. 7, 073B03 (2015) doi:10.1093/ptep/ptv089 [arXiv:1503.03542 [hep-th]].

[198] K. Narayan, "de Sitter entropy as entanglement," Int. J. Mod. Phys. D **28**, no.14, 1944019 (2019) doi:10.1142/S021827181944019X [arXiv:1904.01223 [hep-th]].

[199] K. Narayan, "Further remarks on de Sitter space, extremal surfaces, and time entanglement," Phys. Rev. D **109**, no.8, 086009 (2024) doi:10.1103/PhysRevD.109.086009 [arXiv:2310.00320 [hep-th]].

[200] Y. Hikida, T. Nishioka, T. Takayanagi and Y. Taki, "CFT duals of three-dimensional de Sitter gravity," JHEP **05**, 129 (2022) doi:10.1007/JHEP05(2022)129 [arXiv:2203.02852 [hep-th]].

[201] Y. Hikida, T. Nishioka, T. Takayanagi and Y. Taki, "Holography in de Sitter Space via Chern-Simons Gauge Theory," Phys. Rev. Lett. **129**, no.4, 041601 (2022) [arXiv:2110.03197 [hep-th]].

[202] J. Cotler and A. Strominger, "Cosmic ER=EPR in dS/CFT," [arXiv:2302.00632 [hep-th]].

[203] Y. Nakata, T. Takayanagi, Y. Taki, K. Tamaoka and Z. Wei, "New holographic generalization of entanglement entropy," Phys. Rev. D **103**, no.2, 026005 (2021) [arXiv:2005.13801 [hep-th]].

[204] Z. Li, Z. Q. Xiao and R. Q. Yang, "On holographic time-like entanglement entropy," JHEP **04**, 004 (2023) doi:10.1007/JHEP04(2023)004 [arXiv:2211.14883 [hep-th]].

[205] K. Doi, J. Harper, A. Mollabashi, T. Takayanagi and Y. Taki, "Timelike entanglement entropy," JHEP **05**, 052 (2023) doi:10.1007/JHEP05(2023)052 [arXiv:2302.11695 [hep-th]].

[206] X. Jiang, P. Wang, H. Wu and H. Yang, "Timelike entanglement entropy and TT^{-} deformation," Phys. Rev. D **108**, no.4, 046004 (2023) doi:10.1103/PhysRevD.108.046004 [arXiv:2302.13872 [hep-th]].

[207] Z. Chen, "Complex-valued Holographic Pseudo Entropy via Real-time AdS/CFT Correspondence," [arXiv:2302.14303 [hep-th]].

[208] X. Jiang, P. Wang, H. Wu and H. Yang, "Timelike entanglement entropy in $\mathrm{dS}_3/\mathrm{CFT}_2$," JHEP **08**, 216 (2023) doi:10.1007/JHEP08(2023)216 [arXiv:2304.10376 [hep-th]].

[209] C. S. Chu and H. Parihar, "Time-like entanglement entropy in AdS/BCFT," JHEP **06**, 173 (2023) doi:10.1007/JHEP06(2023)173 [arXiv:2304.10907 [hep-th]].

[210] H. Y. Chen, Y. Hikida, Y. Taki and T. Uetoko, "Complex saddles of Chern-Simons gravity and dS3/CFT2 correspondence," Phys. Rev. D **108**, no.6, 066005 (2023) [arXiv:2306.03330 [hep-th]].

[211] D. Chen, X. Jiang and H. Yang, "Holographic $T\bar{T}$ deformed entanglement entropy in $\mathrm{dS}_3/\mathrm{CFT}_2$," [arXiv:2307.04673 [hep-th]].

[212] P. Z. He and H. Q. Zhang, "Timelike Entanglement Entropy from Rindler Method," [arXiv:2307.09803 [hep-th]].

[213] A. Das, S. Sachdeva and D. Sarkar, "Bulk reconstruction using timelike entanglement in (A)dS," Phys. Rev. D **109**, no.6, 066007 (2024) doi:10.1103/PhysRevD.109.066007 [arXiv:2312.16056 [hep-th]].

[214] D. Basu and V. Raj, "Reflected entropy and timelike entanglement in $T\bar{T}$-deformed CFT2s," Phys. Rev. D **110**, no.4, 046009 (2024) doi:10.1103/PhysRevD.110.046009 [arXiv:2402.07253 [hep-th]].

[215] R. Fareghbal, "Flat-space limit of holographic pseudoentropy in (A)dS space-times," Phys. Rev. D **110**, no.6, 066019 (2024) doi:10.1103/PhysRevD.110.066019 [arXiv:2408.03061 [hep-th]].

[216] M. P. Heller, F. Ori and A. Serantes, "Geometric interpretation of timelike entanglement entropy," [arXiv:2408.15752 [hep-th]].

[217] A. Lewkowycz and J. Maldacena, "Generalized gravitational entropy," JHEP **08**, 090 (2013) doi:10.1007/JHEP08(2013)090 [arXiv:1304.4926 [hep-th]].

[218] X. Dong, A. Lewkowycz and M. Rangamani, "Deriving covariant holographic entanglement," JHEP **11**, 028 (2016) doi:10.1007/JHEP11(2016)028 [arXiv:1607.07506 [hep-th]].

[219] X. Dong, "The Gravity Dual of Renyi Entropy," Nature Commun. **7**, 12472 (2016) doi:10.1038/ncomms12472 [arXiv:1601.06788 [hep-th]].

[220] X. Dong, "Holographic Entanglement Entropy for General Higher Derivative Gravity," JHEP **01**, 044 (2014) doi:10.1007/JHEP01(2014)044 [arXiv:1310.5713 [hep-th]].

[221] H. Casini, M. Huerta and R. C. Myers, "Towards a derivation of holographic entanglement entropy," JHEP **1105**, 036 (2011) [arXiv:1102.0440 [hep-th]].

[222] J. B. Hartle and S. W. Hawking, "Wave Function of the Universe," Phys. Rev. D **28**, 2960-2975 (1983) doi:10.1103/PhysRevD.28.2960

[223] J. Maldacena, "Comments on the no boundary wavefunction and slow roll inflation," [arXiv:2403.10510 [hep-th]].

[224] R. Bousso and S. W. Hawking, "The Probability for primordial black holes," Phys. Rev. D **52**, 5659-5664 (1995) doi:10.1103/PhysRevD.52.5659 [arXiv:gr-qc/9506047 [gr-qc]].

[225] J. B. Hartle, S. W. Hawking and T. Hertog, "The Classical Universes of the No-Boundary Quantum State," Phys. Rev. D **77**, 123537 (2008) doi:10.1103/PhysRevD.77.123537 [arXiv:0803.1663 [hep-th]].

[226] J. Diaz Dorronsoro, J. J. Halliwell, J. B. Hartle, T. Hertog and O. Janssen, "Real no-boundary wave function in Lorentzian quantum cosmology," Phys. Rev. D **96**, no.4, 043505 (2017) doi:10.1103/PhysRevD.96.043505 [arXiv:1705.05340 [gr-qc]].

[227] J. J. Halliwell, J. B. Hartle and T. Hertog, "What is the No-Boundary Wave Function of the Universe?," Phys. Rev. D **99**, no.4, 043526 (2019) doi:10.1103/PhysRevD.99.043526 [arXiv:1812.01760 [hep-th]].

[228] O. Janssen, "Slow-roll approximation in quantum cosmology," Class. Quant. Grav. **38**, no.9, 095003 (2021) doi:10.1088/1361-6382/abe143 [arXiv:2009.06282 [gr-qc]].

[229] T. Hertog, O. Janssen and J. Karlsson, "Kontsevich-Segal Criterion in the No-Boundary State Constrains Inflation," Phys. Rev. Lett. **131**, no.19, 191501 (2023) doi:10.1103/PhysRevLett.131.191501 [arXiv:2305.15440 [hep-th]].

[230] G. W. Gibbons and S. W. Hawking, "Action Integrals and Partition Functions in Quantum Gravity," Phys. Rev. D **15**, 2752-2756 (1977) doi:10.1103/PhysRevD.15.2752

[231] S. W. Hawking and D. N. Page, "Thermodynamics of Black Holes in anti-De Sitter Space," Commun. Math. Phys. **87**, 577 (1983) doi:10.1007/BF01208266

[232] E. Witten, "Anti-de Sitter space, thermal phase transition, and confinement in gauge theories," Adv. Theor. Math. Phys. **2**, 505-532 (1998) doi:10.4310/ATMP.1998.v2.n3.a3 [arXiv:hep-th/9803131 [hep-th]].

[233] T. Hartman and J. Maldacena, "Time Evolution of Entanglement Entropy from Black Hole Interiors," JHEP **1305**, 014 (2013) [arXiv:1303.1080 [hep-th]].

[234] J. M. Maldacena, "Eternal black holes in anti-de Sitter," JHEP **0304**, 021 (2003) [hep-th/0106112].

[235] K. Narayan, "On dS_4 extremal surfaces and entanglement entropy in some ghost CFTs," Phys. Rev. D **94**, no. 4, 046001 (2016) [arXiv:1602.06505 [hep-th]].

[236] D. P. Jatkar and K. Narayan, "Ghost-spin chains, entanglement and *bc*-ghost CFTs," Phys. Rev. D **96**, no. 10, 106015 (2017) [arXiv:1706.06828 [hep-th]].

[237] K. Doi, N. Ogawa, K. Shinmyo, Y. k. Suzuki and T. Takayanagi, "Probing de Sitter Space Using CFT States," [arXiv:2405.14237 [hep-th]].

[238] M. Trodden and S. M. Carroll, "TASI lectures: Introduction to cosmology," [astro-ph/0401547].

[239] D. Baumann, "Inflation," doi:10.1142/9789814327183_0010 [arXiv:0907.5424 [hep-th]].

[240] D. Baumann and L. McAllister, "Inflation and String Theory," Cambridge University Press, 2015, ISBN 978-1-107-08969-3, 978-1-316-23718-2 doi:10.1017/CBO9781316105733 [arXiv:1404.2601 [hep-th]].

[241] N. Ogawa, T. Takayanagi and T. Ugajin, "Holographic Fermi Surfaces and Entanglement Entropy," JHEP **1201**, 125 (2012) [arXiv:1111.1023 [hep-th]].

[242] L. Huijse, S. Sachdev and B. Swingle, "Hidden Fermi surfaces in compressible states of gauge-gravity duality," Phys. Rev. B **85**, 035121 (2012) [arXiv:1112.0573 [cond-mat.str-el]].

[243] X. Dong, S. Harrison, S. Kachru, G. Torroba and H. Wang, "Aspects of holography for theories with hyperscaling violation," JHEP **1206**, 041 (2012) [arXiv:1201.1905 [hep-th]].

[244] K. Narayan, "On Lifshitz scaling and hyperscaling violation in string theory," Phys. Rev. D **85**, 106006 (2012) [arXiv:1202.5935 [hep-th]].

[245] K. Narayan, T. Takayanagi and S. P. Trivedi, "AdS plane waves and entanglement entropy," JHEP **1304**, 051 (2013) [arXiv:1212.4328 [hep-th]].

[246] K. Narayan, "On a lightlike limit of entanglement," Phys. Rev. D **91**, no.8, 086010 (2015) doi:10.1103/PhysRevD.91.086010 [arXiv:1408.7021 [hep-th]].

[247] K. Goswami and K. Narayan, "Small Schwarzschild de Sitter black holes, the future boundary and islands," JHEP **05**, 016 (2024) doi:10.1007/JHEP05(2024)016 [arXiv:2312.05904 [hep-th]].

[248] K. Goswami, K. Narayan and G. Yadav, "No-boundary extremal surfaces in slow-roll inflation and other cosmologies," JHEP **03**, 193 (2025) doi:10.1007/JHEP03(2025)193 [arXiv:2409.14208 [hep-th]].

[249] M. Kontsevich and G. Segal, "Wick Rotation and the Positivity of Energy in Quantum Field Theory," Quart. J. Math. Oxford Ser. **72**, no.1-2, 673-699 (2021) doi:10.1093/qmath/haab027 [arXiv:2105.10161 [hep-th]].

[250] E. Witten, "A Note On Complex Spacetime Metrics," [arXiv:2111.06514 [hep-th]].

[251] I. Mata, S. Raju and S. Trivedi, "CMB from CFT," JHEP **07**, 015 (2013) doi:10.1007/JHEP07(2013)015 [arXiv:1211.5482 [hep-th]].

[252] A. Ghosh, N. Kundu, S. Raju and S. P. Trivedi, "Conformal Invariance and the Four Point Scalar Correlator in Slow-Roll Inflation," JHEP **07**, 011 (2014) doi:10.1007/JHEP07(2014)011 [arXiv:1401.1426 [hep-th]].

[253] I. Dey, K. K. Nanda, A. Roy and S. P. Trivedi, "Aspects of dS/CFT Holography," [arXiv:2407.02417 [hep-th]].